

Document Type: TWR  
Document No: TWR-18901  
Document Rev: -  
Change No: 000  
Work Order: N/A

*1N-37-CR  
247695*

## FINAL REPORT FOR ETP-0403, RESIDUAL STRESS MEASUREMENTS AFTER PROOF AND FLIGHT

NASA/CR- -97- 208242

Prepared for:

NATIONAL AERONAUTICS AND SPACE ADMINISTRATION  
GEORGE C. MARSHALL SPACE FLIGHT CENTER  
MARSHALL SPACE FLIGHT CENTER, ALABAMA 35812

Contract No. NAS8-38100  
DR No. 5-3  
WBS. No. 4C205  
ECS No. 00010932  
ECP No.

**THIOKOL**

P. O. Box 707, Brigham City, UT 84302-0707 (801) 863-3511



V. K. Henson, SA51  
E613-FY98-242

Distribution

R. B. Roth, TC/MSFC  
S. Cash, EE54  
A. Domal, EE53  
T. Shaffner, TC/KSC  
D. Burton, RMO/K68 (2)  
M. Fisher, USBI/K68  
R. Brown, CR65  
D. Hull, CR65  
R. Goins, Hernandez/MSFC  
F. Bugg, ED26  
L. Clayton, ED63  
M. Hill, ED28  
G. Bishop, EE52  
J. Hester, EE51  
D. Ricks, EE54  
R. Nichols, EE51  
D. Hannsz, JSC/CB  
R. Sanders, JSC/MS4  
Central Documentation Repository, CN22D (5)

W/O Enclosure

S. Vigil, E68

CN31S 0 2  
TURNER J/PUBLICATION  
MARSHALL SPACE FLIGHT CENTER  
HUNTSVILLE AL.  
DELETIONS OR CHANGES 544-4494  
RETURN ADDRESS CN31D  
Document Code: 2444



**SPACE OPERATIONS**

P.O. BOX 707  
BRIGHAM CITY, UT 84302-0707  
801-863-3511

**THIOKOL**  
AEROSPACE & INDUSTRIAL TECHNOLOGIES

November 24, 1997  
E611-FY98-242

George C. Marshall Space Flight Center  
National Aeronautics and Space Administration  
Marshall Space Flight Center, AL 35812

Attention Mr. V. K. Henson, SA51

Gentlemen:

Subject: Transmittal of Final Report for ETP-0403, Residual Stress  
Measurements After Proof and Flight, TWR-18901, DR 5-3,  
Type 2 Documentation

Transmittal of Final Report for ETP-0474, Evaluation of  
Electroless Nickel Plating to Eliminate Fretting, TWR-19494,  
DR 5-3, Type 2 Documentation

Transmittal of Final Report for ETP-0492, Measured Residual  
Stresses in Cylinder S/N 53 Fretted Area, TWR-18901, DR 5-3,  
Type 2 Documentation

The subject documents report results of testing completed during the Redesign Program. The test data was used in various Flight Readiness Review presentations, but final documentation was never completed. In an effort to clean up open paperwork, we have recently devoted resources to complete the preparation and release of these three reports. The subject documents are being forwarded for your information.

If you have any questions or comments concerning this transmittal, please direct them to the undersigned at extension 3475.

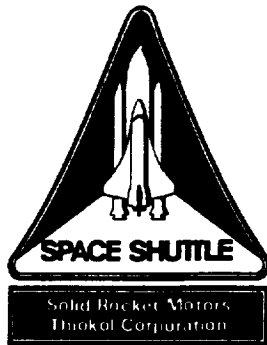
Very truly yours,



Sam Vigil  
Test Management

Encl: a/s





Document Type: TWR  
 Document No: TWR-18901  
 Document Rev: -  
 Change No: 000  
 Work Order: N/A

## FINAL REPORT FOR ETP-0403, RESIDUAL STRESS MEASUREMENTS AFTER PROOF AND FLIGHT

SR&QA Not Required	Date	PREPARER Ronald L. Webster:03681	Date 28-OCT-1997
PM Scott R. Stein:13537	Date 17-NOV-1997	DE_SUPERVISOR Jay V. Daines:03741	Date 31-OCT-1997
DE Vicki B. Call:13022	Date 03-NOV-1997	DATA_MANAGEMENT Irma Nieto:19249	Date 18-NOV-1997

RELEASED  
 18-nov-1997 13:07:26



## ABSTRACT

The intent of this testing was to evaluate the residual stresses that occur in and around the attachment details of a case stiffener segment that has been subjected to flight/recovery followed by proof loading. Not measured in this test were stresses relieved at joint disassembly due to out-of-round and interference effects, and those released by cutting the specimens out of the case segment.

The test article was lightweight case stiffener segment 1U50715, S/N L023 which was flown in the forward stiffener position on flight SRM14A and in the aft position on flight SRM24A. Both of these flights were flown with the 3 stiffener ring configuration. Stiffener L023 had a stiffener ring installed only on the aft stub in its first flight, and it had both rings installed on its second flight. No significant post flight damage was found on either flight. Finally, the segment was used on the DM-8 static test motor in the forward position. No stiffener rings were installed. It had only one proof pressurization prior to assignment to its first use, and it was cleaned and proof tested after each flight. Thus, the segment had seen 3 proof tests, two flight pressurizations, and two low intensity water impacts prior to manufacturing for use on DM-8. On DM-8 it received one static firing pressurization in the horizontal configuration.

Residual stresses at the surface and in depth were evaluated by both the x-ray diffraction and neutron beam diffraction methods. The x-ray diffraction evaluations were conducted by Technology for Energy Corporation (TEC) at their facilities in Knoxville, TN. The neutron beam evaluations were done by Atomic Energy of Canada Limited (AECL) at the Chalk River Nuclear Laboratories in Ontario. The results showed general agreement with relatively high compressive residual stresses on the surface and moderate to low subsurface tensile residual stresses.



**Table Of Contents**

1. INTRODUCTION .....	1
1.1 TEST ARTICLE DESCRIPTION .....	3
2. OBJECTIVES .....	5
3. EXECUTIVE SUMMARY .....	5
3.1 SUMMARY .....	5
3.2 CONCLUSIONS .....	7
3.3 RECOMMENDATIONS .....	7
4. INSTRUMENTATION .....	8
5. PHOTOGRAPHY .....	8
6. RESULTS AND DISCUSSION .....	8
6.1 TEST DESCRIPTION .....	8
6.2 DESCRIPTION AND JUSTIFICATION OF DEVIATIONS FROM THE TEST PLAN .....	11
6.3 TEST PREPARATIONS .....	11
6.4 TEST FACILITIES .....	11
6.5 TEST PROCEDURES AND INSTRUMENTATION .....	11
6.6 SIGNIFICANT FINDINGS .....	12
6.6.1 GENERAL OBSERVATIONS .....	12
6.6.2 TEST DATA EVALUATIONS .....	12
6.6.3 INFORMATION FROM STRESS ANALYSES .....	15
7. APPLICABLE DOCUMENTS .....	19
8. REFERENCES .....	19

APPENDIX A - VENDOR REPORT FOR X-RAY DIFFRACTION MEASUREMENTS

APPENDIX B - VENDOR REPORT FOR NEUTRON BEAM DIFFRACTION MEASUREMENTS

**LIST OF FIGURES**

Figure 1 Configuration of Factory Joint Alignment Slot Region .....	4
Figure 2 Configuration of Case Stiffener Stubs .....	4
Figure 3 Summary of Hoop Residual Stresses on Factory Joint Features .....	6
Figure 4 Summary of Residual Stresses on Stiffener Stubs .....	6
Figure 5 Comparison of Neutron Beam Measured and Analytical Residual Strains .....	7
Figure 6 Tang and Clevis Measurement Locations .....	9
Figure 7 X-ray Diffraction Evaluation Points for Tang Specimens .....	9
Figure 8 X-ray Diffraction Evaluation Points For Stiffener Stubs .....	10
Figure 9 Comparative Measurement Trends .....	15
Figure 10 Finite Element Model of Typical Factory Joint Pin Locations .....	16
Figure 11 FE Analysis Results for Tang Nodes .....	16
Figure 12 FE Analysis Results for Outer Clevis Leg Nodes .....	17
Figure 13 FE Analysis Results for Inner Clevis Leg Nodes .....	17
Figure 14 Yield Zones for a Typical Pin Hole and an Alignment Slot .....	18
Figure 15 Finite Element Model of the Alignment Slot Zone .....	18



LIST OF TABLES

Table 1 Test Evaluation Sequence For X-Ray Diffraction.....8  
Table 2 Test Evaluation Sequence For Neutron Beam Diffraction .....10  
Table 3 Comparison Of Key Residual Stress Values .....14  
Table 4 Typical Dislocation Density Readings By X-Ray Diffraction.....15



## 1. INTRODUCTION

The steel case components of the Space Shuttle Reusable Solid Rocket Motor (RSRM) are fracture critical items. One important issue in assuring flight safety for the motor components of the booster rockets is the fracture sensitivity for each use (mission). This includes both basic flaw growth driven by repeated loads and stress corrosion cracking. The conditions for stress corrosion cracking to occur are a combination of the following:

1. A sustained surface (or near surface) tensile stress exceeding the stress corrosion cracking susceptibility limit (about 30 ksi for a 0.100 in. deep crack in the RSRM case material).
2. A sustained corrosive environment (salt water, humid air exposure)

There are two periods of sustained exposure to corrosion environments. The first is in sea air with high humidity prior to flight. This occurs during the launch site storage, flight system assembly, roll-out, and on-pad operations. A significant sea water exposure of case components occurs during recovery operations in the splashdown and tow back phases. Most of the external surface of the case is painted to avoid corrosion exposure. Those areas where structural joints are to be made cannot be painted and absolute corrosion protection cannot be assured even though a coating of CONOCO HD-2 grease is used to protect the exposed surfaces and a sacrificial anode is attached to the case soon after splashdown. The joints addressed by this set of tests are at the factory and field joints of the cylinder segments and the attachment stubs for the stiffener rings on the aft segment.

Where absolute protection cannot be assured, the critical issue for stress corrosion cracking is what the stresses are at or near the surfaces during the unlikely corrosive exposure. The residual stresses are a potential means of obtaining sustained surface stresses. The residual stress distributions of most concern for stress corrosion cracking are tensile surface stresses and in-depth distributions that can contribute to the development of high stress intensity factors at the location of the tip of a potential macroscopic surface flaw (crack).

Although a major one, the stress corrosion cracking is not the only concern for the presence of residual stresses in the RSRM case. Since the residual stresses are present for all loading applied after the residual stresses are developed, they combine with the loading to increase or decrease the final stresses. Knowing the location, sign, and magnitude of the residual stresses is required to assess the structural adequacy of the RSRM case.

Residual stresses result from nonuniform plastic deformations or from an assembly operation that stresses the mating parts. There are several processes in motor manufacture and flight use which can produce residual stresses in the case components. Some of them are:

1. Quenching during heat treatment
2. Machining during case segment manufacturing
3. Local yielding during proof test
4. Blasting with grit or glass beads for surface cleaning
5. Fixturing and curing during motor manufacturing
6. Assembly with interferences and pre-loads
7. Local yielding during flight and recovery

Often the stresses produced from assembly are only present while the components are mated. They are released on disassembly if no plastic deformations have occurred in the interim. Plastic deformations of assembled components can alter the interference that produced the assembly stresses and lead to a different pattern of residual stresses in the components after disassembly. Proof testing and water impact are two examples of loads that can produce plastic deformations on an assembly.

Quenching stresses are usually highest on the surfaces of thick regions, and they often result in compressive residual stresses which decrease with depth into the material. The residual stresses caused by machining after heat treatment are highest at the surface and decrease rapidly into the depth of the material. This decay is much more rapid for machining

residual stresses than for quenching residual stresses. Tensile residual stresses may be found interior to the parts but at much lower magnitude over a large volume.

Residual stresses developed by machining usually do not penetrate deep enough to be a concern for macroscopic cracks. Their influence is mostly at the surface. The machining and hole drilling can produce microscopic surface tearing in some situations. These offer an opportunity for crack initiation in high load or repeated load situations.

The grit or glass bead blasting in cleaning operations produce a thin layer of compressive residual stresses at the blasted surface. Since these are compressive stresses, they are likely to overwhelm any tensile surface stresses developed previous to the cleaning.

Residual stresses from proof testing and flight/recovery loadings tend to be localized around attachments and other structural details. These vary through the thickness at the details, but at a much slower rate and over a larger region than do the quenching, machining, and surface blasting residuals. Both tensile and compressive surface stresses can be produced. The highest residual stresses tend to be very localized and surrounded by a larger regions of residual stress at a lower magnitude and opposite sign.

The proof and flight/recovery loadings are the most concern for critical crack growth. The highest internal pressure seen by the case components is the proof pressure. It is intentionally from 10% to 20% higher than the maximum expected operating pressure for flight. The pressure histories in proof and flight are relatively short so that they have little direct contribution to crack growth enhancement by stress corrosion cracking. The main contributions of these pressure loadings are the development of residual stresses and incremental crack growth. The factory and field joints experience stresses high enough to locally yield the details around the pin holes, the base of the alignment slots, and the special ports used in joint assembly and leak checking. When the pressure is released, a portion of the yielded zone is forced into a reversed yielding by the elastic recovery of the larger volume of adjacent material. This cyclic plastic deformation leads to a complex pattern of residual stresses in the joint details. The size of cracks potentially allowed in flight components is limited by the refurbishment proof test and the NDE inspections for cracks prior to the next use.

The assembly of the field joints requires an interference between the tang capture feature and the inner clevis leg. This interference adds locally to the residual stresses in the assembled RSRM. Although the factory joints do not have the capture feature to induce the interference fit on assembly, there are unavoidable incongruencies that must be forced to accommodate the assembly of either joint type. Each clevis joint has shims installed that take up radial slack around the pins. Some of these may become hard contact points as the assembly is closed out. Additional long term stresses are produced by the gravity loads imposed on the RSRM case while supporting the entire flight assembly on the MLP during flight preparations.

Launch and flight loads are not long term loads, but (as noted above) the pressure loading combined with other flight loads has the potential for altering the residual stress distribution by adjusting the local yielding and for growing existing cracks.

The recovery for reuse of the RSRM case components involves a water impact event that is well known for its ability to produce high external side loading on the aft portions of the motor casing. This highly variable loading can produce permanent deformation in the components of the aft segment of the case. This deformation is manifest as an out-of-round condition at the factory joints and the stiffener ring attachment stub details after case disassembly. Local damage experienced in the stiffener stub details can include hole and stub deformations and bolt hole ligament cracking. Local deformations also occur in the factory joint details around the pin holes, alignment slots, and leak check ports. These all contribute to the development of residual stresses.

Stiffener segments with bolt hole ligament cracks are not allowed in flight motors. They can be cleared for flight only if they have the cracked material removed in an approved "repair" processes. Stiffener stubs reworked to remove cracks are not considered in this test effort.

The refurbishment process for preparing segments for their next use involves removal of bonded insulation and paint by high pressure water jet, glass bead blasting for cleaning of tang and clevis details, grinding and blending to remove surface anomalies, and hydroproof testing at pressures higher than flight and with support conditions not fully simulating flight conditions. The refurbishment process modifies the state of the residual stresses in a way that needs to be quantified to

assure surface tensile residual stress are not developed that exceed the stress corrosion cracking susceptibility limit for the D6AC case material.

The intent of this testing was to evaluate the residual stresses that occur in and around the attachment details of a case stiffener segment that has been subjected to flight/recovery followed by proof loading. Not measured in this test were stresses relieved at joint disassembly due to out-of-round and interference effects, and those released by cutting the specimens out of the case segment.

## 1.1 TEST ARTICLE DESCRIPTION

The test article was lightweight case stiffener segment 1U50715, S/N L023 which was flown in the forward stiffener position on flight SRM14A and in the aft position on flight SRM24A. Both of these flights were flown with the 3 stiffener ring configuration. Stiffener L023 had a stiffener ring installed only on the aft stub in its first flight. It had both rings installed on its second flight. No visible post flight damage was found for either flight. Finally, the segment was used on the DM-8 static test motor in the forward position. No stiffener rings were installed. It had only one proof pressurization prior to assignment to its first use, and it was cleaned and proof tested after each flight. Thus, the segment had seen 3 proof tests, two flight pressurizations, and two low intensity water impacts prior to manufacturing for use on DM-8. On DM-8 it received one static firing pressurization in the horizontal configuration.

The RSRM cylinder segments are fabricated from D6AC steel per STW4-2606 and heat treated according to STW7-2608.

**NOTE:** The test plan (reference 1) gives two incorrect designations for this segment. The title page refers to 1U50716-06 S/N L023 (*a lightweight attach segment*). The test component description in Section 2.0 refers to 1U50715 S/N L032 (*a lightweight stiffener segment flown on flight 21A*). The DM-8 motor used the lightweight attach segment S/N L032 and the lightweight stiffener segment S/N L023. The correct designation of the test item is lightweight stiffener segment S/N L023 flown on flights 14A and 24A. The similarity of the segment numbering gave opportunity for the confusion.

At the end of the DM-8 static firing, part of the case deluge system failed, and the ET attach segment was heat damaged along with the forward end of the L023 stiffener segment for part of the circumference (the L032 attach segment had major heat damage). The heat damage was due to static firing heat soak and the accumulation of slag in the bottom of the motor. The heating was focused on the 0° angular position, which was the bottom in the static firing configuration. The aft half of the L023 attach segment appeared unaffected. The segment was scrapped and allocated to various investigations and evaluations.

The failure investigation for DM-8 included a Rockwell C hardness survey and a dye penetrant crack survey to assure the heat affected areas were delineated. The cutting plan for the DM-8 accident investigation allocated portions of the unaffected areas for this test as well as pieces from the damaged area for the accident investigation (see reference 2). Seven large pieces were assigned to this residual stress investigation.

The excess heat from the DM-8 deluge failure produced various local deformations of the forward end of the segment which would alter the residual stress state. Since it was necessary to cut out the test pieces from the case, the assembly and test stand induced stresses were relieved along with both the out-of-round and heat affected residual stresses in the segment. There is no way to estimate what they were, but studies of out-of-round conditions suggest that the case is a thin shell that does not require large forces to move it to an out-of-round condition. The residual stresses from any heat effects are considered to have been small and of no consequence to this testing. The post flight inspection of this segment showed no measurable damage from water impact on either flight. This suggests that the residual stresses relieved by removing the test pieces from the cylinder (ignoring heat effects) were less than 2 ksi. This is an order of magnitude less than the typical measurement accuracy of the x-ray diffraction process.

The case cleaning operations in refurbishment involve glass bead blasting which induces compressive residual stresses on the blasted surfaces. This process tends to overwhelm (replace) the residual stresses that existed prior to blast cleaning on the surface and to a depth of a few mils. This suggests the residual stresses prior to DM-8 manufacturing should have been similar to the state after the acceptance proof testing and cleaning for first motor manufacturing. The static firing and flight stresses are not as high as the proof stresses, so negligible disturbance of the residual stress fields would have occurred over the two flights and one static firing.

REVISION \_\_\_\_\_

DOC NO.	TWR-18901	VOL
SEC	PAGE	3

This sequence of observations suggest that the tested pieces of the lightweight stiffener S/N L023 were representative of RSRM case material that has seen repeated refurbishments and proof tests. The effects of flight, water impact, repeated blast cleaning, and static firing are expected to be negligible on this component. Thus the S/N L023 cylinder is considered to be representative of the RSRM lightweight stiffener segments that have had three proof cycles applied. The major contributors to the residual stress state are considered to be the repeated local plastic deformations from the 3 proof tests and the compressive surface residuals from the last blast cleaning.

Figures 1 and 2 show the general configurations the alignment slot and stiffener stub features of a stiffener segment.

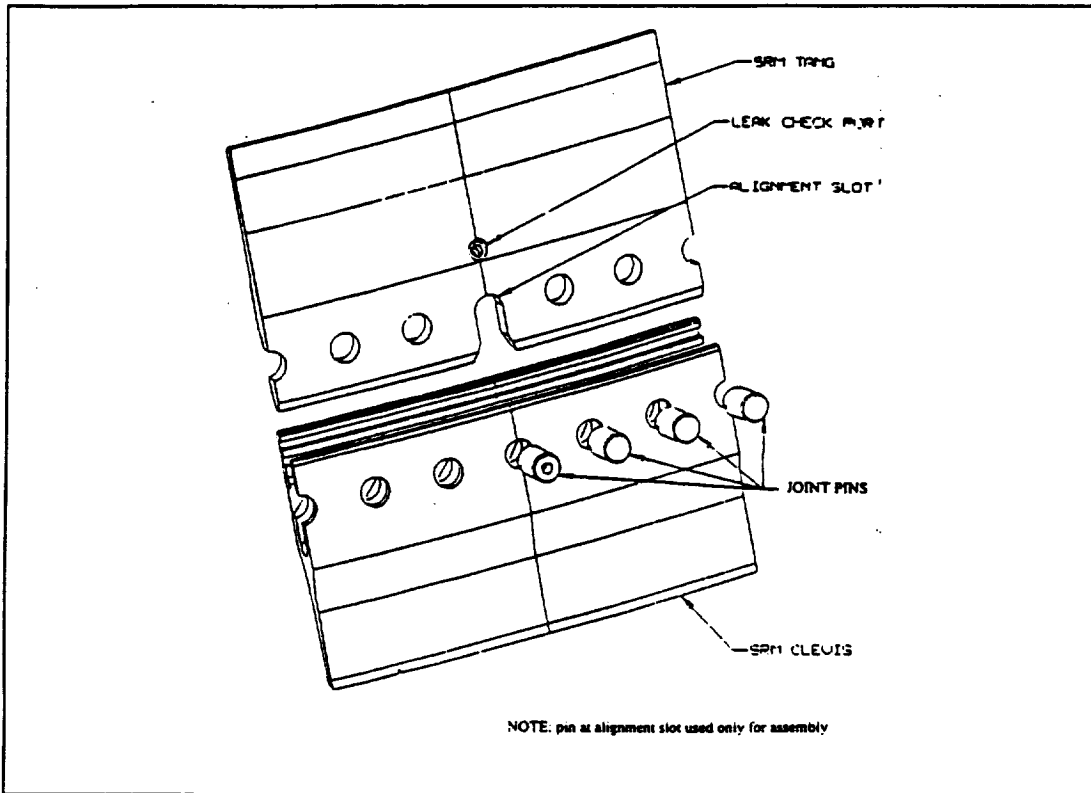


Figure 1 Configuration of Factory Joint Alignment Slot Region

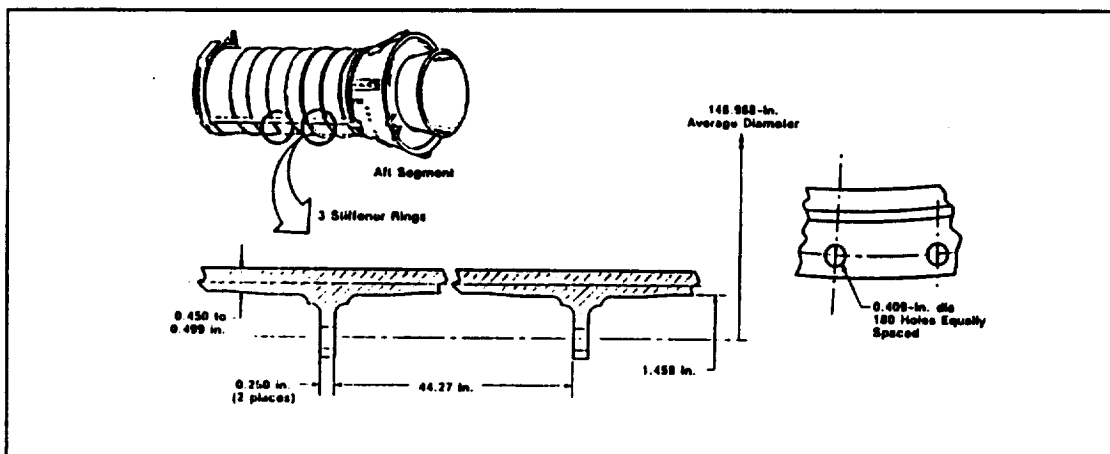


Figure 2 Configuration of Case Stiffener Stubs

The cutting plan associated with this test is shown in the test plan (Reference 1, Figures 1-3). The seven pieces produced were labeled with the following identification codes:

Tang - 000  
Tang - 118  
Tang - 240  
Clevis - 118  
Clevis - 240  
F Stub - 166  
A Stub - 166

The numbers for the specimens indicate the case reference angle to the center of the specimens. The three tang specimens were centered on the alignment slots, providing 3 pin holes on either side of the alignment slot. The first pin holes on either side of the slot see the largest pin loads from pressurization and were the specific targets of this testing. The two clevis specimens were at corresponding locations on the forward end of the segment where there was no heat damage. Each of the two stiffener stub specimens spanned a 20° arc centered on the same angular position, again avoiding the heat affected zone. Each stiffener stub specimen had 9 bolt holes available for evaluation. Each of the pieces were flame cut from the segment and abrasively trimmed to the final sizes using a hydrolaser to remove any heat affected material produced by the flame cutting.

Two pieces of case membrane (9 in. long with a 16° arc) were used as material comparison standards in measurements of grain dislocation density. One piece was supplied in the "as cut" condition, and the other received a laboratory heat treatment to remove any residual stresses.

## 2. OBJECTIVES

The objective of this test was to measure the residual stresses near the structural details (factory joint and stiffener attachment stubs) in a case segment that had experienced both flight loads and subsequent proof testing. The intent was to use this data to compare with analytical computations and to assess basic structural integrity and the sensitivity of the case components to stress corrosion cracking. A side objective was to compare the effectiveness of measuring residual stresses by the x-ray and neutron beam diffraction methods.

## 3. EXECUTIVE SUMMARY

### 3.1 SUMMARY

All test objectives were met. There were no abnormal occurrences or adverse findings. Figures 3 and 4 summarize the residual stress results obtained from the x-ray diffraction evaluations. Although the lightweight stiffener S/N L023 test article had seen two flight uses, the effects of water impact and recovery were found to be minimal. The primary effects represented in the residual stresses retained in the test pieces were from 3 proof tests and 2 refurbishments prior to the DM-8 static firing.

It should be noted that a general review of these test results was presented in Reference 3 to support an evaluation of damaged stiffener segments with the intent of defining conditions for their continued use.

This testing found no evidence of tensile residual stresses at the surface locations evaluated. No concerns were raised about the stress corrosion potential at the surface or near surface in the cylinder joints or the stiffener stub bolt holes.

The magnitudes of the surface compressive stresses found were generally in the range of 100 to 150 ksi at all points evaluated. They decreased rapidly with depth from the surface, extending inward less than 10 mils. The combination of x-ray diffraction and material removal was not precise enough to estimate the actual depth of this effect. These surface compressive stresses are most likely to be the result of the shot-peening effect from cleaning using glass bead blasting.

The subsurface residual stress readings at depths approaching 10 mils were mixed low tension and compression. The majority of the readings were compressive with magnitudes less than 90 ksi. At locations that found tensile residual

REVISION \_\_\_\_\_

DOC NO.	TWR-18901	VOL
SEC	PAGE	5

stresses, most of them had magnitudes less than 10 ksi. Somewhat higher tensile residual stresses were found at a few subsurface locations. The highest tensile reading found by the x-ray diffraction process was  $28.1 \pm 2.7$  ksi. This was measured in the hoop direction at point T4C on the Tang-240 specimen. Taking the measurement uncertainty at that point, the hoop residual stress could be as high as 30 ksi. A similar (but lower) reading was obtained at the same location on the Tang-118 specimen. Test point T4C was on the outboard surface of the tang midway from the edge of the pin hole and the tip of the tang on the second hole from the alignment slot (4") at a depth of about 10 mils. The estimated crack tip residual stress patterns must be combined with these upper bound estimates to determine if a risk of stress corrosion augmented cracking indicated for such a flaw. What is indicated by this finding is a need for careful and accurate surface crack detection in the refurbishment process.

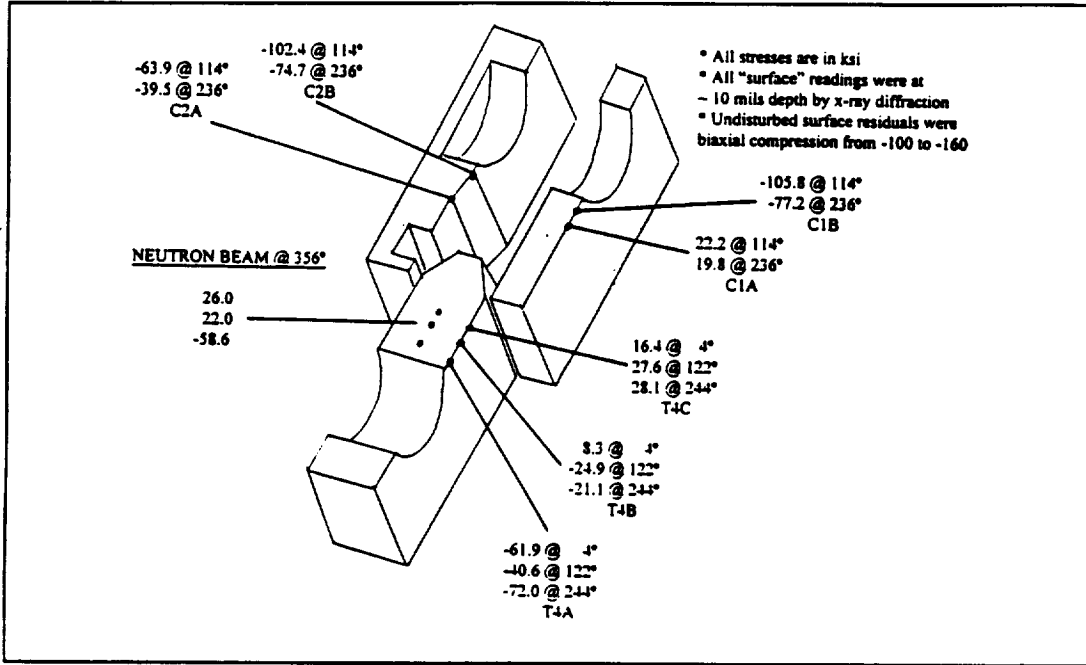


Figure 3 Summary of Hoop Residual Stresses on Factory Joint Features

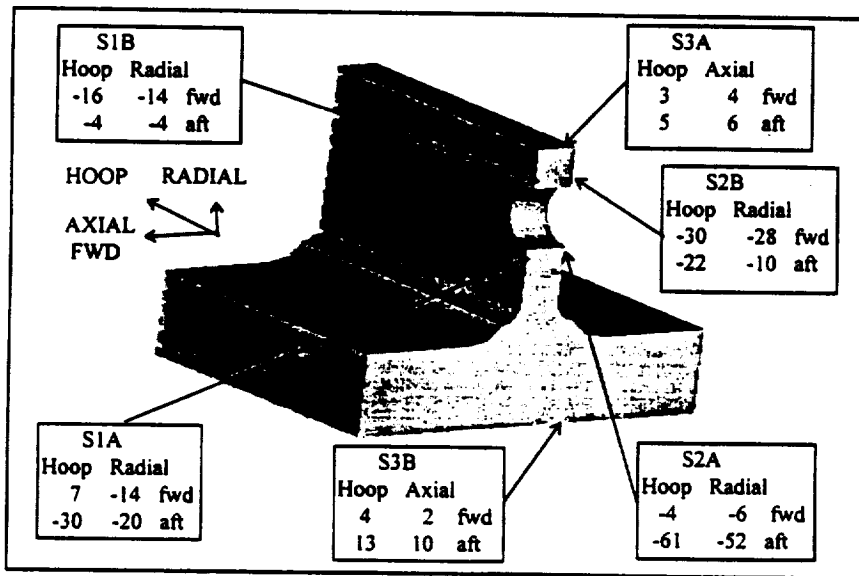


Figure 4 Summary of Residual Stresses on Stiffener Stubs

### 3.2 CONCLUSIONS

The neutron beam diffraction investigation of a 4" hole on the Tang-000 specimen succeeded in evaluating the in-depth residual stresses between the edge of the pin hole and the tip of the tang. These are considered to be representative of the in-depth residual stresses produced by three proof tests. Measurements were made of the tang radial, hoop, and axial residual strains at 57 interior points. No material removal was needed in this process. Each of these points were used to compare the patterns of residual strain variation between the experimental and analytical distributions. There was reasonably good agreement. In most cases the values computed from the finite element model were found to lie within the error band of the experimental data. This level of agreement is about as good as can be expected with the differences that exist between actual hardware (properties, geometry, and loading) and the worst case conditions assumed in the finite element analysis [4]. Figure 5 shows the level of agreement between measured and analytical estimates of residual strains with a graph of the values along the mid-thickness line between the pin hole and the tip of the tang.

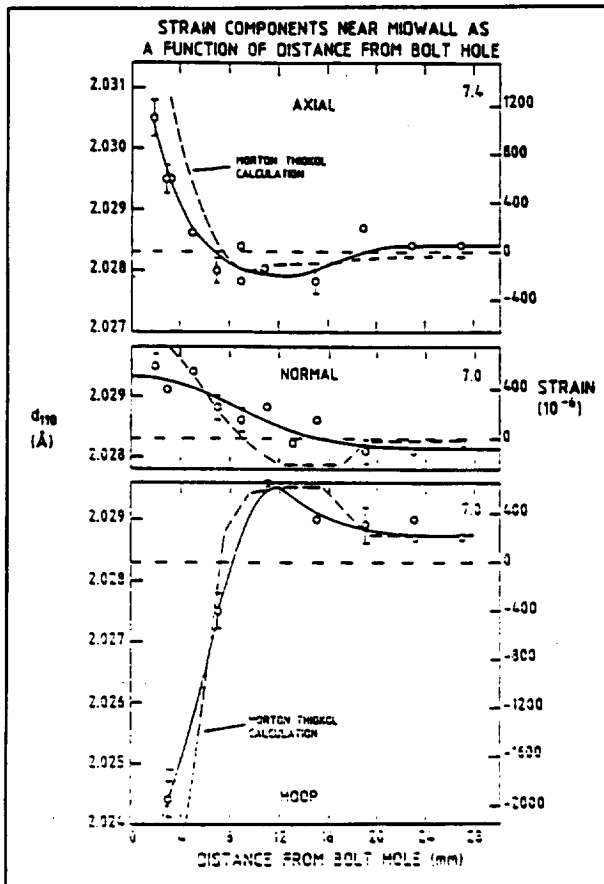


Figure 5 Comparison of Neutron Beam Measured and Analytical Residual Strains

The neutron beam diffraction process was found to be very effective in measuring in-depth residual strains (stresses). Its major limitation is in the size of parts that can be accommodated by the measuring equipment. It is impossible to use this method in a nondestructive mode on flight hardware because the test pieces must be relatively small and must be excised from the case.

The x-ray diffraction process was found to be effective for surface measurements of residual strains (stresses) in a nondestructive mode, and it is portable so it can be used on full scale hardware. The test equipment is relatively bulky so the process cannot be used in the nondestructive mode in tight quarters such as the inner surfaces of the clevis, dome y-joint/skirt regions, or in holes. It becomes a destructive process when measurement of subsurface conditions are required because material removal is necessary.

Direct comparisons of the readings obtained by the two methods were not possible because no common points were measured. A crudely extrapolated comparison showed they gave similar trends for the hoop and axial stresses on the region aft of the pin holes that are 4" away from an alignment slot.

### 3.3 RECOMMENDATIONS

Because of the positive effect from the shallow compressive residual stresses developed from glass bead cleaning operations, it is recommended that local glass beading be repeated, wherever feasible, on regions where it is necessary to do local rework that is likely to disturb the surface residual stresses (e.g. blending) after the final cleaning.

Nondestructive Test Evaluations for crack detection must be capable of reliable surface crack detection with surface length of 0.200 in. (depths of 0.100 in.) or greater. This size is driven by the magnitude of the subsurface tensile residual stresses found in the tang at a depth of about 0.100 in. These inspections must be conducted with every case segment refurbishment just prior to release for motor manufacture. Any positive crack indication should mean loss of flight worthiness.

The levels of these residual stresses in combination with long term fixturing, handling, and assembly stresses should be evaluated with the upper bound exposure times to estimate the stress corrosion potential for pre-flight activities.

This effort did not deal with the upper bound values of recovery damage that could be accepted for reuse. Additional attention should be focused on the post water impact period of exposure to sea water with more representative water impact damage than was produced in the hardware evaluated here. There should also be a study of the changes in residual stresses as well as the altered assembly stresses that are released at post flight segment disassembly.

#### 4. INSTRUMENTATION

The only instrumentation required was supplied by the testing vendors as part of the diffraction system used to measure the residual stresses. The x-ray diffraction equipment conformed to MIL-STD-45662.

#### 5. PHOTOGRAPHY

Still photographs were taken of the seven test specimens at various stages of the x-ray diffraction measurement process. These are presented in Appendix A. A photograph of the neutron diffraction test set up with the specimen in place is included in the vendor report (Appendix B).

### 6. RESULTS AND DISCUSSION

#### 6.1 TEST DESCRIPTION

The test was conducted in accordance with the test plan, ETP-0403 (reference 1, ECS-2078). There was one deviation from this plan that is discussed in Section 7.1.1. It was the addition of test measurements using the neutron beam diffraction process.

Surface residual stress measurements using beam diffraction processes are nondestructive for steel. When subsurface evaluations are sought using the x-ray diffraction method, it is necessary to locally remove material between measurements. This is because the low power x-ray beam can penetrate only a few microns below the surface. The material removal makes the process destructive. Both methods require dismantling portions of the details to get readings in constricted areas (e.g. inside the clevis slot).

The x-ray diffraction measurements were taken at the full set of test points at the undisturbed surface and after a small amount of material was removed. Some dismantling of the clevis pieces was needed to get access to the points inside the clevis. This was done after the readings were taken on the external points.

Two pieces of case membrane were used as material comparison standards in measurements of grain dislocation density. One piece was supplied in the "as cut" condition, and the other received a laboratory stress relief heat treatment to remove any residual stresses.

X-ray diffraction measurements were taken before and after local material removal by electropolishing (etching). The depth of the material removed at each evaluation point was intended to be about 5 mils. This depth was selected to investigate the residual stresses that could exist at the depth of a surface crack that may not be detected. Table 1 lists the sequence of steps used in the test measurements at the points shown in Figures 6-8.

Table 1 Test Evaluation Sequence For X-Ray Diffraction

STEP	TASK DESCRIPTION
1	Measure dislocation densities in the two pieces of reference material.
2	Layout measurement locations on the seven test pieces, and photograph the test pieces to record measurement locations.
3	Measure residual strains at prescribed locations. Measure dislocation densities at prescribed locations.
4	Locally electropolish the test pieces to remove approximately 0.005 in. (5 mils) of material from the surface of the pieces at the measurement locations.
5	Restore the layout of the measurement locations.
6	Re-measure the residual stresses at each prescribed location. Re-measure the dislocation density at each point.

The actual material removal for the second set of readings were not sufficiently controllable to guarantee 5 mils depth. The depths obtained were closer to 10 mils.

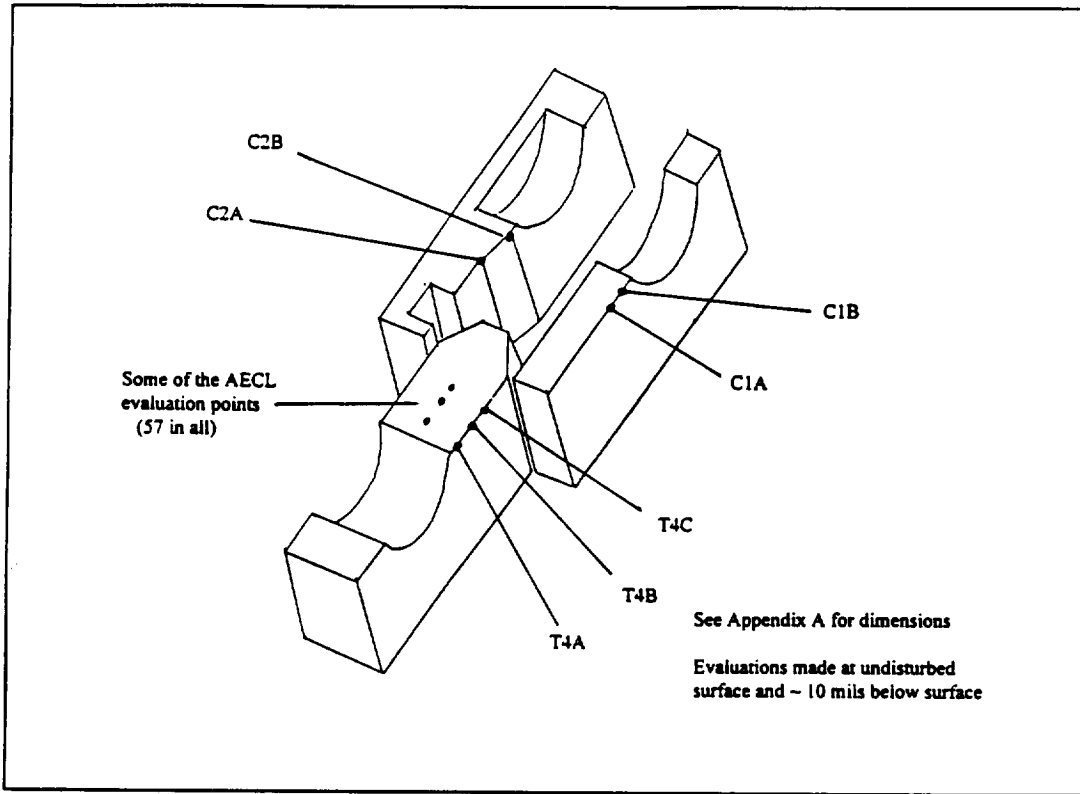


Figure 6 Tang and Clevis Measurement Locations

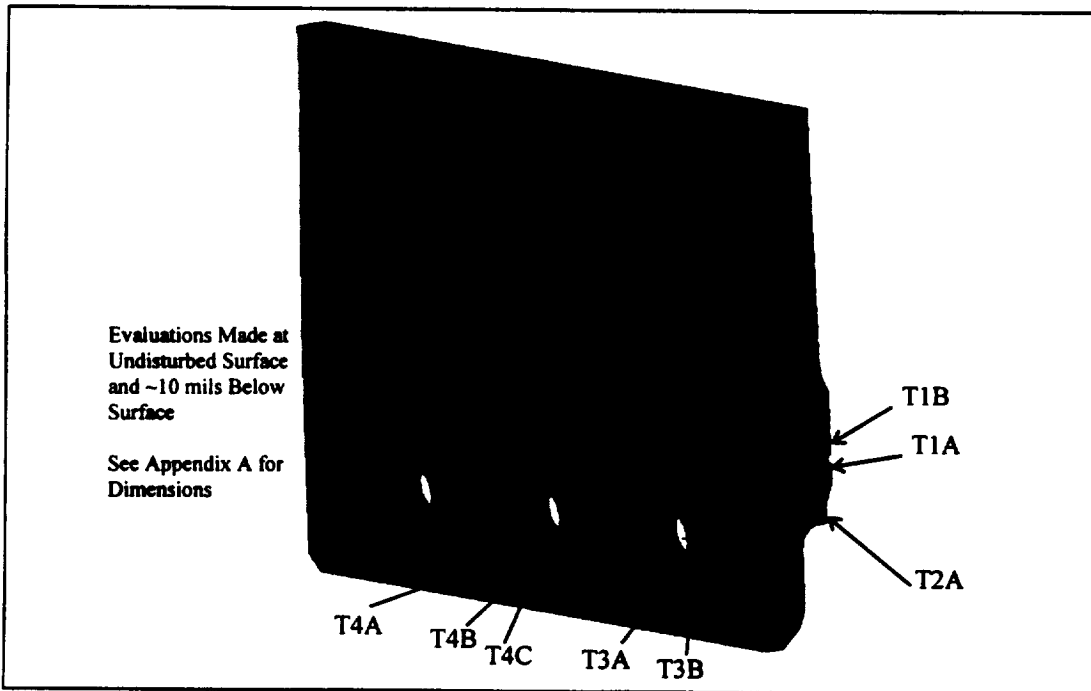


Figure 7 X-ray Diffraction Evaluation Points for Tang Specimens

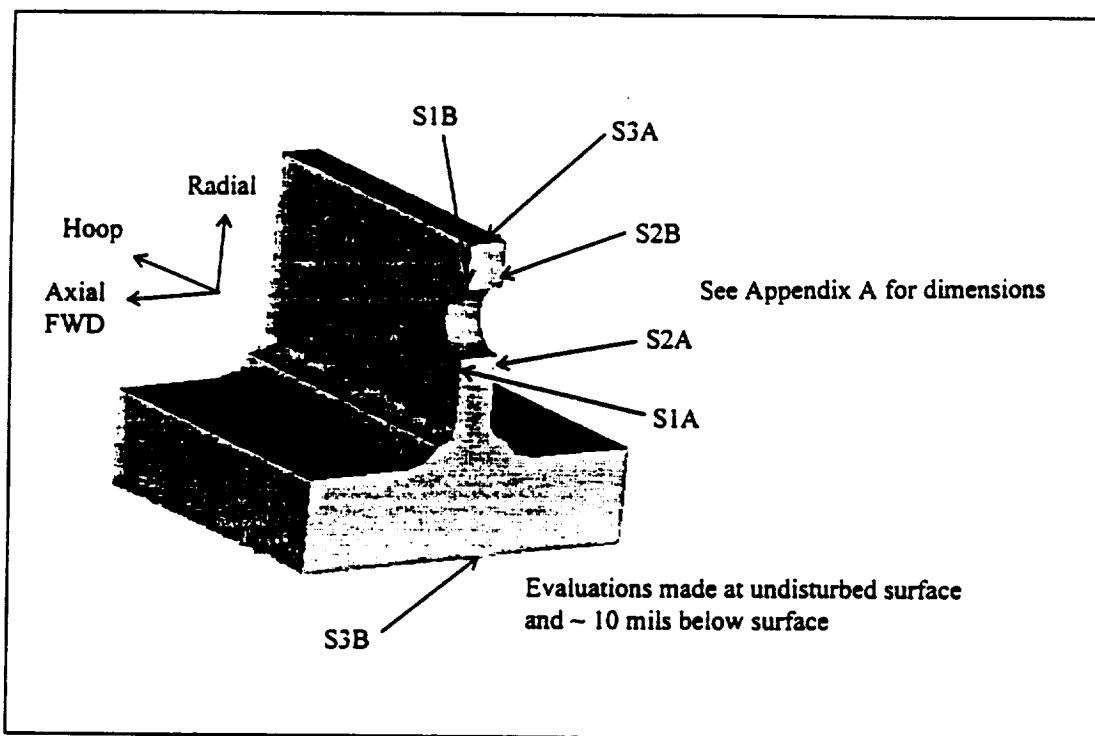


Figure 8 X-ray Diffraction Evaluation Points For Stiffener Stubs

Following the x-ray diffraction work on the Tang-000 specimen, the piece was sent to the second test vendor to be evaluated using the neutron beam diffraction method. The region forward of the second pin hole from the slot (4") was investigated out to the tip of the tang (the hole on the opposite side of the slot that was investigated by x-ray diffraction). The neutron beam was able to penetrate the entire thickness with no material removal. The stress relieved calibration sample cut from the case was also evaluated. Table 2 outlines the test procedures.

Table 2 Test Evaluation Sequence For Neutron Beam Diffraction

STEP	TASK DESCRIPTION
1	Trim the test specimen to fit into the test fixture with the evaluation zone positioned for the range of movement needed to span the evaluation zone.
2	Mount the test specimen in the measurement fixture and establish the geometric reference points. The reference points used were the tang outside and inside diameters at the midplane of the pin hole, and the outboard (aft) edge of the pin hole at the midplane. Check the range of motion for the evaluation zone.
3	Program the x-y drive controls to select each of the evaluation points and check the positioning.
4	Energize the measurement system and set the orientation. Evaluate the beam diffraction while focused on each of the pre-programmed evaluation sites. Take the average of three readings at each point and record it.
5	Repeat step 4 for each beam orientation.
6	Repeat steps 1 through 5 for each specimen.
7	Review the data for consistency and convert beam diffraction readings to strains.

## 6.2 DESCRIPTION AND JUSTIFICATION OF DEVIATIONS FROM THE TEST PLAN

After the test plan was written and released it was decided to involve two testing vendors to compare the effectiveness of two testing methods. The primary vendor selected was Technology for Energy Corporation (TEC) in Knoxville, TN. The measurement method they used was x-ray diffraction. The second vendor selected was Atomic Energy of Canada, Ltd. (AECL) at the Chalk River National Laboratories in Chalk River, Ontario, Canada. The measurement method they used was neutron beam diffraction. A description of the x-ray diffraction method is given in Appendix A. The neutron beam diffraction method is described in Appendix B.

TEC conducted the test as described in the test plan. When TEC had finished the Tang-000 testing, it was sent to AECL to measure the residual stresses in the volume forward of a generic pin hole. This report presents the comparison of the results.

**NOTE:** The test plan (reference 1) gives two incorrect designations for this segment. The title page refers to 1U50716-06 S/N L023 (*a lightweight attach segment*). The test component description in Section 2.0 refers to 1U50715 S/N L032 (*a lightweight stiffener segment flown on flight 21A*). The DM-8 motor used the lightweight attach segment S/N L032 and the lightweight stiffener segment S/N L023. The correct designation of the test item is lightweight stiffener segment S/N L023 flown on flights 14A and 24A. The similarity of the segment numbering gave opportunity for the confusion.

## 6.3 TEST PREPARATIONS

The test preparations consisted of identifying the case segment to be evaluated and selecting the pieces to be excised. The test specimens were extracted and prepared by Thiokol and then shipped to the test vendors' facilities. The locations for the test measurements were marked on each test piece by the primary vendor (TEC).

## 6.4 TEST FACILITIES

Two types of testing were employed in measuring residual stresses. They were x-ray diffraction and neutron beam diffraction. The x-ray diffraction tests were conducted at the TEC facilities in Knoxville, TN. The neutron beam diffraction tests were conducted by AECL in the Chalk River National Laboratories in Chalk River, Ontario, Canada. The test vendors provided the equipment needed to conduct the tests.

## 6.5 TEST PROCEDURES AND INSTRUMENTATION

The test procedures were those appropriate for beam diffraction measurements of residual strains in steel. This included the beam generator (x-ray tube or nuclear reactor) and the equipment to measure the diffraction angle. The x-ray diffraction equipment was augmented with equipment and material to do local material removal by the electropolishing process. All of this equipment and the depth measuring devices were provided and certified by the testing vendor.

Electropolishing was used to remove material from the test points in the x-ray diffraction method because the x-ray is only capable of penetrating the steel a few microns. Electropolishing minimizes the disruptions to the residual stress field by not inducing thermal/mechanical forces during material removal.

The neutron beam method is capable of measuring in-depth strains so material removal was not needed. No additional instrumentation was required in either process.

Both procedures are based on electromagnetic wave diffraction at the grain boundaries where the beam is focused and utilize Bragg's Law. They use the wave diffraction angle to estimate the strains present in the material at the focus point. Having the strain estimates at various directions at a point, they compute the stresses using Hooke's Law for the material. Qualitative estimates of the dislocation density are obtained from the full-width half-maximum (FWHM). This is the diffraction peak width at half of its maximum intensity. The relative dislocation density is a qualitative measure of the intensity of the dislocations in the grain lattice structure of the material that is a signal of local plastic deformation. Increasing dislocation density suggests higher amounts of plastic deformation have occurred. (See the Recommended Reading list in Appendix A for more detail.)

## 6.6 SIGNIFICANT FINDINGS

### 6.6.1 GENERAL OBSERVATIONS

The testing provided generally consistent and reasonable data. No "bad" data readings were obtained because of the interactive nature of the data collection process. A few of the test data points were re-evaluated and showed the intrinsic variation. Each data point measurement provided an estimate for the residual stress and an uncertainty level. Only in the low values of residual stress were the uncertainty levels near the magnitude of the measured value. Uncertainty levels ranged between 2 and 20 ksi with the higher uncertainty values corresponding to the higher residual stress magnitudes. In general the residual stresses were found to be low with the exception of the surface compressive stresses that are attributed to the shot-peening effect of the glass bead blast cleaning.

Although the test measurements were interpreted as strains that are readily converted to stresses, the relatively high uncertainty levels for low readings interfered with the computation of principal stresses from the x-ray diffraction data. This was because the measurements in each direction at a point are essentially independent and are not required to be self-consistent by the measurement process. This shows up in differences between the results using the 0,45,90 measurements compared to the 0,135,90 measurements. The readings obtained by repeating the evaluations at the "same" point showed more variations than the error term. This was assumed to be due to the difficulty of assuring the beam is focused on the same spot and the inherent level of variability of the metal grain structure.

Neutron beam measurements of strain dealt only with three orthogonal directions at points that were on a plane of geometric symmetry. Since no oblique directions were evaluated, it was not possible to demonstrate that this was also a plane of symmetry for the strain. The evaluation of stresses was further complicated because independent readings were taken in the axial, radial, and hoop directions, and they were not always taken at the same location in all three directions.

An overview of the results are given in Figures 3 and 4. Detailed data listings of the readings can be obtained from the two Appendices. Appendix A gives the information for the x-ray diffraction measurements, and Appendix B gives the information for the neutron beam measurements. The x-ray diffraction residual strain measurements were converted to stresses by the vendor.

The neutron beam diffraction measurements were reported as strains. The strain measurements were taken at three orthogonal directions (axial, radial, and hoop) with no readings at intermediate angles. This means there is no way to estimate the shear strains. A quick look at the x-ray diffraction data shows that there are possibly significant shear strains away from symmetry lines (e.g. around the pin holes that are next to the alignment slots or on the stiffener stub), and it would be inappropriate to assume they were zero in some cases. There is enough uncertainty for the points located where there is geometric symmetry (e.g. point locations T4A, T4B, and T4C) that it cannot be claimed with certainty there is strain symmetry. The shear stress values obtained in the geometric symmetry conditions are small, however, and may be resulting from measurement noise. It is often not possible to distinguish between measurement uncertainty (noise) and actual strain values where the strains are small and the noise is of the same order.

The only points evaluated by the neutron beam method were on the geometric symmetry plane extending aft from the center of the pin hole on one of the 4' pin holes on Tang-000. (Note: x-ray diffraction measurements were taken on the other 4' pin hole on the opposite side of the alignment slot on this specimen.) Stress estimates for the neutron beam measurements have been computed as part of the test data evaluations using the isotropic form of Hooke's Law. Assuming shear strains are small on this geometric symmetry plane allows these to be treated as principal stresses.

Photographs of the test specimens at various stages of the x-ray diffraction testing are shown Appendix A. Appendix B has a photograph of the neutron beam diffraction test facility.

### 6.6.2 TEST DATA EVALUATIONS

The x-ray diffraction evaluations were successful in showing the surface residual stresses and observing the generally rapid decline of those residual stresses with depth into the material. All surface evaluations showed large biaxial compressive residual stresses. They were in the range of -100 to -150 ksi with uncertainty values under 30 ksi. Typical uncertainty

values were around 10 ksi. No tensile surface residual stresses were found at the surface across all points evaluated on all of the specimens.

Subsurface evaluations at depths of up to 10 mils showed mixed compression and tension values. The compression values were substantially decreased from the surface values. The largest magnitudes of the compression residual stresses were below 90 ksi with most of them below 20 ksi. The tensile residual stresses found at depths up to 10 mils ranged in magnitude of 2 ksi to about 29 ksi. Uncertainty values for the subsurface measurements were generally under 10 ksi, with typical values under 5 ksi.

The residuals measured by x-ray diffraction tell similar stories on the tang (pin holes, alignment slot, and leak check port), the clevis legs, and the stiffener stubs. In general, there is a biaxial compressive residual on all surfaces in the order of -130 ksi. These stresses drop off rapidly with depth into the part. At 10 mils depth there are mixed compressive and small tensile residual stresses that are consistent with local yielding from proof and flight. No particular pattern could be found on the stiffener stub holes. Noting the relatively low water impact effects encountered in the two flights, it is to be expected that there would be irregular variations from hole to hole on the stiffener stubs. Detailed residual stress data are included in Appendix A.

The maximum tensile residual stresses found at the 10 mil depth were in the outboard surface of the tang between the pin hole and the tip of the tang. The highest readings were at the T4C evaluation points. These were between the edge of the pin hole and the tang tip on the second hole from the alignment slot (4'), about 0.56 in. aft of the edge of the pin hole. The peak values for the Tang-000, Tang-118, and Tang-240 test pieces were  $+16.4 \pm 5.2$ ,  $+27.6 \pm 4.2$ , and  $+28.1 \pm 2.7$  ksi, respectively. A repeat of the reading on the Tang-240 specimen gave  $+22.7 \pm 3.6$  ksi. These were all for the 0° measurement direction (hoop) at point T4C. Using the measurements at the 0°, 135°, and 90° directions for the largest Tang-240 reading suggests the 0° direction is a principal direction. Using the 0°, 45°, and 90° directions suggests there is a shear stress of about 2 ksi. As noted above, this may simply be due to measurement uncertainty. In either case, the maximum principal stress of about 30 ksi is indicated by the first reading on Tang-240. This estimate includes measurement uncertainty and the possibility of some small shear strains. The average of the two readings on Tang-240 is 25.4 ksi, which would suggest a maximum principal stress around 28 ksi.

The holes next to the alignment slots are known to have the highest pin hole loading because they must support both the axial bearing loading and a component of hoop loading to bridge across the missing pin at the alignment slot. This loading must be distributed between the tang and the clevis legs across the slot through the pins adjacent to the slots. This load redistribution carries on to the 4' and 6' holes in much smaller proportions compared to the 2' holes. This could account for some lack of strain symmetry at the 4' holes. The effect is probably small enough at the 4' (and even smaller at the 6') holes that it is masked by the measurement noise level.

The in-depth residual strains measured by the neutron beam diffraction method were successfully obtained for a large number of points between the edge of the pin hole and the tip of the tang at the second pin hole from the alignment slot (4'). A pattern of tensile and compressive strains were obtained that were compared to the analysis predictions for a generic pin hole after unloading from a proof test pressure cycle. Part of the comparison plots are presented in Figure 5, and the complete set is presented in the vendor report in Appendix B. The measured results showed trends in general agreement with the analysis results. The AECL estimate of the upper bound on the strain measurement error was  $\pm 310 \times 10^{-6}$  in/in. This is equivalent to about  $\pm 9$  ksi. This is a conservative upper bound (95% confidence level) that places the error bounds of both methods at about the same level. The AECL data did not give a specific error bound for each reading.

Comparisons of the data from the two vendors must recognize that they used different conventions for the measurement directions. TEC data (x-ray diffraction) used the hoop direction as the first evaluation direction (0°). The direction for the second reading depended of the location of the measurement. The determiner was the normal direction at the surface point. Readings could only be taken in the surface plane of the test piece. The normal stresses on a free surface are zero. On the tang and clevis points the axial direction was at the 90° orientation. On the stiffener stub, regions 1 and 2 had the radial direction corresponding to the 90° direction. In region 3 it was the axial direction. The AECL data (neutron beam diffraction) assumed the evaluation order was axial, radial (normal), and hoop at all points. Since these were all internal points, the normal stresses were not zero.

No direct comparisons between the two measurement methods were possible because they had no common points evaluated. The x-ray diffraction work focused on surface and near surface residuals, the neutron beam diffraction work emphasized in-depth measurements. An approximate comparison between the two methods was done on the outboard surface of the tang near the location of evaluation points T4A, T4B, and T4C for all three tang specimens for the x-ray beam and the points through the tang thickness at about the same positions relative to the pin hole measured by the neutron beam. As noted above, tensile residual stresses were found at a depth of about 10 mils. The neutron beam evaluations made nearest the surface were at a depth of 1 mm (~39 mils). Looking at the trend of the stresses obtained through the tang thickness at points near the x-ray measurement points, an extrapolation from the 39 mils depth to the 10 mils was used as a basis for comparison. Table 3 shows the results. These values indicate very similar patterns measured by the two methods. The trends of the average of the TEC tang data and the crudely extrapolated AECL data are shown in Figure 9.

Table 3- Comparison Of Key Residual Stress Values

X-RAY			NEUTRON BEAM					
POSITION			STRESS - KSI		STRESS - KSI		POSITION	
ID	AXIAL IN.	DEPTH IN.	HOOP	AXIAL	AXIAL	HOOP	AXIAL MM/IN.	DEPTH MM/IN.
T4A 000	0.088	-0.01	-61.9	-13.0	18.2	-36.4	3 0.118	1 0.039
T4B 000	0.305	-0.01	8.3	-15.2	-0.8	-58.6	3 0.118	7.+ 0.291
T4C 000	0.545	-0.01	16.4	-1.5	16.1	-60.2	3 0.118	11.+ 0.448
T4A 118	0.075	-0.01	-40.6	-9.8	-12.6	-8.1	7 0.276	1 0.039
T4B 118	0.320	-0.01	-24.9	-43.4	-7.9	-13.4	7 0.276	7.+ 0.291
T4C 118	0.565	-0.01	27.6	-22.3	4.1	-4.0	7 0.276	11.+ 0.448
T4A 240	0.105	-0.01	-72.0	-14.7	-7.8	8.1	11 0.433	1 0.039
T4B 240	0.324	-0.01	-21.1	-40.2	7.8	26.0	11 0.433	7.+ 0.291
T4C 240	0.555	-0.01	22.7	-6.1	-10.1	10.1	11 0.433	11.+ 0.448
T4A ave			-58.2	-12.5	-0.8	-0.8	15 0.591	1 0.039
T4B ave			-12.6	-32.9	-1.9	11.9	15 0.591	7.+ 0.291
T4C ave			22.2	-9.8	1.4	16.1	15 0.591	11.+ 0.448

Residual measurements taken 45° off-axis at the 2" holes in the tang (locations T3A and T3B) showed surface and subsurface values similar to the T4 measurements. There was a general biaxial compressive stress on the surface which dropped off quickly below the surface. The subsurface residual stresses found on the 2" holes (next to the alignment slot) were somewhat less than those found at the 4" holes. There were too few measurements taken to establish the pattern of residual stress around the hole to determine at what angle the highest residuals occurred.

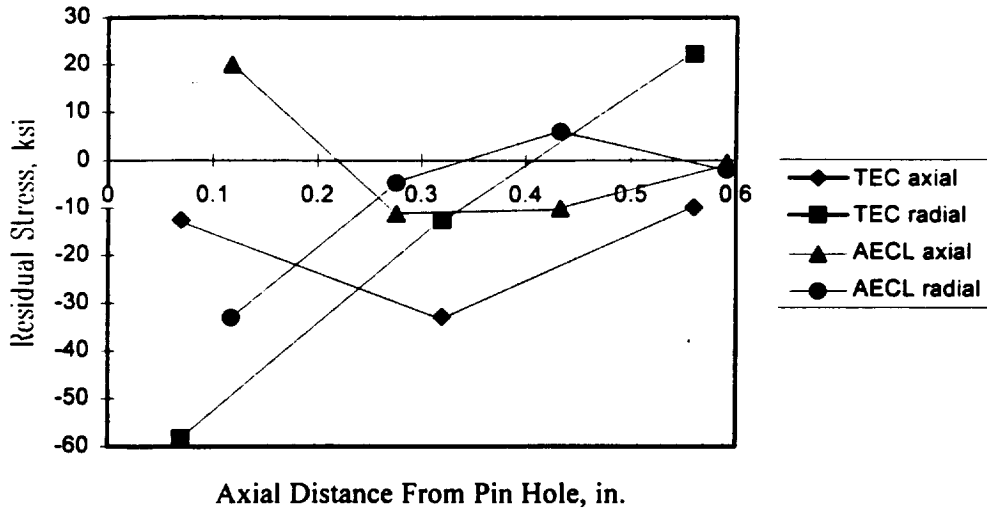


Figure 9 Comparative Measurement Trends

Evaluations of the dislocation density readings obtained by the x-ray diffraction method showed small variations from the case membrane control samples, with the stress relieved specimen showing a slightly lower reading. This was taken to be an indication that even though there were some plastic deformations, the amount of deformation was relatively small. Dislocation density readings for the case wall samples are presented in Table 4. Figure 9 of Appendix B shows a general trend of the dislocation density that decreases with the axial distance from the tang pin hole.

Table 4 Typical Dislocation Density Readings By X-Ray Diffraction

	RESIDUAL STRESS KSI	DISLOCATION DENSITY INDICATOR*
CASE SAMPLE A (no stress relief)	-50.2 ± 5.4	2.3
CASE SAMPLE B (stress relieved)	-14.7 ± 3.4	1.9

### 6.6.3 INFORMATION FROM STRESS ANALYSES

An overview of the nonlinear stress analysis results for the case factory joint is given in Figures 10-13. They are based on computer runs reported in Reference 4. These are the analyses used in the results comparisons reported in Appendix B. The analysis of the factory joint was done for a generic pin location subjected to a pressure of 1070 psig. This is significantly higher than the maximum expected operating pressure (MEOP). The pressures imposed in flight and static firing involving this stiffener segment were considerably lower than MEOP at the forward case field joint. This is because the gas dynamics of motor operation results in a pressure drop in the aft regions of the motor and MEOP is a statistically conservative number. The proof pressure, on the other hand, is selected to be higher than case MEOP. The peak proof pressure at the time Lightweight Stiffener SN L23 was proof tested and used was 1070 psig. The proof pressure currently imposed on the lightweight stiffener proof tests is 1055+30,-0 psig. Figure 14 gives a qualitative view of the yield zones developed around the pin holes, leak check port, and alignment slot from successive pressurizations. The yielding effects around the pin holes adjacent to the alignment slots (2' holes) are not shown, but they have slightly larger yield zones that are not aligned with the axial direction, but are skewed toward the alignment slot. Figure 15 shows the finite element model use to study the behavior of alignment slot region [5].

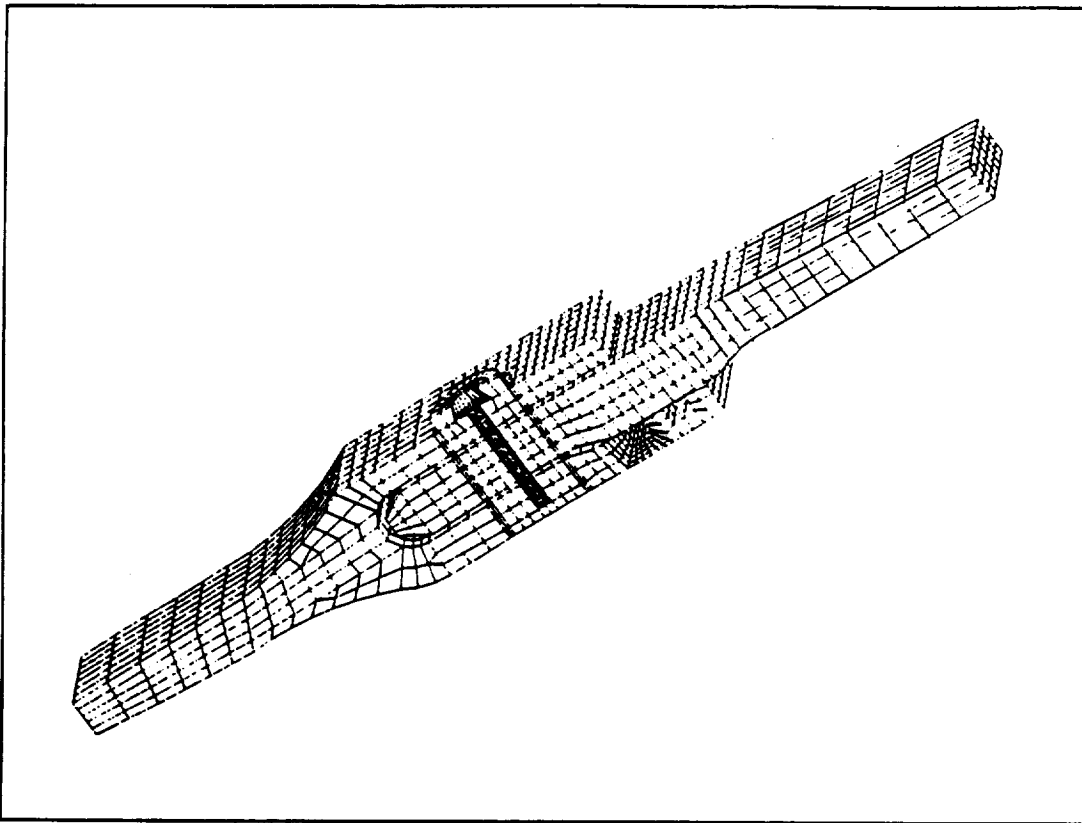


Figure 10 Finite Element Model of Typical Factory Joint Pin Locations

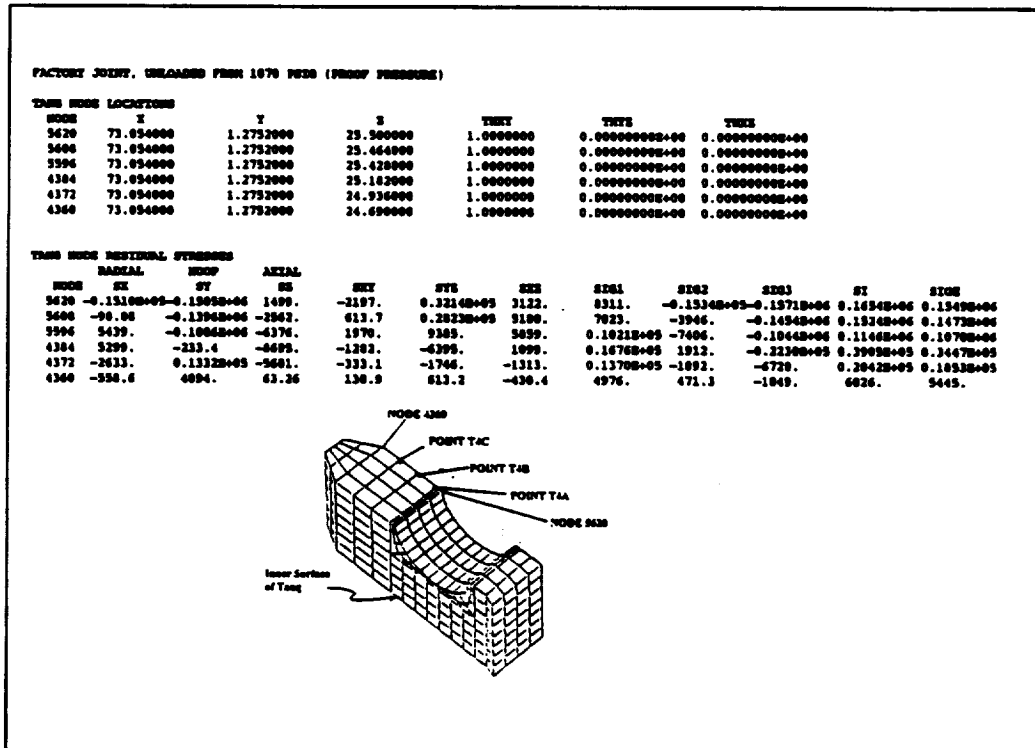


Figure 11 FE Analysis Results for Tang Nodes

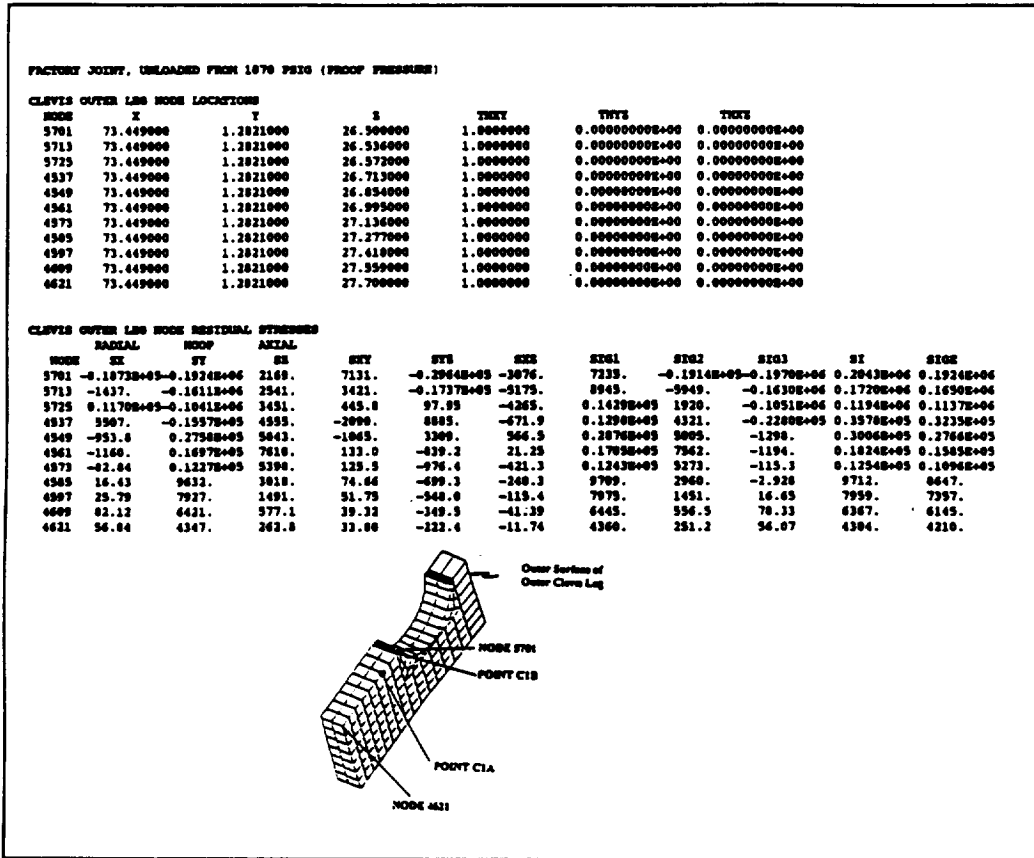


Figure 12 FE Analysis Results for Outer Clevis Leg Nodes

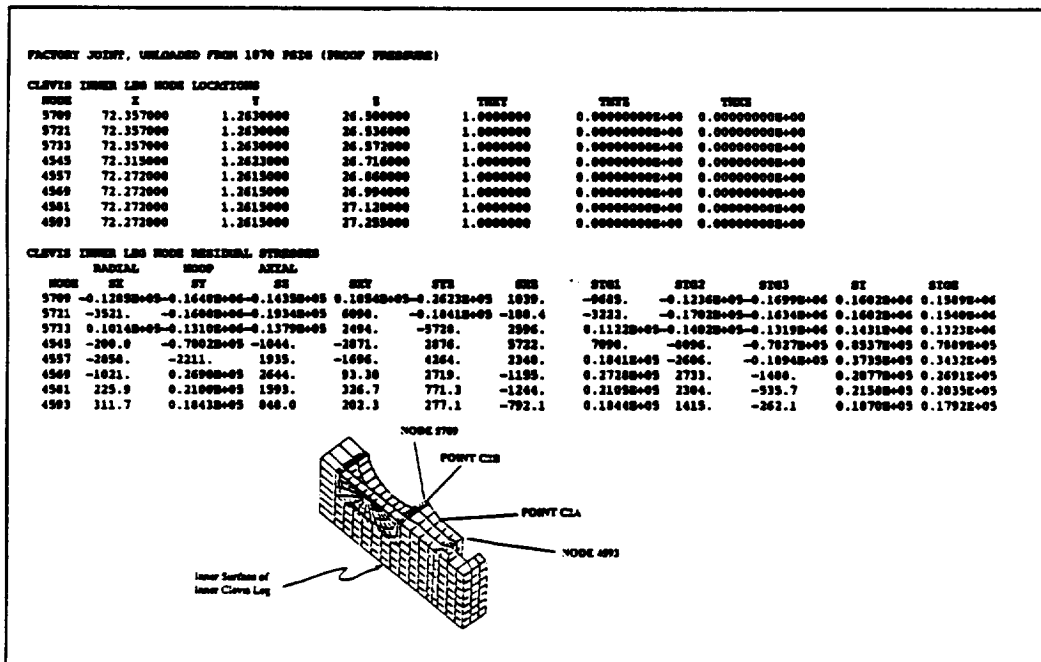


Figure 13 FE Analysis Results for Inner Clevis Leg Nodes

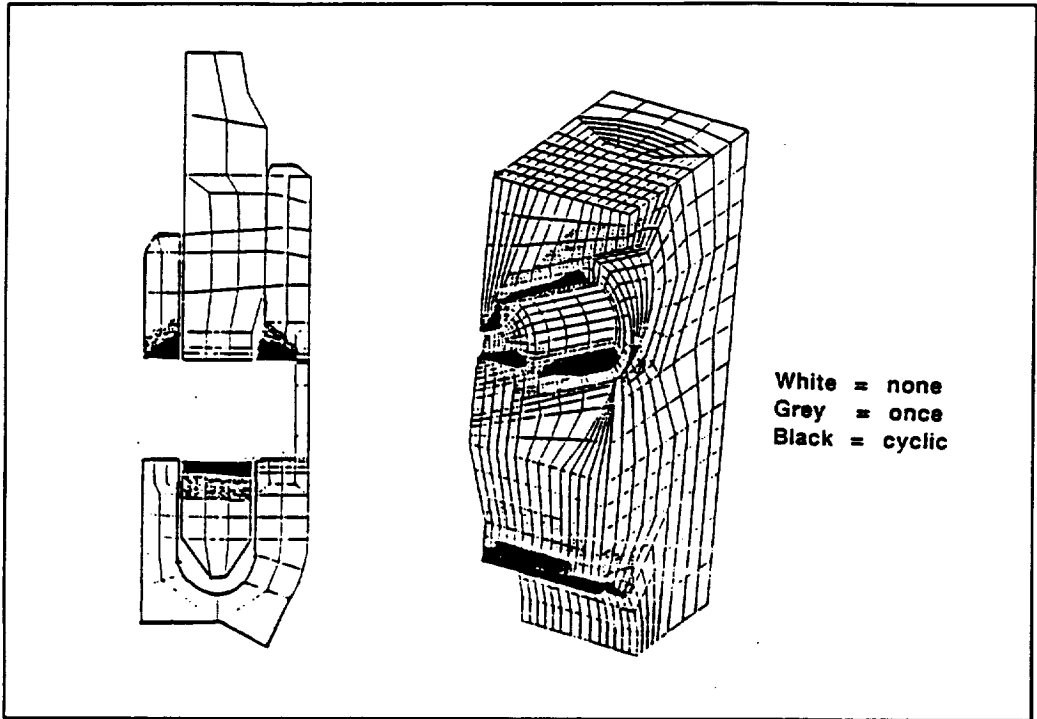


Figure 14 Yield Zones for a Typical Pin Hole and an Alignment Slot

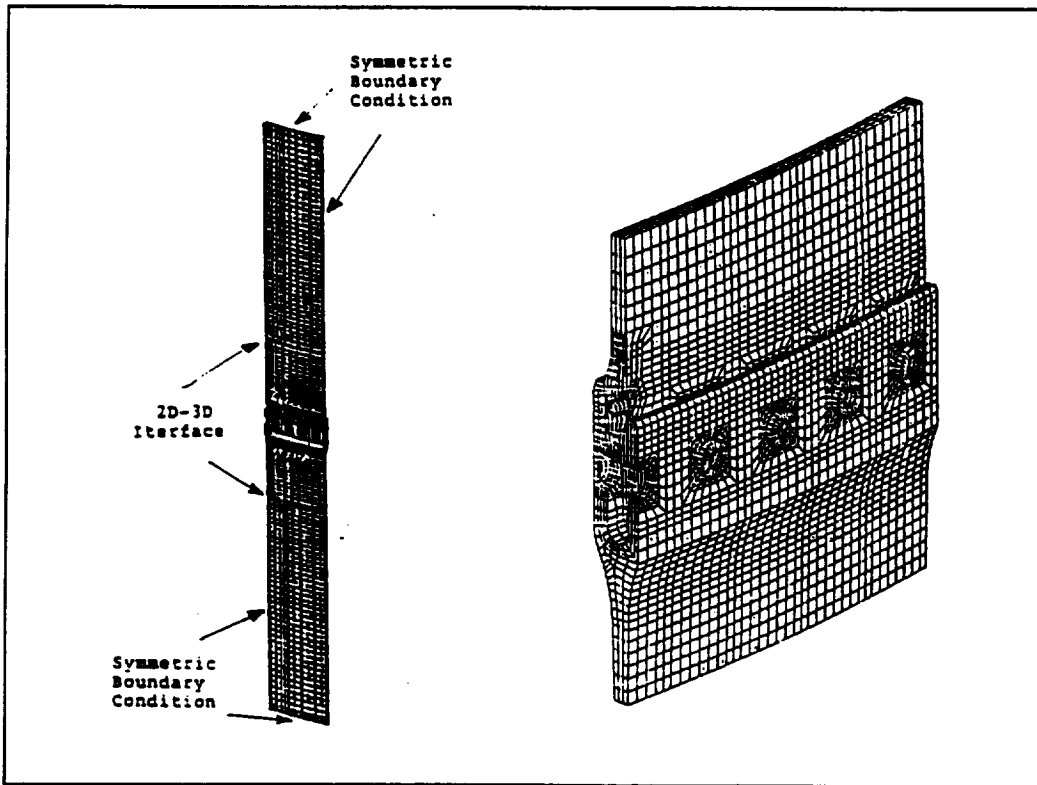


Figure 15 Finite Element Model of the Alignment Slot Zone

## 7. APPLICABLE DOCUMENTS

<u>Number</u>	<u>Title</u>
1U50715	Stiffener Segment, Lightweight Case
STW4-2606	Steel, Alloy, High Strength, D6AC (for Space Shuttle SRM Case Components).
STW7-2608	Heat Treatment, Alloy Steel, D6AC (for Space Shuttle SRM Case Components).
MIL-STD-45662	Calibrate System Requirements.
---	Electropolishing Machine Instruction Book

## 8. REFERENCES

1. ETP-0403, MEASUREMENT OF RESIDUAL STRESSES AFTER HYDROPROOF AND FLIGHT IN RSRM CASE SEGMENT 1U50716-067 SERIAL NO. L023. (*should be* 1U50715), August 1988
2. ETP-0221 Rev A, EVALUATION OF OVERHEATED AFT CASE SEGMENT FROM DM-8, Sept. 1988
3. TWR-19326, STIFFENER SEGMENT DAMAGE CAUSED BY WATER IMPACT LOADS, July 1991
4. TWR-17118 Rev A, RSRM CASE STRUCTURAL ANALYSIS SUMMARY, April 1988
5. TWR-65866, FACTORY JOINT ALIGNMENT SLOT/LEAK CHECK PORT ANALYSES (4 volumes), Feb. 1994

APPENDIX A - VENDOR REPORT FOR X-RAY DIFFRACTION MEASUREMENTS

The attached report and data summary pages were submitted by Technology for Energy Corporation (TEC) at the completion of the residual stress (strain) evaluations made on the seven pieces excised from the heat damaged forward stiffener segment from the DM-8 static firing. These pieces were selected from portions of the case segment where there was no evidence of heat damage. This test article is considered to be representative of a case stiffener segment that has experienced three proof tests and negligible flight/recovery damage.

REVISION \_\_\_\_\_



**TECHNOLOGY for ENERGY CORPORATION**

**November 29, 1988**

**In reply, refer to:  
1188-EBSP-1705-32946**

**Morton Thiokol, Inc.  
Utah Tactical Division Building X-20  
1080 North Main Street  
Brigham City, Utah 84302**

**Attention: Dr. Dan Sutherland**

**Subject: Morton Thiokol, Inc. Purchase Order No. 9MN026  
Transmittal of R-88-049**

**Enclosure: TEC Report R-88-049**

**Dear Dr. Sutherland:**

**In accordance with the above subject contract, Technology for Energy Corporation (TEC) transmits herewith the data as required in the subject purchase order.**

**If additional information and/or clarification is required, please advise.**

**Sincerely,**

**TECHNOLOGY FOR ENERGY CORPORATION**

*Annette Lewin*  
*for*

**Beth Pardue  
Project Manager**

**EBP:bsh**

**cc: R.D. Wright, TEC  
K.T. Woods, TEC  
Morton Thiokol, Inc. Purchasing Department (Letter only)**



**MORTON THIOKOL, INC.**  
**RESIDUAL STRESS SUMMARY**

**TEC Report R-88-049**

**TEC PON 9MN026**  
**VOLUME 1 of 3**

**Prepared for:**

**Morton Thiokol, Inc.**  
**Utah Tactical Division Building X-20**  
**1080 North Main Street**  
**Brigham City, Utah 84302**

**Submitted by:**

**Technology for Energy Corporation**  
**One Energy Center, Lexington Drive**  
**P. O. Box 22996**  
**Knoxville, Tennessee 37933-0996**  
**(615)966-5856**  
**Telex: 810-570-1770**

**November 29, 1988**



**MORTON THIOKOL**  
**Residual Stress Summary**  
**RSRM Case Segment**

Surface and subsurface residual stress measurements were made on seven pieces of D-6 ac solid rocket booster casing sections. These sections were identified as follows:

Clevis 118  
Clevis 240  
Tang 000  
Tang 118  
Tang 240  
Forward Stiffener Stub 166  
Aft Stiffener Stub 166

Photographs and drawings of measurement locations are attached.

The testing followed Morton Thiokol Document ETP-0403, "Measurement of Residual Stresses After Hydroproof and Flight Loadings in RSRM Case Segment 1U50716-06 Serial No. L023."

Surface preparation consisted solely of removing paint on the painted sections. Paint was removed without mechanical abrasion, which would alter the surface residual stress. The paint remover, KS-3 Paint Remover\*, was applied to the surface until the paint loosened from the surface. The paint was then removed by wiping with a soft cloth. Alcohol was wiped over the surface to remove any residual KS-3.

The measurement locations were marked and photographed. Surface measurements were made at all accessible locations. After these measurements were made, sections of the stiffener stubs were removed to allow access to the S1 and S2 locations and sections of the clevises were removed to allow access to the C2 locations. This sectioning was done by EDM milling. Upon completion of the surface measurements, 10 mils of material were removed by electropolishing. Electropolishing

\* Contains Methylene Chloride, Isopropanol, Ethylene Glycol Monobutyl Ether, and less than 4% Methanol.

solutions used were 91% Butyl Cellulose, 9% Perchloric Acid or 50% Nitric Acid, 50% Water. These solutions were rinsed from the surfaces with water immediately after electropolishing. Alcohol was used as a final rinse. The measurement locations were again marked and subsurface measurements made.

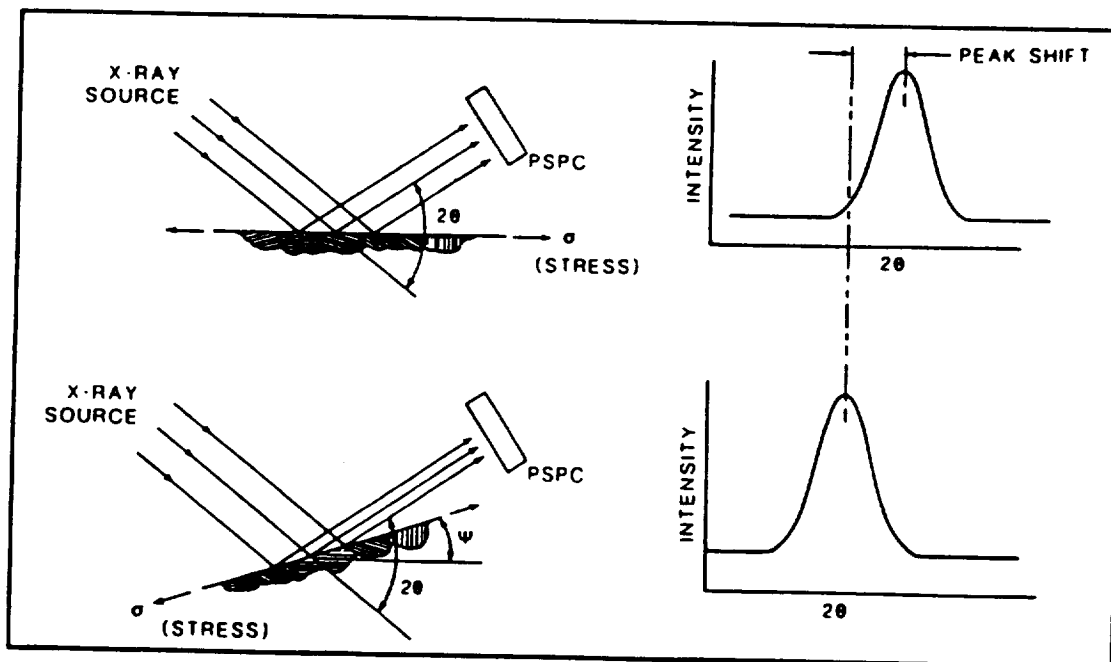
### Measurement of Stress by X-Ray Diffraction

Of the various techniques for measuring residual stresses, the x-ray diffraction method is the most developed and widely used. It is the only technique that is applicable to all crystalline materials, that can measure the absolute stress in the component without the need for a measurement of the sample in the unstressed state, and that is capable of making measurements in a localized region as small as 1mm in diameter. Because the penetration of the long wavelength X-rays is only a few tens of microns, the Model 1600 Stress Analysis Systems are used to measure surface stresses.

Stresses are determined by measuring the strain in the atomic lattice and by relating the strains to stresses through the elasticity theory. An incident beam of essentially monochromatic radiation of wavelength  $\lambda$  is diffracted at an angle  $2\theta$  which obeys Bragg's Law

$$n\lambda = 2d \sin\theta,$$

where  $n$  is the order of the reflection and  $d$  is the atomic spacing of the selected crystalline lattice planes. The sample surface is at an angle  $\theta$  to the incident beam, and only grains with atomic planes parallel to the surface diffract. From the  $2\theta$  position of the peak, the atomic spacing of the diffracting planes may be determined.



When the sample is tilted at an angle  $\psi$ , the atomic planes that make an angle  $\psi$  with respect to the surface now diffract. If there is no stress in the sample, the two diffraction curves superimpose. However, in the presence of surface stresses, the atomic planes in different orientations are compressed or dilated and a peak shift results. The stress,  $\sigma$ , can be determined from the shift through the relationship

$$\sigma = \frac{E}{1 + \nu} \frac{1}{\sin^2 \psi} \frac{(d_\psi - d_0)}{d_0}$$

where  $d_\psi$  is the lattice spacing at a tilt angle  $\psi$  and  $E$  and  $\nu$  are Young's modulus and Poisson's ratio appropriate to the selected crystallographic planes. The values of  $d_\psi$  are obtained from Bragg's Law (Equation 1) by careful analysis of the diffraction peak. Note that it is not necessary to know the d-spacing of the unstressed material. Thus, an accurate and rapid measurement of the location of the diffraction peaks can be used to determine the presence of loading or residual stresses.

The specific parameters used in this test program included:

Radiation: Cr K $\alpha$  ( $\lambda = 2.29092\text{\AA}$ )  
Power: 35kV, 1.5 mA  
Beam Size: ~2 mm diameter  
Data Acquisition Time: 60s at  $\psi = 0$

A summary of the data along with the computer-generated data sheets are attached. The standard reference material data for the as-received and stress relieved conditions are included for comparison.

The full-width half-maximum (FWHM), the diffraction peak width at half of its maximum intensity, is a qualitative measurement of dislocation density. In other words, the larger the FWHM is, the higher the dislocation density is.

The repeatability (precision) of the x-ray stress measurements on steel is generally within 5% or 5 ksi, whichever is greater. The error bar reported with the stress value is comprised of both counting statistics errors and uncertainty due to metallurgical and mechanical factors (i.e., preferred orientation, large grain size, stress gradients, shear stresses). This number is, in general, very conservative.

The accuracy of the technique is within  $\pm 10$  to  $\pm 15$  ksi. A discussion of sources of error can be found in James and Cohen, "The Measurement of Residual Stresses by X-Ray Diffraction Techniques," Treatise on Materials Science and Technology, Vol. 19A, 1980. The largest source of error is the x-ray elastic constant,  $(1 + \nu) / E$ . This term generally varies from the bulk value by 10%, but can vary as much as 50%. The x-ray elastic constant is multiplied by the slope of the d-spacing versus  $\sin^2\psi$  line as part of the conversion from strain to stress. The value used in this program was measured experimentally and reported in the open literature.

**D-6ac Standard Reference Material**

	<u>Residual Stress, ksi</u>	<u>FWHM, °</u>
<b>As Received</b>	-50.2 ± 5.4	2.3
<b>Stress Relieved</b>	-14.7 ± 3.4	1.9

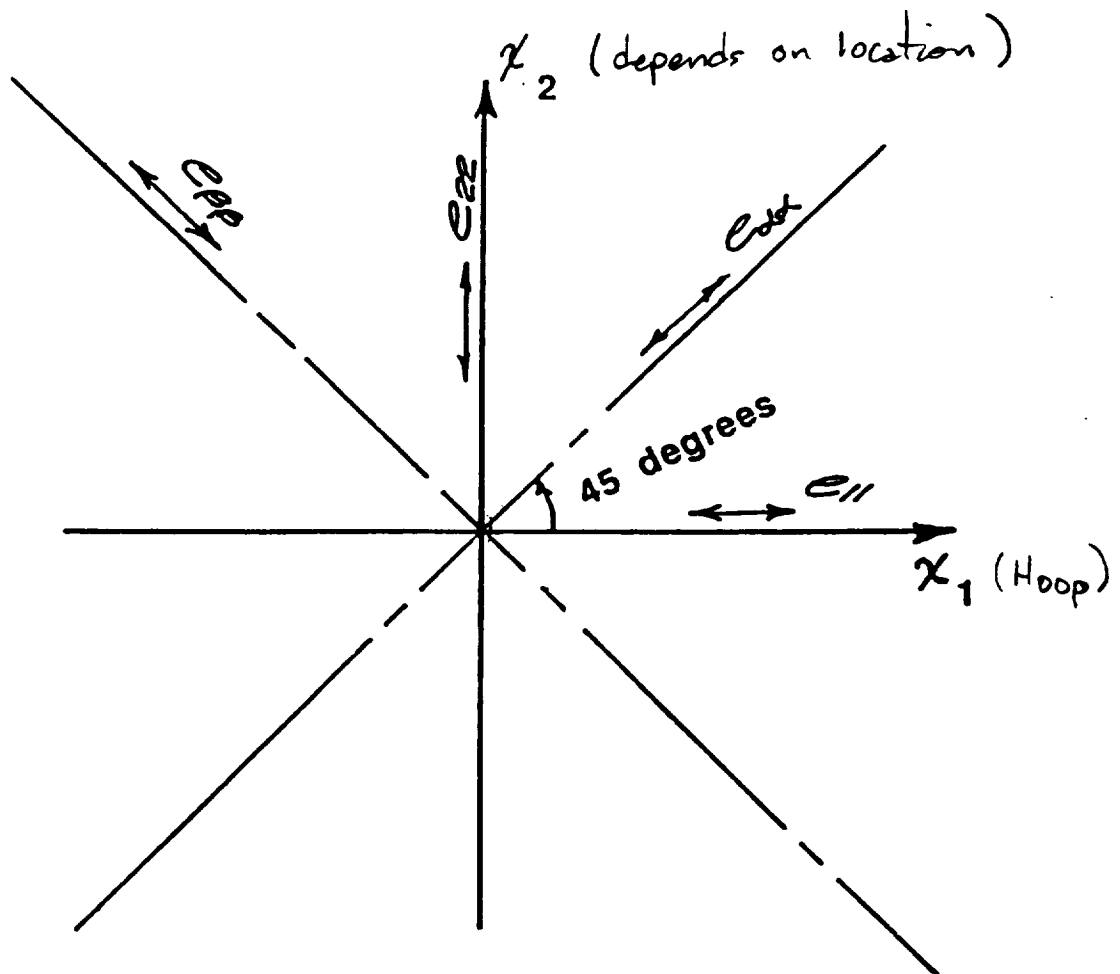
### **Recommended Reading**

**B. D. Cullity, Elements of X-Ray Diffraction, Addison-Wesley, Reading, MA, 2nd Edition, 1977, pp. 447-477.**

**M. E. Hilley et al., (eds.), Residual Stress Measurement by X-Ray Diffraction - SAE J784a, SAE, Warrendale, PA, 1971.**

**Noyan and Cohen, Residual Stress Measurement by Diffraction and Interpretation, Springer-Verlag, New York, 1987.**

**Metals Handbook, ASM, Metals Park, Ohio, 9th Ed. Vol. 10, 1986, pp. 380-392.**



**$x_1, x_2$  ARE LOCAL DIRECTIONS OF THE ANSYS  
FINITE ELEMENT COORDINATE SYSTEM**

\*\*\*\*\*

Residual Stress Analysis Report

\*\*\*\*\*

Date: 01-OCT-88 Time: 11:05:19

Sample Description :  
MORTON THIOKOL/REFERENCE SAMPLE/STRESS RELIEVED  
LONG DIRECTION

System Hardware Configuration :  
Auto Psi Angle Drive  
Psi Angle Position Encoder

ADC Channels Full Scale		256
Collimator Slit Type -	Rectangular	1.50
X-ray Target Material and Wavelength	Chromium	2.29092
Detector Mounting Block Bragg Angle		156.00
PSI Oscillation Angle Range		0.00
High Voltage and Beam Current	35000.	1.50
Peak Bounding Range (percent)		20.

Material ID Number		55
Material Type	D-6AC	(Cr 211)

Stress Spectra File Specifications		000408.SPC
Stress Spectra Acquisition Date:	01-OCT-88	11:03:54
Stress Spectra Count Time (sec)		60

Calibration File Specifications		CLC256.156
---------------------------------	--	------------

Detector Calibration Coefficients			
A -0.675706E-08	B 0.254374E-05	C 0.0593568	D 148.3517

Psi	Sin <sup>2</sup> (Psi)	Pk Chan	Intens	FWHM	Kalp Cor	2-Theta	D Spacing	St. Dev.
-45.0	0.50457	139.75	737.8	2.13	0.15424	156.52	1.169926	0.000029
-25.0	0.18138	137.91	812.6	2.17	0.15374	156.41	1.170159	0.000031
0.0	0.00001	136.35	933.6	2.12	0.15287	156.32	1.170355	0.000027
25.0	0.17613	137.18	857.0	2.13	0.15326	156.37	1.170250	0.000029
45.0	0.49592	138.80	807.7	2.12	0.15382	156.47	1.170045	0.000026

Fitted Delta D vs Sin<sup>2</sup>(Psi) Data

D Spacing Intercept	1.170344
Slope of Fitted Line	-7.236994E-04
Material Stress Constant	3.240000E-08

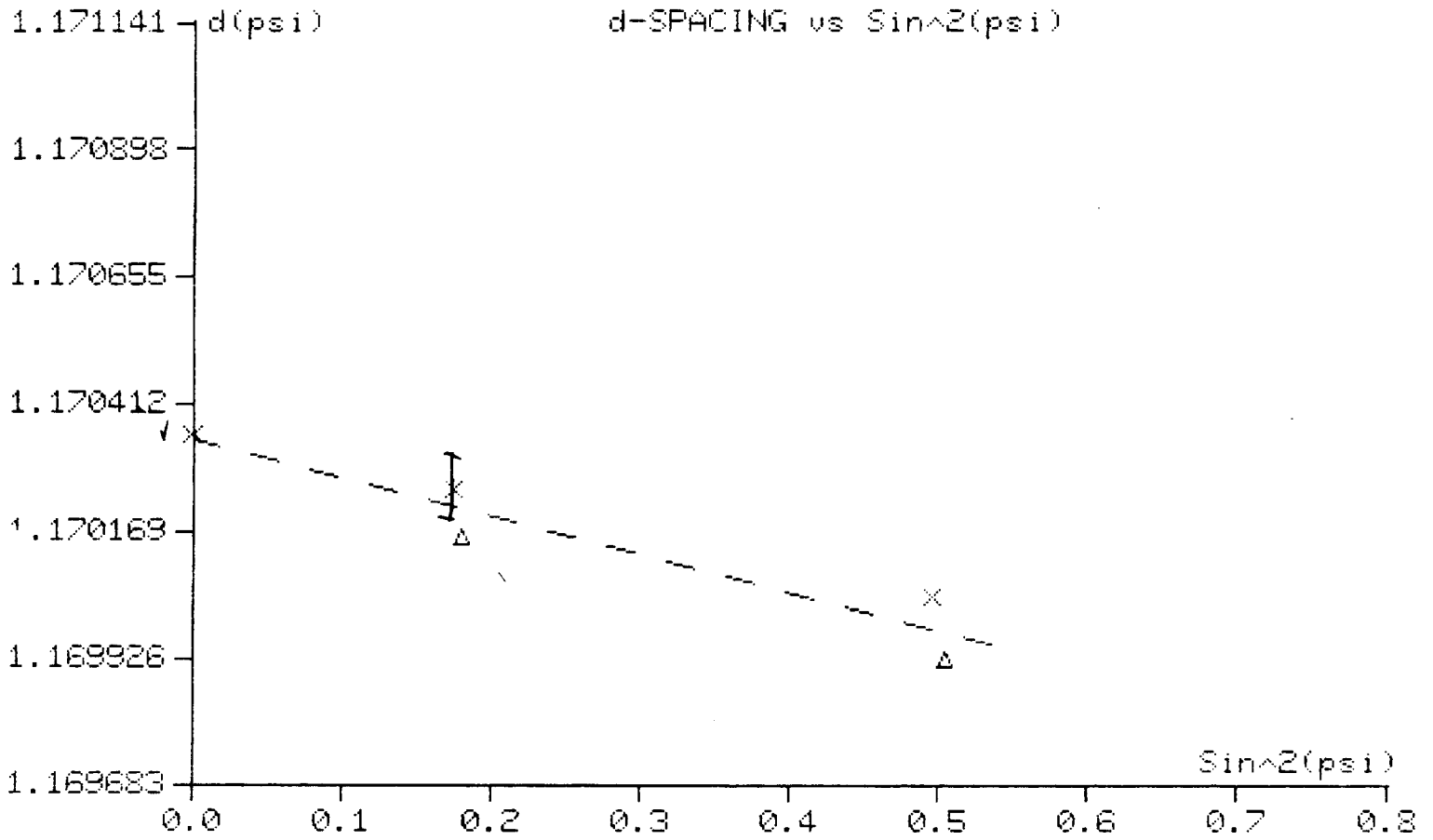
Residual Stress	-19.1 ksi	-131.6 MPa
Counting Statistics Stress Error (+/-)	1.6 ksi	11.3 MPa
Goodness of Fit Stress Error (+/-)	4.1 ksi	28.5 MPa
Total Stress Error (+/-)	4.4 ksi	30.6 MPa

Sample Description :  
MORTON THIOKOL/REFERENCE SAMPLE/STRESS RELIEVED  
IG DIRECTION

Stress Spectra File Specifications

000408.SFC

Residual Stress	(ksi)	-19.09	(mpa)	-131.59
Statistical Error (+/-)	(ksi)	4.44	(mpa)	30.65



\*\*\*\*\*

Residual Stress Analysis Report

\*\*\*\*\*

Date: 01-OCT-88 Time: 10:46:20

Sample Description :  
MORTON THIOKOL/REFERENCE SAMPLE/AS RECEIVED  
LONG DIRECTION/ROTATED 180 DEG.

System Hardware Configuration :  
Auto Psi Angle Drive  
Psi Angle Position Encoder

ADC Channels Full Scale 256  
Collimator Slit Type - Rectangular 1.50

X-ray Target Material and Wavelength Chromium 2.29092  
Detector Mounting Block Bragg Angle 156.00  
PSI Oscillation Angle Range 0.00  
High Voltage and Beam Current 35000. 1.50  
Peak Bounding Range (percent) 20.

Material ID Number 55  
Material Type D-6AC (Cr 211)

Stress Spectra File Specifications 000407.SPC  
Stress Spectra Acquisition Date: 01-OCT-88 10:45:01  
Stress Spectra Count Time (sec) 60

Calibration File Specifications CLC256.156

Detector Calibration Coefficients  
A -0.675706E-08 B 0.254374E-05 C 0.0593568 D 148.3517

Psi	Sin <sup>2</sup> (Psi)	Pk Chan	Intens	FWHM	Kalp Cor	2-Theta	D Spacing	St. Dev.
-45.0	0.51038	151.01	17.0	2.64	0.16033	157.19	1.168535	0.000033
-25.0	0.18037	135.40	45.3	2.76	0.15443	156.26	1.170480	0.000155
0.0	0.00000	133.32	60.7	2.59	0.15347	156.14	1.170745	0.000127
25.0	0.17660	136.02	46.8	2.47	0.15404	156.30	1.170400	0.000170
45.0	0.49203	146.35	18.3	2.91	0.15897	156.91	1.169108	0.000088

Fitted Delta D vs Sin<sup>2</sup>(Psi) Data

D Spacing Intercept 1.171001  
Slope of Fitted Line -4.221517E-03  
Material Stress Constant 3.240000E-08

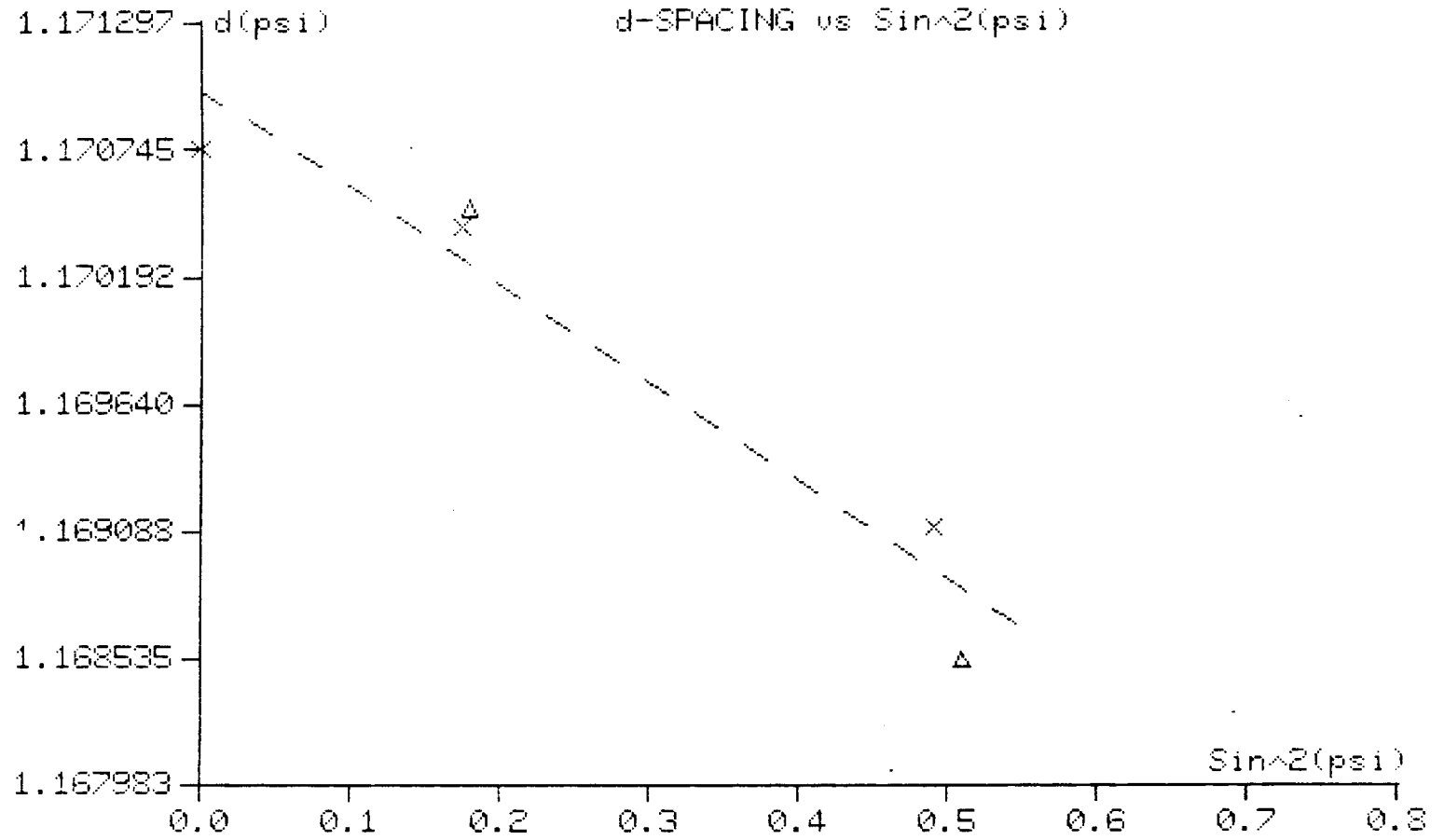
Residual Stress -111.3 ksi -767.2 MPa  
Counting Statistics Stress Error (+/-) 6.1 ksi 42.3 MPa  
Goodness of Fit Stress Error (+/-) 21.1 ksi 145.3 MPa  
Total Stress Error (+/-) 22.0 ksi 151.4 MPa

Sample Description :  
MORTON THIOKOL/REFERENCE SAMPLE/AS RECEIVED  
JG DIRECTION/ROTATED 180 DEG.

Stress Spectra File Specifications

000407.SPC

Residual Stress	(ksi)	-111.27	(mpa)	-767.16
Statistical Error (+/-)	(ksi)	21.96	(mpa)	151.38







**TECHNOLOGY for ENERGY CORPORATION**

December 22, 1988

In reply, refer to:  
1288-EBSP-1772-32946

Dr. D. W. Sutherland  
Morton Thiokol, Inc.  
Structures Design, Aerospace Group  
P. O. Box 707  
Brigham City, Utah 84302-0707

Dear Dan:

The exact locations of the stress measurements have been measured using a set of calibrated calipers. They are reported below and compared to locations in your letter of 9/26/88 (L221:FY89:L06). These locations represent the after etching locations. The electropolishing removed some material near the edge of the hole thus affecting the precise location of the measurement. Since TEC no longer has the Tang 000 sections, locations from this piece are not included.

If you need additional information, please contact me. It's been my pleasure working with you this year, and I look forward to working with you next year.

Sincerely,

TECHNOLOGY FOR ENERGY CORPORATION

E. Beth Pardue  
Supervisor  
Stress Analysis Laboratory

EBP/bsh

cc: L. A. Lowery  
J. C. Robinson

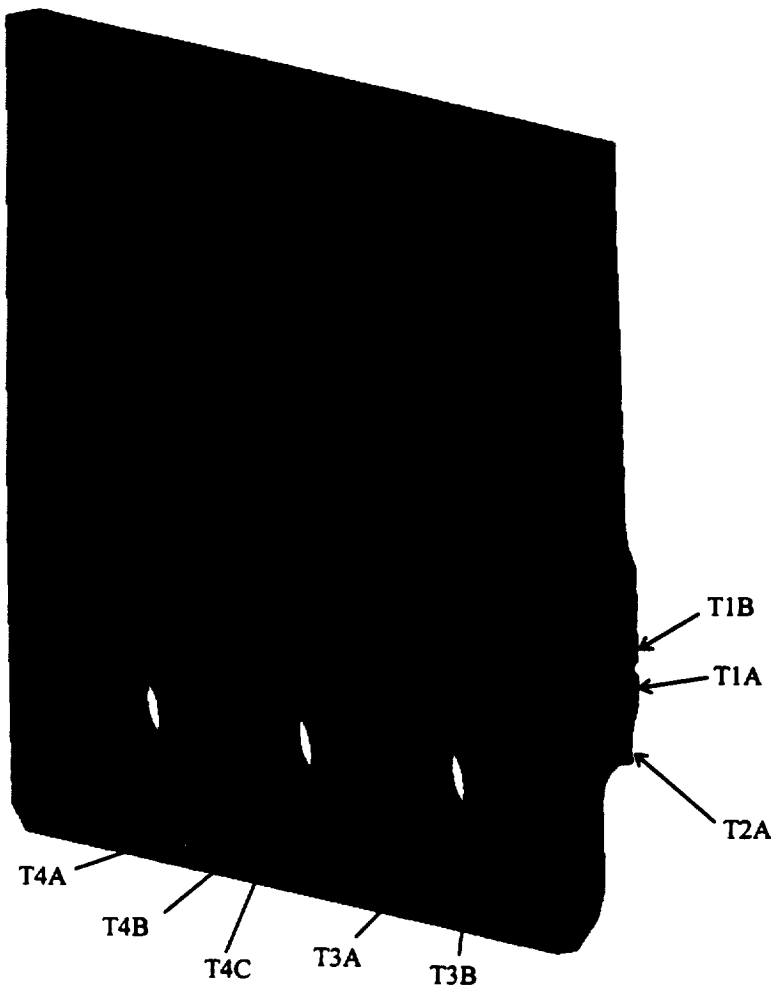


<u>Sample</u>	<u>Number</u>	<u>Nominal Location from Edge of Hole, in.</u>	<u>Actual Location from Edge of Hole, in.</u>
Tang 118	T3A	0.15	0.151
	T3B	0.31	0.304
	T4A	0.07	0.072 .075
	T4B	0.32	0.314 .320
	T4C	0.56	0.533 .565
Tang 240	T3A	0.15	0.149
	T3B	0.31	0.316
	T4A	0.07	0.063 .105
	T4B	0.32	0.308 .325
	T4C	0.56	0.546 .555
Clevis 118	C1A	0.35	0.366
	C1B	0.07	0.076
	C2A	0.36	0.327
	C2B	0.07	0.074
Clevis 240	C1A	0.35	0.358
	C1B	0.07	0.074
	C2A	0.36	0.326
	C2B	0.07	0.110

		Tang-000
T4 A	.072	T4A 0.088
T4 B	.318	T4B 0.305
T4 C	.564	T4C 0.545
C1A	.354	
C1B	.072	
C2A	.360	
C2B	.072	

Evaluations Made at  
Undisturbed Surface  
and ~10 mils Below  
Surface

See Appendix A for  
Dimensions



Tang 000  
Residual Stress, ksi

Measurement Point		Angle Directions			
		$e_{11}(0^\circ)$	$e_{\alpha\alpha}(45^\circ)$	$e_{22}(90^\circ)$	$e_{\beta\beta}(135^\circ)$
T1A	Surface	-147.4 ± 6.1	-137.7 ± 18.1	-127.2 ± 28.3	-135.8 ± 17.0
	Subsurface	+3.1 ± 3.9	+7.8 ± 2.6	+3.6 ± 6.6	+0.7 ± 4.5
T1B	Surface	-145.8 ± 8.7	-141.0 ± 10.6	-121.6 ± 21.1	-136.0 ± 14.3
	Subsurface	+5.9 ± 5.7	-1.1 ± 4.6	+2.9 ± 5.4	+7.3 ± 5.4
T2A	Surface	-137.1 ± 6.7	-128.0 ± 13.3	-116.7 ± 22.5	-126.7 ± 20.0
	Subsurface	-45.2 ± 5.8	-26.7 ± 4.7	-16.3 ± 4.8	-24.6 ± 5.4
T3A	Surface	-142.7 ± 8.9	-137.1 ± 7.1	-136.8 ± 5.2	-140.4 ± 7.3
	Subsurface	-89.8 ± 6.3	-78.0 ± 4.1	-31.8 ± 7.6	-45.7 ± 4.1
T3B	Surface	-140.0 ± 11.6	-138.4 ± 4.7	-138.1 ± 7.1	-152.1 ± 4.2
	Subsurface	-53.6 ± 5.4	-16.1 ± 3.8	+1.8 ± 5.9	-145.3 ± 6.2 -29.5 ± 3.4
T4A	Surface	-147.1 ± 8.5	-131.9 ± 9.1	-116.2 ± 9.3	-134.3 ± 5.0
	Subsurface	-61.9 ± 7.1	-47.6 ± 4.8	-13.0 ± 3.0	-36.9 ± 3.1
T4B	Surface	-139.5 ± 8.2	-133.9 ± 4.0	-136.1 ± 4.8	-139.7 ± 8.5
	Subsurface	+8.3 ± 4.7	-7.5 ± 4.9	-15.2 ± 8.2	+1.5 ± 6.5
T4C	Surface	-143.4 ± 5.2	-137.3 ± 4.0	-140.8 ± 4.8	-149.0 ± 6.5
	Subsurface	+16.4 ± 5.2	+15.0 ± 7.4	-1.5 ± 7.5	+3.9 ± 5.4

## Tang 118

## Residual Stress, ksi

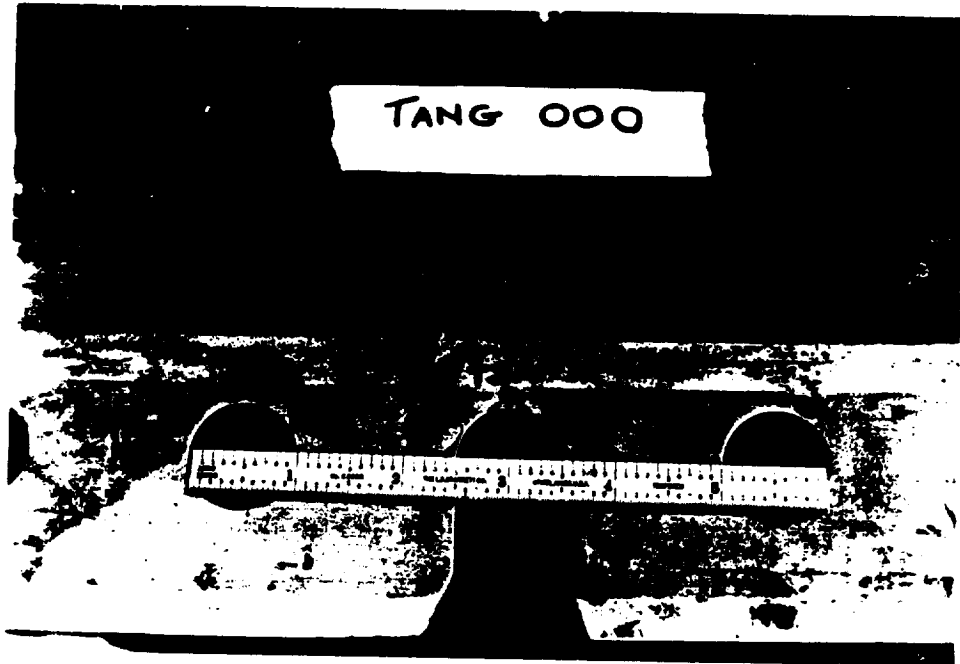
Measurement Point	Angle Directions				
	$\epsilon_{11}(0^\circ)$	$\epsilon_{\alpha\alpha}(45^\circ)$	$\epsilon_{22}(90^\circ)$	$\epsilon_{\beta\beta}(135^\circ)$	
T2A	Surface	-142.0 $\pm$ 7.3	-139.5 $\pm$ 14.1	-134.8 $\pm$ 10.7	-136.3 $\pm$ 24.1
	Subsurface	-50.3 $\pm$ 3.5	-33.1 $\pm$ 5.4	-10.0 $\pm$ 7.0	-37.8 $\pm$ 8.8
T3A	Surface	-128.9 $\pm$ 24.3	-128.9 $\pm$ 8.3	-136.0 $\pm$ 11.5	-145.9 $\pm$ 14.3
	Subsurface	-56.5 $\pm$ 3.9	-66.2 $\pm$ 4.3	-35.2 $\pm$ 4.2	-28.6 $\pm$ 2.6
T3B	Surface	-139.4 $\pm$ 13.7	-132.6 $\pm$ 7.7	-130.8 $\pm$ 6.1	-135.6 $\pm$ 9.1
	Subsurface	-22.2 $\pm$ 2.7	+10.3 $\pm$ 5.0	+13.3 $\pm$ 2.9	-17.9 $\pm$ 3.4
T4A	Surface	-129.8 $\pm$ 4.9	-123.8 $\pm$ 5.7	-123.9 $\pm$ 10.6	-134.6 $\pm$ 5.5
	Subsurface	-40.6 $\pm$ 5.0	-36.4 $\pm$ 4.4	-9.8 $\pm$ 5.7	-17.1 $\pm$ 3.9
T4B	Surface	-140.5 $\pm$ 7.3	-125.0 $\pm$ 4.7	-125.6 $\pm$ 4.3	-138.9 $\pm$ 7.3
	Subsurface	-24.9 $\pm$ 5.0	-38.8 $\pm$ 2.8	-43.4 $\pm$ 2.5	-30.6 $\pm$ 4.8
T4C	Surface	-138.7 $\pm$ 7.1	-129.6 $\pm$ 8.3	-129.7 $\pm$ 4.4	-138.7 $\pm$ 6.0
	Subsurface	+27.6 $\pm$ 4.2	+2.1 $\pm$ 3.5	-22.3 $\pm$ 5.5	-2.6 $\pm$ 4.3

Tang 240

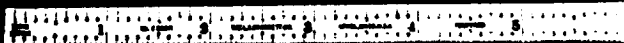
Residual Stress, ksi

Measurement Point		Angle Directions			
		$\epsilon_{11}(0^\circ)$	$\epsilon_{\alpha\alpha}(45^\circ)$	$\epsilon_{22}(90^\circ)$	$\epsilon_{\beta\beta}(135^\circ)$
T2A	Surface	-135.3 ± 12.7	-124.8 ± 16.7 } -129.4 ± 16.2 }	-127.4 ± 18.6	-125.1 ± 14.8 } -135.9 ± 16.1 }
	Subsurface	-73.7 ± 6.8	-93.0 ± 5.4	-9.5 ± 4.4	-35.6 ± 7.6
T3A	Surface	-133.2 ± 6.1	-126.3 ± 8.7	-136.4 ± 3.8	-137.1 ± 6.7
	Subsurface	-57.3 ± 2.9	-57.8 ± 4.5	-27.9 ± 4.9	-27.3 ± 4.2
T3B	Surface	-187.2 ± 4.8	-123.2 ± 4.3	-127.3 ± 5.1	-143.0 ± 3.1
	Subsurface	-21.1 ± 6.3	+7.8 ± 3.4	+15.2 ± 2.4	-13.5 ± 3.8
T4A	Surface	-131.1 ± 3.6	-127.2 ± 5.9	-134.6 ± 5.8	-141.4 ± 5.2
	Subsurface	-72.0 ± 5.5	-41.9 ± 2.9	-14.7 ± 4.0	-49.8 ± 3.0
T4B	Surface	-125.9 ± 8.0	-124.1 ± 8.0	-133.3 ± 10.4	-132.6 ± 5.8
	Subsurface	-21.1 ± 6.2	-26.3 ± 3.2	-40.2 ± 5.7	-25.6 ± 4.2
T4C	Surface	-132.6 ± 4.6	-118.0 ± 10.3	-131.2 ± 10.0	-132.7 ± 6.0
	Subsurface	+28.1 ± 2.7 } +22.7 ± 3.6 }	+7.7 ± 2.9	-6.1 ± 3.1	-0.0 ± 3.4

TANG 000

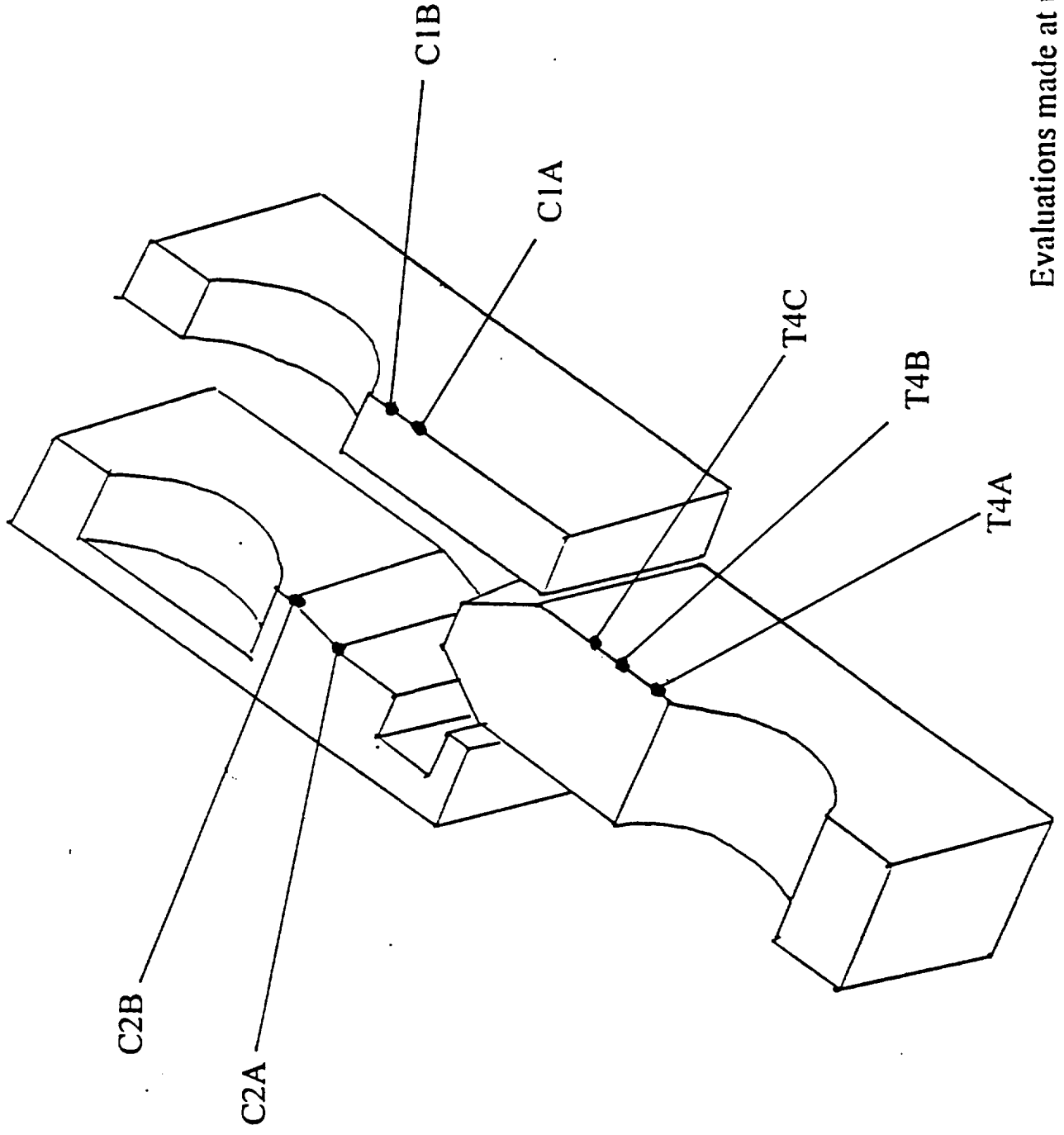


TANG 118



TANG 240





Evaluations made at undisturbed surface and ~ 10 mils below surface

Clevis 118

Residual Stress, ksi

Measurement Point	Angle Directions				
	$\epsilon_{11}(0^\circ)$	$\epsilon_{\alpha\alpha}(45^\circ)$	$\epsilon_{22}(90^\circ)$	$\epsilon_{\beta\beta}(135^\circ)$	
C1A	Surface	-121.0 ± 5.8	-112.4 ± 24.4	-118.0 ± 23.9 -120.7 ± 24.4	-119.2 ± 18.9
	Subsurface	+22.2 ± 6.5	-14.1 ± 7.2	-19.5 ± 7.8	-18.2 ± 5.6
C1B	Surface	-146.8 ± 7.0	-121.4 ± 14.1	-85.9 ± 17.5	-112.0 ± 20.0
	Subsurface	-105.8 ± 4.7	-77.5 ± 6.2	-56.8 ± 6.2	-68.8 ± 9.2
C2A	Surface	-115.1 ± 16.5	-128.2 ± 25.8	-124.5 ± 15.2	-128.7 ± 11.9
	Subsurface	-63.9 ± 19.6	-85.4 ± 3.9	-69.6 ± 8.6	-87.0 ± 3.2
C2B	Surface	-127.6 ± 8.0	-121.9 ± 7.0	-126.8 ± 4.9	-129.8 ± 12.3
	Subsurface	-102.4 ± 5.8	-47.4 ± 8.6	-6.9 ± 6.8	-32.6 ± 5.4

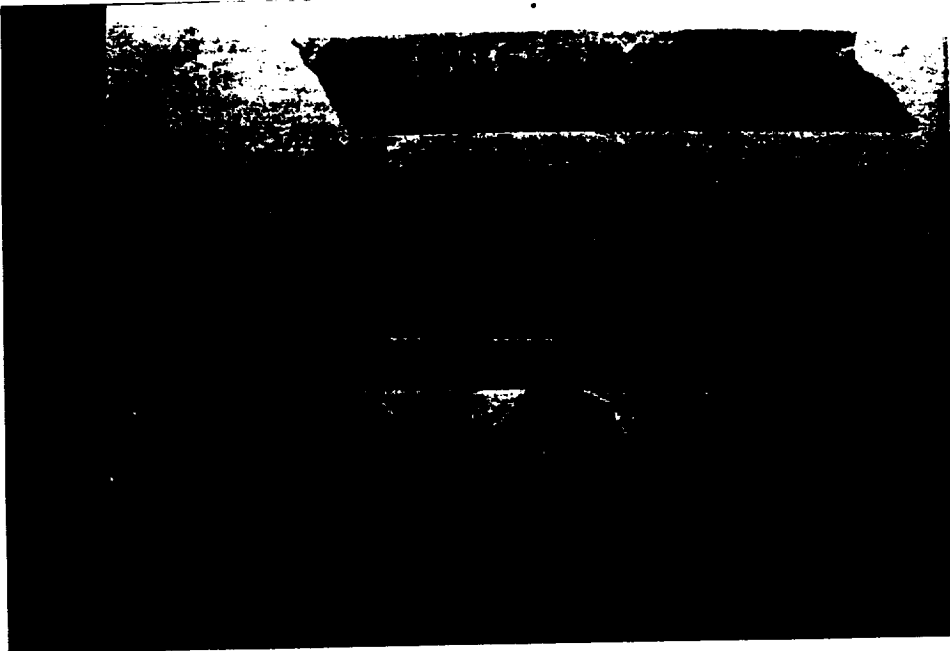
*measurements made @ 112°*

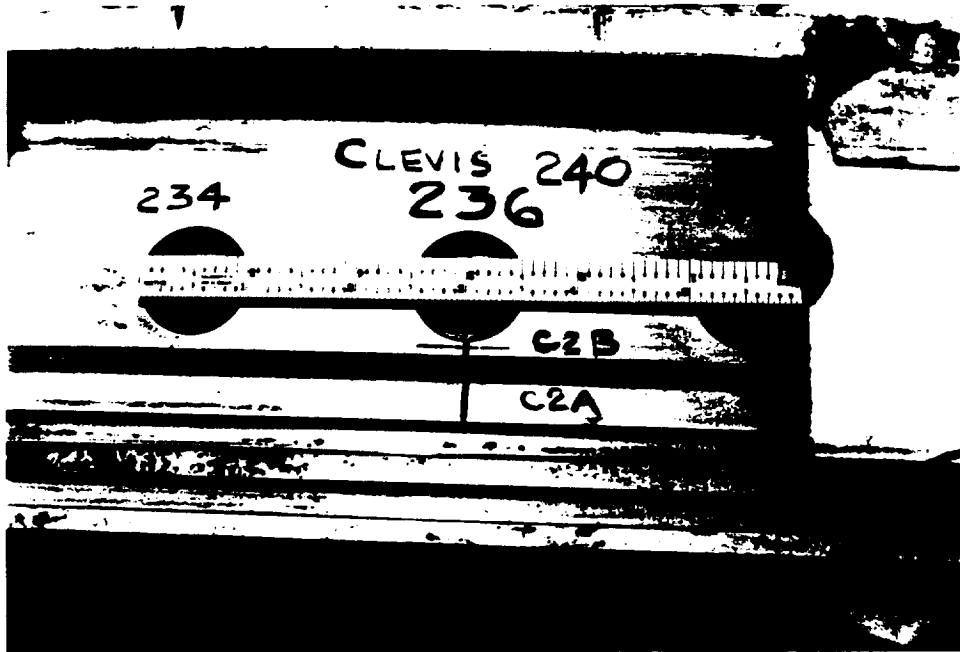
Clevis 240

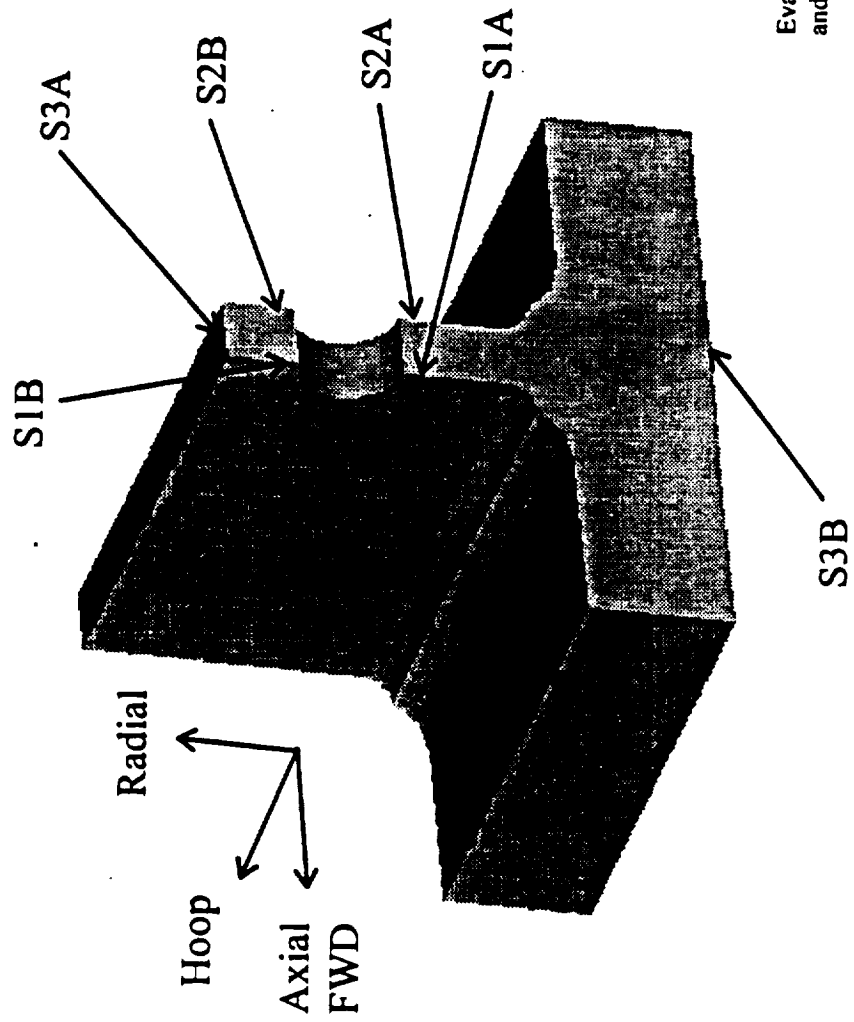
Residual Stress, ksi

Measurement Point	Angle Directions				
	$\epsilon_{11}(0^\circ)$	$\epsilon_{\alpha\alpha}(45^\circ)$	$\epsilon_{22}(90^\circ)$	$\epsilon_{\beta\beta}(135^\circ)$	
C1A	Surface	-111.4 ± 5.4	-119.8 ± 9.8	-118.8 ± 21.6	-113.7 ± 18.1 -105.8 ± 17.1
	Subsurface	+19.8 ± 8.2	-0.8 ± 5.2	-7.5 ± 6.2	+7.3 ± 7.3
C1B	Surface	-137.6 ± 5.1	-96.7 ± 8.2	-51.2 ± 13.2 -32.9 ± 17.6	-98.2 ± 10.6
	Subsurface	-77.2 ± 5.8	-35.3 ± 3.2	-22.5 ± 4.2	-56.5 ± 5.5
C2A	Surface	-114.8 ± 9.6	-117.1 ± 22.3	-120.3 ± 21.4	-127.7 ± 15.4
	Subsurface	-39.5 ± 5.9	-58.7 ± 3.5	-46.6 ± 5.1	-59.5 ± 5.7
C2B	Surface	-134.8 ± 7.3	-131.5 ± 11.9	-134.4 ± 8.9	-122.3 ± 23.0
	Subsurface	-74.7 ± 8.7	-85.8 ± 7.5	-4.9 ± 4.2	-42.5 ± 4.8

measurements made @ 256°







Evaluations made at undisturbed surface  
and ~ 10 mils below surface

Forward Stiffener Stub 166

Residual Stress, ksi

Measurement Point		Angle Directions			
		$\epsilon_{11}(0^\circ)$	$\epsilon_{\alpha\alpha}(45^\circ)$	$\epsilon_{22}(90^\circ)$	$\epsilon_{\beta\beta}(135^\circ)$
S1A	Surface	-134.9 ± 18.6		-129.4 ± 8.3	
	Subsurface	+6.8 ± 4.5		-14.0 ± 5.0	
S1B	Surface	-147.0 ± 13.8		-140.4 ± 9.2	
	Subsurface	-15.8 ± 7.9		-14.0 ± 3.7	
S2A	Surface	-129.3 ± 13.3		-147.9 ± 8.7	
	Subsurface	-3.5 ± 7.1		-6.0 ± 3.6	
S2B	Surface	-123.6 ± 8.7		-125.8 ± 11.6	
	Subsurface	-80.0 ± 4.5		-28.0 ± 5.5	
S3A	Surface	-189.7 ± 7.9	-193.3 ± 19.3	-148.8 ± 8.1	-142.2 ± 8.6
	Subsurface	+3.4 ± 5.7	+4.9 ± 6.6	+3.8 ± 6.0	+8.1 ± 7.6
S3B	Surface	-115.8 ± 8.6	-118.8 ± 20.1	-109.1 ± 21.6 } -116.1 ± 19.2 }	-117.7 ± 11.5 } -114.9 ± 12.6 }
	Subsurface	+4.1 ± 6.5	+3.2 ± 3.3	+2.4 ± 4.8	+8.0 ± 7.2 } +2.3 ± 6.3 }

Aft Stiffener Stub 166

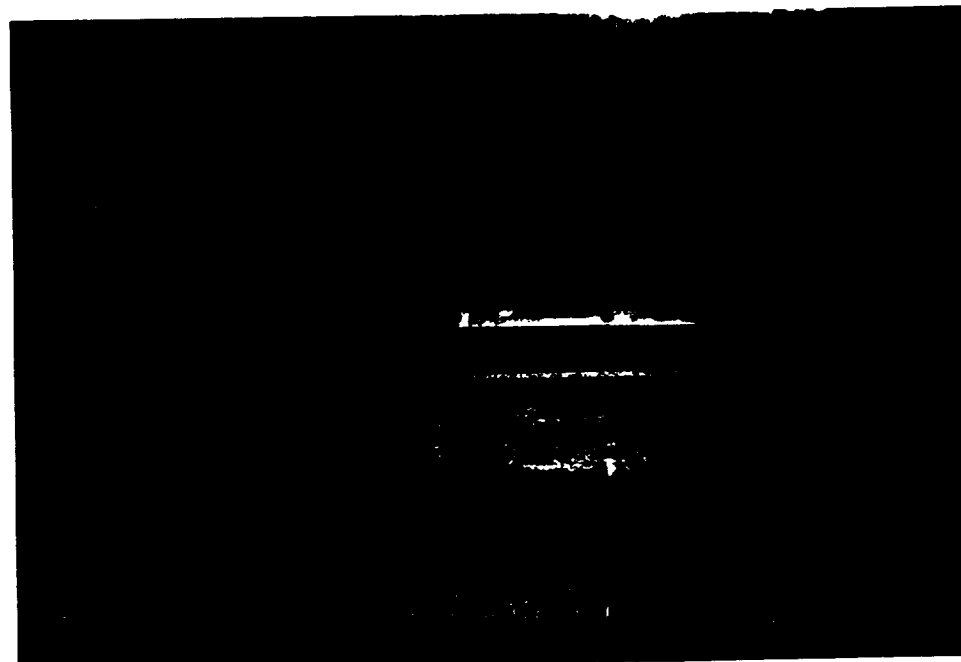
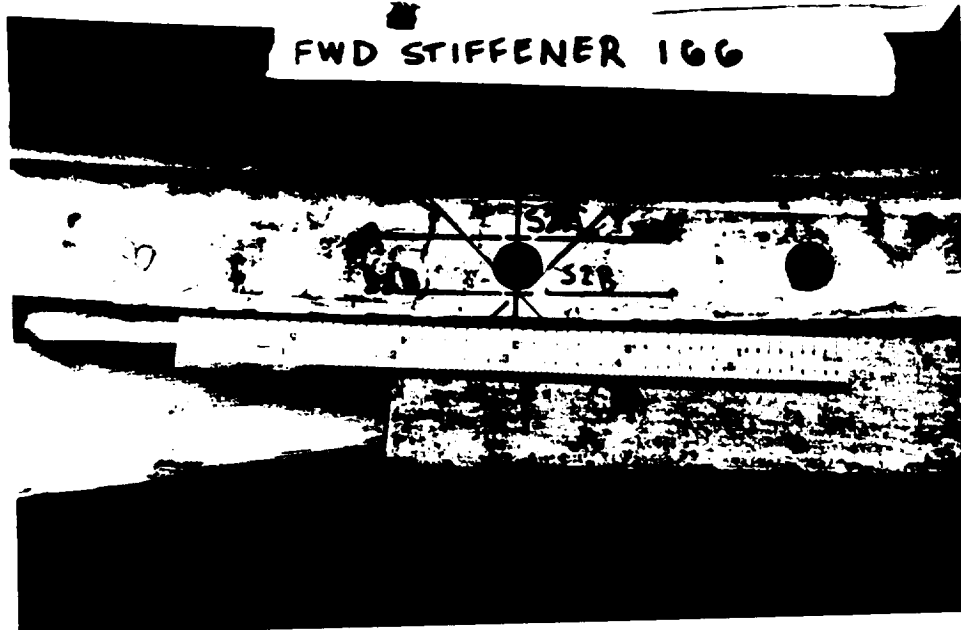
Residual Stress, ksi

Measurement Point		Angle Directions			
		$e_{11}(0^\circ)$	$e_{\alpha\alpha}(45^\circ)$	$e_{22}(90^\circ)$	$e_{\beta\beta}(135^\circ)$
S1A	Surface	-140.3 ± 12.1		-133.8 ± 10.0	
	Subsurface	-30.1 ± 5.6	-7.3 ± 7.3	-28.8 ± 5.5	
S1B	Surface	-141.2 ± 10.9		-141.0 ± 5.6	
	Subsurface	-3.6 ± 4.8	-26.8 ± 4.2	-4.0 ± 3.9	
S2A	Surface	-120.8 ± 10.1		-134.2 ± 5.7	
	Subsurface	-60.6 ± 5.3		-51.8 ± 9.3	-56.2 ± 24.3
S2B	Surface	-137.1 ± 7.3		-170.2 ± 6.4	
	Subsurface	-21.5 ± 3.8		-10.1 ± 3.2	-26.6 ± 6.9
S3A	Surface	-146.2 ± 4.5	-148.6 ± 15.2	-139.7 ± 19.8	-141.7 ± 12.1
	Subsurface	+4.8 ± 7.5	+5.6 ± 5.5	+5.8 ± 8.1	-4.3 ± 6.2
S3B	Surface	-122.0 ± 4.2	-115.2 ± 12.0	-114.6 ± 15.2	-117.1 ± 10.0
	Subsurface	+12.8 ± 10.2	+5.4 ± 6.6	+10.1 ± 9.1	+5.6 ± 4.8

FWD STIFFENER 166



FWD STIFFENER 166

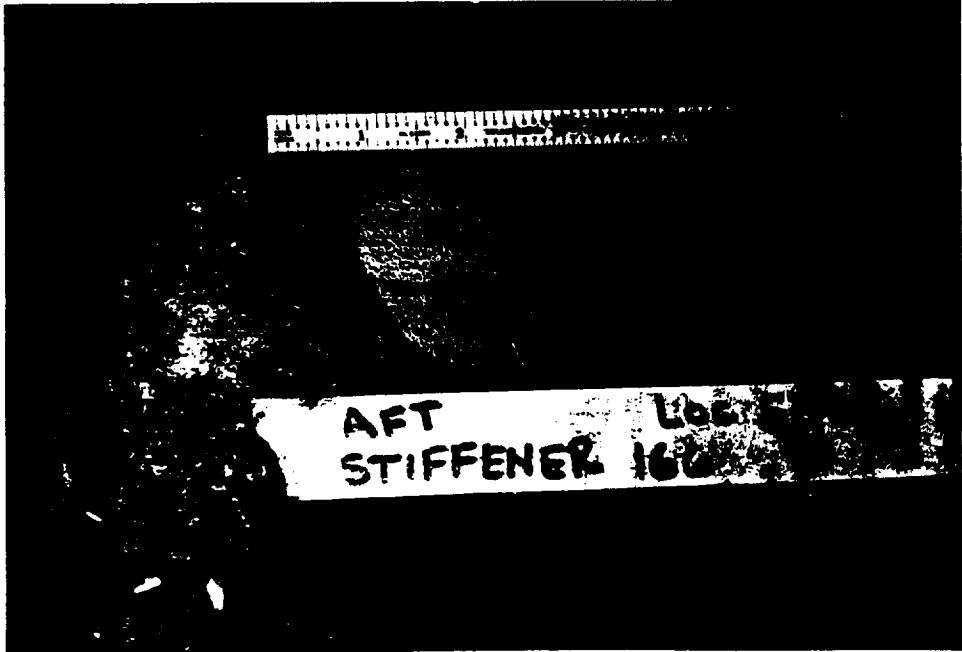
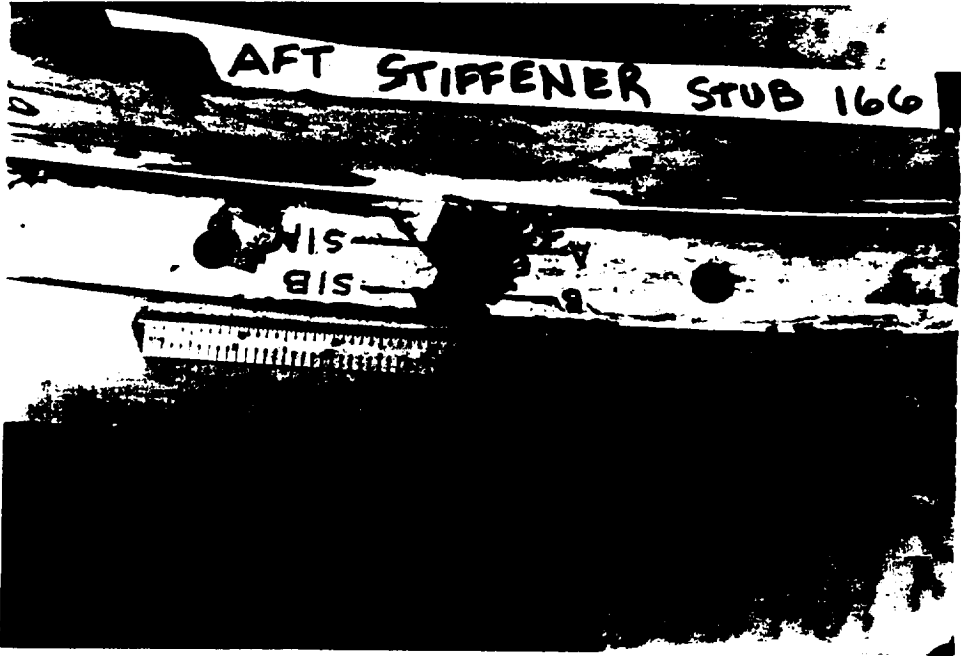


FORWARD

LOC S3B

STEFFNER 166





APPENDIX B - VENDOR REPORT FOR NEUTRON BEAM DIFFRACTION MEASUREMENTS

The attached report was submitted by Atomic Energy of Canada Limited (AECL) at the completion of the measurements of the residual strains on Tang 000 in the region of the tang forward of the pin hole at the 4' position. It provides a description of the neutron beam measurement process, identifies the region evaluated, presents the measured data, and compares the results to an elasto-plastic analysis of the residual strains around a generic (not next to an alignment slot) pin hole in a factory joint tang.

**NOTE:** The test plan gives two incorrect designations for this segment. The title page refers to 1U50716-06 S/N L023 (*a lightweight attach segment*). The test component description in Section 2.0 refers to 1U50715 S/N L032 (*a lightweight stiffener segment flown on flight 21A*). The DM-8 motor used the lightweight attach segment S/N L032 and the lightweight stiffener segment S/N L023. The correct designation of the test item is lightweight stiffener segment S/N L023 flown on flights 14A and 24A. The similarity of the segment numbering gave opportunity for the confusion.

Unfortunately the erroneous description of the case stiffener segment was carried into this vendor report in Section 2.1. That reference should be 1U50715 S/N L023 with history noted above.

This test article was the other half of Tang-000 tested earlier by TEC using the x-ray diffraction method.

**PROTECTED - Morton Thiokol**

THIS REPORT WAS PREPARED UNDER CONTRACT BY AECL. THE INFORMATION IS OWNED BY THE CONTRACTOR. NO EXPLOITATION OR TRANSFER OF ANY INFORMATION CONTAINED HEREIN IS PERMITTED IN THE ABSENCE OF AN AGREEMENT WITH THE OWNERS. NEITHER THE DOCUMENT NOR ANY INFORMATION IN THE DOCUMENT MAY BE RELEASED TO ANY THIRD PARTY WITHOUT THE WRITTEN CONSENT OF THE OWNERS.

**ATOMIC ENERGY  
OF CANADA LIMITED**



**ÉNERGIE ATOMIQUE  
DU CANADA LIMITÉE**

**NEUTRON DIFFRACTION MEASUREMENTS  
OF RESIDUAL STRAINS NEAR A PIN HOLE  
IN A SOLID FUEL BOOSTER ROCKET CASING**

**ANDI-25**

by

**T.M. HOLDEN, J.H. ROOT and R.R. HOSBONS**

**Neutron and Solid State Physics Branch**

**Chalk River Nuclear Laboratories**

**Chalk River, Ontario K0J 1J0**

**1989 June**



PROTECTED  
MORTON THIOKOL

ANDI-25

THIS REPORT WAS PREPARED UNDER CONTRACT BY AECL. THE INFORMATION IS OWNED BY THE CONTRACTOR. NO EXPLOITATION OR TRANSFER OF ANY INFORMATION CONTAINED HEREIN IS PERMITTED IN THE ABSENCE OF AN AGREEMENT WITH THE OWNER(S). NEITHER THE DOCUMENT NOR ANY INFORMATION IN THE DOCUMENT MAY BE RELEASED TO ANY THIRD PARTY WITHOUT THE WRITTEN CONSENT OF THE OWNER(S).

NEUTRON DIFFRACTION MEASUREMENTS  
OF RESIDUAL STRAINS NEAR  
A PIN HOLE IN A SOLID FUEL  
BOOSTER ROCKET CASING

T.M. Holden\*, J.H. Root\* and R.R. Hosbons\*\*

Abstract

The elastic strains corresponding to residual stresses in the region between the pin hole and the end of the tang were measured using a neutron diffraction technique.

The largest strains were found to be near the pin hole in the region which yields under a combination of pin bearing and hoop tension loadings. The largest elastic compressive hoop strain observed was  $-2300 \times 10^{-6}$ . In the same region tensile axial strains of  $1200 \times 10^{-6}$  and tensile normal strains of  $1400 \times 10^{-6}$  were observed.

\* Neutron and Solid State Physics Branch  
\*\* Advanced Materials Research Branch

Neutron and Solid State Physics Branch  
Atomic Energy of Canada Limited  
Chalk River Nuclear Laboratories  
Chalk River, Ontario, Canada, KOJ 1J0

1989 June



## 1.0 INTRODUCTION

The cases of the motors for NASA's Space Shuttle booster rockets are assembled from a number of case segments. Each of these segments is machined from a single forging. The forgings are made from D6AC, a High Strength Low Alloy Steel.

During proof testing of the case segments, local regions near some of the structural details yield. When the proof test pressure is released local elastic residual stress fields must develop to maintain compatibility between the yielded and non-yielded regions of the case. D6AC steel is known to be moderately susceptible to stress corrosion cracking if exposed to sufficiently high tensile stresses for a long enough period of time in a water or humid air environment. It is important therefore that the design engineers be able to determine the sign and magnitude of the residual stresses associated with local yielding, since tensile residual stresses of sufficient magnitude could, if present, lead to stress corrosion cracking.

Residual stresses are presently being determined from elastic plastic finite element analyses. To obtain a direct experimental check on the accuracy of these computed residual stresses, Morton Thiokol, Inc. decided to obtain measured values for the residual stresses near some of the structural details in an actual piece of flight hardware. As part of this effort a contract was awarded to The Chalk River Nuclear Laboratories of Atomic Energy of Canada Limited to measure the residual stresses near a pin hole in a factory joint tang using a neutron diffraction technique. This report presents the results of those measurements.

## 2. EXPERIMENTAL

### 2.1 Sample

The specimen examined is a portion of the tang of Case segment 1U50715 S/N 032, a lightweight stiffener segment. This segment was flown in the aft position on motor 21A, and was used in the forward position on test motor DM-8. A proof test was performed on the case before Flight 21 and before its use in the DM-8 test motor. At the conclusion of the DM-8 test, the ET attach case

*See NOTE  
on Prelim page.*

segment and lightweight stiffener S/N 032 were subjected to a localized overheating as the result of a failure in the external case cooling system. The forward end of S/N L032 was damaged along a band centered on the zero degree longitudinal line, but the remainder of the case was unaffected. As a result of the local overheating, the case segment was scrapped, and it was possible to obtain residual stress test specimens from portions of the case which had not been overheated.

Tensile coupons cut from the case segment forging after heat treatment had been tested to verify the mechanical properties of the forging. These tests indicated the yield strength of the material to be  $199.7 \times 10^3$  psi (1398 MPa). This strength level is within specification.

Three residual stress specimens were cut from the tang. Each specimen was centered on one of the three alignment slots. Figure 1 shows the cutting sketch for the tang specimens. One of the three specimens was supplied to AECL. This specimen contains the alignment slot which was originally located at zero degrees on the case. Note that the measurements were made on a pin hole four degrees around a complete tang from the alignment slot.

A small piece of case membrane which had been stress relieved at 1000° F (538° C) in a laboratory furnace was also provided to AECL. This material was examined as an example of a reference interplanar spacing.

## 2.2 Neutron Diffraction

It is possible to make measurements of the interplanar spacing of the atomic lattice through the complete thickness of a rocket casing by neutron diffraction because thermal neutrons of the wavelength used in the experiment are only attenuated by a factor of 10 in passing through 16 mm of steel. The neutron diffraction method is the only way of getting this information directly and non-destructively by experiment. The measured strains may then be compared with the results of computer modeling.

In the presence of residual tensile stress the atomic planes in the grains which make up the casing are slightly pulled apart. The lattice spacing,  $d_{hkl}$ , is related to the diffraction angle,  $2\theta_{hkl}$ , by the Bragg equation,

$$2d_{hkl} \sin \theta_{hkl} = \lambda \quad (1)$$

where (hkl) labels the family of crystallographic planes and  $\lambda$  is the calibrated neutron wave length 2.6139 Å. The shift in the angular position of the diffraction peaks can thus be used as a miniature internal strain gauge. If the lattice spacing can be measured in a strain-free component, or in a part of the casing believed not to be subjected to a perturbing influence such as a pin hole, the residual strain can be computed. Finally if the elastic constants are known, the residual stress components may be calculated from the measured residual strain components.

### 2.3 Experimental Procedure

The measurements were made with the L3 spectrometer at the NRU reactor, Chalk River Nuclear Laboratories, employing the (113) planes of a squeezed Ge crystal as monochromator to provide a neutron beam of wavelength 2.6139 Å. The collimations of the beams before and after the sample were 0.19 and 0.21 degrees respectively.

Slits in absorbing cadmium sheet, each 1.3 mm wide and 2 mm high placed in both the incident and diffracted beams, defined the gauge volume, a column 2 mm high whose cross section in the horizontal plane is a parallelogram centered over the sample table of the spectrometer. By moving the sample on a computer controlled X-Y drive any desired point may be brought into the gauge volume. Each diffraction measurement gives the average interplanar spacing of those grains in the gauge volume whose normals lie along the bisector of the included angle between the incident and diffracted beams. Positioning of the gauge volume in the casing was achieved with an accuracy of  $\pm 0.1$  mm. Reference positions were established at the ID and OD of the casing and at the position of the outside diameter of the pin hole by moving the wall, or hole surface, through the gauge volume and examining the characteristic intensity change. Three different geometrical arrangements of the component are needed to set the required directions in the component along the bisector of the incident and scattered beams. Fig. 2 shows a photograph of the set-up for measuring the hoop strain near the pin hole.

The instrumental lineshape for neutron diffraction is Gaussian so that the angular position of the diffraction peak was obtained, to a precision of  $\pm 0.012$  deg. in this experiment, by fitting a Gaussian peak on a sloping background to the experimental data. The important parameters are peak position, peak width and integrated intensity. By measuring the linewidth of the diffraction peaks of standard Ge and KCl powders the instrumental linewidth at the diffraction angle for the component was found to be  $0.42 \pm 0.01$  degree. The average linewidth observed in the present measurements,  $0.83 \pm 0.05$  degree, is much greater than this indicating that there is an intrinsic linewidth stemming from the tempered martensite microstructure.

The experiments reported here were carried out with the (110) reflection of the ferritic phase. No surface preparation was required for the measurement.

#### 2.4 Determination of Lattice Spacing in the Stress Free Condition

Three axial d-spacing measurements were made at different locations through the thickness of the sample wall at a point located 100 mm from the edge of the pin hole. The results of these measurements are shown in Table 1. There was no through-wall variation of lattice spacing at 100 mm. The average spacing was found to be  $2.0283 \pm 0.0002$  Å.

Seventeen through-wall measurements of lattice spacing in the axial, hoop and normal orientations were made on the piece of stress relieved reference material. The results of these measurements are summarized in Table 2. There is no significant through-wall variation and the average spacing is  $2.0281 \pm 0.0002$  Å. The average peak width is  $0.76 \pm 0.04$  deg. which is slightly less than the average peak width in the component.

The average value for the three measurements on the sample itself ( $2.0283$ Å) was selected as the reference value with respect to which strains were calculated.

### 3. RESULTS

Three strain components (axial, hoop and normal) were measured at a number of points between the pin hole and the end of the tang. All of the points lie in a plane defined by the axis of the pin hole and the North-South axis through

the pin hole shown in the schematic diagram of the tang end of the casing (see Figure 3).

### 3.1 Axial Strain Measurements

The results of eighty-two (110) lattice spacing measurements in the axial direction are tabulated in Table 3 and plotted in Figure 4. The location of the center of the gauge volume is indicated by its distance from the edge of the hole and its distance from the outer surface of the tang. The outer surface of the tang is chamfered near its end. Two of the axial measurement stations (23 and 27 mm from the edge of the hole) are in the chamfered portion of the tang. Note that the location of the measurement points at these positions is measured from the local outer diameter of the case segment.

At 3 mm from the hole the axial strain is tensile at every point through the thickness with a maximum at the ID. Between 7 and 15 mm from the hole compressive strains are observed. These strains vary somewhat through the thickness with higher compressive strains occurring on the ID of the tang. Finally, we note that beyond 19 mm from the hole the axial strains are essentially zero.

A total of twenty readings of the diffraction angle were taken at the nine stations located 3 mm from the edge of the hole. Figure 5 shows a third order polynomial curve to fit to this data. The standard deviation of the data points from this curve is 0.014 deg. For a normal distribution of errors we expect one-third of the observations to depart from a fitted curve by more than one standard error. In the present case seven out of twenty observations lie more than one standard error from the curve. Assuming an error band equal to  $\pm 2\sigma$  we have  $\Delta(2\theta) = \pm 0.028$  degrees. The error in the d-spacing is given in terms of the error in  $(2\theta)$  and the error in  $\lambda$  by

$$\Delta d_{hkl} = d_{hkl} \left[ \frac{\Delta\lambda}{\lambda} - \frac{1}{2} \cot(\theta_{hkl}) \Delta(2\theta_{hkl}) \right] \quad (2)$$

Setting  $d_{hkl} = 2.0283\text{\AA}$ ,  $\lambda = 2.6139\text{\AA}$ ,  $\Delta\lambda = \pm 5 \times 10^{-5}\text{\AA}$ ,  $\theta_{hkl} = 40$  deg., and  $\Delta(2\theta_{hkl}) = \pm 0.028$  deg., we obtain  $\Delta d_{hkl} = \pm 0.00063\text{\AA}$  which corresponds to an error in strain measurement of  $\pm 310 \mu$  ( $1 \mu$  is equal to a strain of  $10^{-6}$ ). The data points plotted in Figures 4, 6, 7 and 8 should be considered to have

this error band which corresponds to a 95% confidence limit. The errors derived from the Gaussian fitting procedure (in Tables 1-5) are standard errors ( $\pm\sigma$ ) with a 91% confidence limit.

### 3.2 Normal Strain Measurements

The component of residual strain normal to the surface of the tang was measured at 57 points. The results of these measurements are tabulated in Table 4 and plotted in Figure 6. The normal strain is tensile all through the wall at 3 mm from the pin hole and shows a marked maximum close to the inner surface. Note that the measurements were made 1 mm from the two surfaces.

The results at 7 mm indicate tensile normal strains near the inner surface falling to nearly zero at the outer surface. The through-wall variation is negligible at 11 mm from the pin hole and beyond.

### 3.3 Hoop Strain Measurements

The hoop component of residual strain is plotted in Fig. 7 as a function of distance from the outside wall at various distances from the pin hole. The data are summarized in Table 5.

The hoop strain is strongly compressive at 3 mm from the hole. The hoop strain becomes more compressive as we pass from the OD to the ID which matches the increasing tensile axial component of strain along this path. At distances of 15 and 19 mm the strains are tensile, matching a compressive tendency in the axial component. The hoop strain beyond 19 mm is near zero although it shows a tendency to increase from the OD to the ID.

### 3.4 Variation of Strains Along the Mid Surface of the Shell

Figure 8 shows all three strain components as a function of distance from the pin hole near the mid-wall of the component: this figure conveniently summarizes the trends.

The largest strains observed occur in the hoop direction. The hoop strain at 3 mm from the hole is about  $-1920 \mu$ . The compressive strain decreases in magnitude with distance from the pin hole, falling to zero at about 8 mm from the hole. Beyond 8 mm the residual hoop strain becomes tensile reaching a maximum value of  $640 \mu$  at 12 mm from the hole. At larger distances the hoop

strain remains tensile but falls towards zero with increasing distance from the pin hole.

The axial strain and normal strain at any given location usually have the opposite sign from the hoop stress. At 3 mm from the pin hole they have values of 590  $\mu$  and 390  $\mu$ , respectively.

The linewidth of diffraction peaks has contributions from the instrumental linewidth and any intrinsic effects. As mentioned previously, the measured linewidths (FWHM) are much wider than the known instrumental linewidth. We have obtained the intrinsic linewidth,  $\Delta^s$ , by subtracting the instrumental linewidth  $\Delta^i$  from the measured linewidth  $\Delta$  in quadrature,  $(\Delta^s)^2 = \Delta^2 - (\Delta^i)^2$ . This procedure assumes that both linewidth contributions are Gaussian in form. If we assume further that the intrinsic linewidth has its origin in a distribution of strains in the gauge volume, then the root mean square strain may be calculated from  $\Delta$  by differentiating Bragg's law and relating the standard deviation of the intrinsic width to the half-width

$$\left(\frac{\Delta d}{d}\right)_{\text{rms}} = \left(\frac{\Delta^s}{2.72}\right) \cot \theta \quad (3)$$

The result, derived from measurements of diffraction peaks in the normal, hoop and axial strains near the midwall, is shown in Fig. 9. There is very little extra linewidth in the regions of the component which have high residual strain. The large rms strain distribution is therefore mainly a property of the starting material.

#### 4.0 ANALYTICAL RESULTS

The residual stresses induced in a factory joint tang by proof testing have been calculated in reference 1. The results of that analysis were supplied by Morton Thiokol to AECL in the form of contour diagrams of hoop, axial and normal residual stress in the region between the pin hole and the end of the tang.

The following assumptions were made in the finite element analysis:

- a. A classical incremental elastic-plastic material model was used. Kinematic hardening was assumed with a bilinear uniaxial stress/strain curve.
- b. The material was assumed to have a 0.2 percent offset yield strength of 180 ksi (1260 MPa) a Young's modulus of  $29.6 \times 10^3$  ksi (207 GPa) and a plastic modulus of 400 ksi (2800 MPa).
- c. The finite element model was based on minimum geometry and minimum membrane thickness.
- d. A maximum proof test pressure of 1070 psi (7.5 MPa) was assumed.

### 5.0 COMPARISON OF EXPERIMENTAL AND ANALYTICAL RESULTS

The stresses were read off the contour diagrams on a 2 mm x 2 mm grid in the plane of measurement and the three components of residual strain calculated from the three components of residual stress with the aid of the following equations,

$$\epsilon_H = \frac{\sigma_H}{E} - \frac{\nu\sigma_A}{E} - \frac{\nu\sigma_N}{E} \quad (4)$$

$$\epsilon_A = -\frac{\nu\sigma_H}{E} + \frac{\sigma_A}{E} - \frac{\nu\sigma_N}{E} \quad (5)$$

$$\epsilon_N = -\frac{\nu\sigma_H}{E} - \frac{\nu\sigma_A}{E} + \frac{\sigma_N}{E} \quad (6)$$

In equations 4 through 6, H, A, N stand for hoop, axial and normal. The values of E, Young's modulus and  $\nu$ , Poisson's Ratio, were taken to be 200 GPa and 0.3 respectively. The computed strains are shown by short dashed lines in Figures 4,6,7 and 8.

Most of the measured values of strain are rather small. Only five measured strains are greater than 1500  $\mu$ , a value for which the experimental error band is still  $\pm 20$  percent. Almost half of the measured values are essentially zero; i.e., the magnitude of the measured strain is less than the half width of the error band.

Nevertheless there is reasonably good agreement between the analytical and experimental values. In most cases the value calculated using finite element

analysis lies within the error band of the measured data.

The agreement is about as good as one could expect given the differences which exist between the dimensions and mechanical properties of the actual hardware and the worst case dimensions and properties assumed in the finite element analysis.

#### 6.0 ACKNOWLEDGEMENT

We wish to acknowledge the expert technical assistance of D.C. Tennant, H.F. Nieman, M.M. Potter, G.A. Tapp and L. MacEwan. The help given by J.F. Daines in discussions and for sending numerical data, contributed greatly to the understanding of the problem.

#### 7.0 REFERENCE

1. M.J. Sandor, et. al., TWR-17118, Supplement A, Revision A, "RSRM Case Structural Analysis - Factory Joint", Section 5.4 'Residual Stresses and Strains', April 2, 1988, Morton Thiokol, Inc., Brigham City, Utah.

TABLE 1  
MEASUREMENT OF AXIAL D-SPACING 100 MM FROM PIN HOLE

Distance from pin hole mm	Distance from outside wall mm	$2\theta$ deg.	$\Delta(2\theta)$ deg.	$d_{110}$ Å
100.00	3.4	-80.058(12)	0.76(3)	2.0283(3)
	5.4	-80.056(8)	0.77(2)	2.0283(2)
	7.4	-80.053(6)	0.73(1)	2.0284(1)

$(d_{110})_{av} 2.0283 \pm 0.0002 \text{ \AA}$

TABLE 2  
MORTON THIOKOL REFERENCE SAMPLE

Component	Distance from outside wall mm	$2\theta$ deg	$\Delta(2\theta)$ deg	$d_{110}$ Å
Axial	10	-80.044(9)	0.80(2)	2.0279(2)
	8	-80.031(7)	0.81(2)	2.0282(2)
	6	-80.040(7)	0.79(2)	2.0280(2)
	4	-80.037(7)	0.77(2)	2.0281(2)
	2	-80.024(12)	0.78(2)	2.0284(3)
Hoop	11	-80.033(8)	0.77(2)	2.0282(2)
	9	-80.035(8)	0.79(2)	2.0281(2)
	7	-80.055(8)	0.75(2)	2.0277(2)
	5	-80.031(10)	0.78(2)	2.0282(3)
	3	-80.033(7)	0.74(2)	2.0282(2)
	1	-80.037(7)	0.79(2)	2.0281(2)
Normal	11	-80.030(7)	0.70(2)	2.0282(2)
	10	-80.027(6)	0.70(1)	2.0283(2)
	9	-80.026(7)	0.69(1)	2.0283(2)
	7	-80.022(9)	0.80(2)	2.0284(2)
	5	-80.034(10)	0.80(3)	2.0281(2)
	3	-80.033(8)	0.77(2)	2.0281(2)

Average 2.0281 ± .0002 Å

TABLE 3

AXIAL STRAINS

Distance from pin hole mm	Distance from outside wall mm	$2\theta$ deg.	$\Delta(2\theta)$ deg.	$d_{110}$ Å	Strain ( $\times 10^6$ )
3	15.7	80.120(15)	0.82(4)	2.0307(3)	1180
	15.7	80.136(14)	0.83(4)	2.0304(2)	1040
	15.3	80.146(16)	0.83(4)	2.0302(3)	940
	15.3	80.114(14)	0.78(3)	2.0308(3)	1230
	15.3	80.110(14)	0.85(3)	2.0309(3)	1280
	11.4	80.138(13)	0.84(3)	2.0303(3)	990
	11.4	80.142(14)	0.79(3)	2.0302(3)	940
	9.4	80.150(13)	0.71(3)	2.0301(3)	890
	9.4	80.152(10)	0.83(3)	2.0300(2)	840
	7.4	80.178(15)	0.79(4)	2.0295(3)	590
	7.4	80.178(13)	0.84(3)	2.0295(3)	590
	5.4	80.206(15)	0.90(4)	2.0289(3)	300
	5.4	80.172(11)	0.84(3)	2.0296(2)	640
	3.4	80.190(12)	0.83(3)	2.0292(3)	440
	3.4	80.177(13)	0.88(3)	2.0295(3)	590
	1.8	80.181(12)	0.82(3)	2.0294(3)	540
	1.8	80.205(12)	0.86(3)	2.0289(3)	300
	1.8	80.197(11)	0.87(3)	2.0291(2)	390
	1.0	80.148(10)	0.85(2)	2.0301(2)	890
	1.0	80.176(13)	0.88(4)	2.0295(3)	590
7	15.7	80.274(11)	0.86(3)	2.0275(2)	-390
	14.5	80.246(15)	0.83(4)	2.0281(3)	-100
	14.5	80.268(13)	0.82(3)	2.0276(3)	-350
	11.4	80.237(16)	0.87(4)	2.0282(3)	-50
	11.4	80.218(9)	0.79(2)	2.0286(2)	150
	9.4	80.253(9)	0.83(2)	2.0279(2)	-200
	9.4	80.231(13)	0.81(3)	2.0284(3)	50
	7.4	80.249(9)	0.79(2)	2.0280(2)	-150
	5.4	80.250(12)	0.78(3)	2.0280(2)	-150
	3.4	80.276(9)	0.78(2)	2.0274(2)	-440
	2.2	80.258(12)	0.82(3)	2.0278(3)	-250
	2.2	80.265(12)	0.81(3)	2.0276(3)	-350
	1.0	80.268(10)	0.79(3)	2.0276(2)	-350
	11	15.7	80.306(10)	0.81(2)	2.0268(2)
14.9		80.306(12)	0.83(3)	2.0268(3)	-740
14.9		80.280(13)	0.80(3)	2.0273(3)	-490
11.4		80.276(12)	0.82(3)	2.0274(3)	-440

	9.4	80.254(11)	0.77(3)	2.0279(2)	-200
	7.4	80.247(14)	0.80(4)	2.0280(3)	-150
	5.4	80.268(13)	0.83(3)	2.0276(3)	-350
	3.4	80.279(13)	0.80(3)	2.0273(3)	-490
	2.2	80.270(12)	0.83(3)	2.0276(2)	-350
	2.2	80.272(9)	0.78(2)	2.0275(2)	-390
	1.0	80.264(9)	0.77(2)	2.0277(2)	-300
15	15.7	80.277(8)	0.80(2)	2.0274(2)	-440
	14.3	80.277(8)	0.80(2)	2.0274(2)	-440
	14.3	80.274(9)	0.76(2)	2.0275(2)	-390
	11.4	80.242(13)	0.88(3)	2.0281(3)	-100
	10.4	80.240(12)	0.81(3)	2.0282(2)	-50
	9.4	80.243(11)	0.76(3)	2.0281(2)	-100
	8.4	80.231(10)	0.76(2)	2.0284(2)	50
	7.4	80.258(13)	0.81(3)	2.0278(3)	-250
	6.4	80.260(11)	0.77(3)	2.0278(2)	-250
	5.4	80.239(11)	0.76(3)	2.0282(2)	-50
	3.4	80.237(11)	0.79(3)	2.0282(2)	-50
	1.8	80.248(10)	0.81(2)	2.0280(2)	-150
	1.8	80.260(9)	0.81(2)	2.0278(2)	-250
	1.0	80.236(8)	0.75(2)	2.0283(2)	0
19	14.7	80.253(10)	0.77(2)	2.0279(2)	-200
	11.4	80.234(10)	0.77(3)	2.0283(2)	0
	9.4	80.238(10)	0.75(1)	2.0282(2)	-50
	7.4	80.214(10)	0.74(2)	2.0287(2)	200
	5.4	80.231(10)	0.76(2)	2.0284(2)	50
	3.4	80.248(10)	0.75(2)	2.0280(2)	-150
	1.8	80.238(7)	0.77(2)	2.0282(2)	-50
23	13.0	80.227(6)	0.73(1)	2.0285(1)	100
	10.6	80.238(11)	0.74(1)	2.0282(2)	0
	8.6	80.227(10)	0.74(1)	2.0285(2)	100
	6.6	80.231(10)	0.73(2)	2.0284(2)	50
	4.6	80.231(11)	0.73(2)	2.0284(2)	50
	2.6	80.227(12)	0.76(1)	2.0285(2)	100
	1.0	80.238(6)	0.71(2)	2.0282(1)	-50
27	9.3	80.241(6)	0.71(1)	2.0282(1)	-50
	8.4	80.248(10)	0.69(1)	2.0280(2)	-150
	6.4	80.227(13)	0.70(1)	2.0285(2)	100
	4.4	80.231(12)	0.71(1)	2.0284(2)	50
	2.4	80.231(10)	0.70(1)	2.0284(2)	50
	1.6	80.243(5)	0.70(1)	2.0281(1)	-100
2	7.4	80.130(14)	0.84(4)	2.0305(3)	1090
5	7.4	80.219(16)	0.87(4)	2.0286(3)	150
9	7.4	80.256(13)	0.72(3)	2.0278(3)	-250
9	7.4	80.236(17)	0.80(5)	2.0283(4)	0

TABLE 4

NORMAL STRAINS

Distance from pin hole mm	Distance from outside wall mm	$2\theta$ deg.	$\Delta(2\theta)$ deg.	$d_{110}$ Å	Strain ( $\times 10^6$ )
3	1.0	80.190(7)	0.70(2)	2.0292(2)	440
	2.0	80.175(10)	0.71(2)	2.0295(2)	590
	5.0	80.182(8)	0.73(2)	2.0294(2)	540
	7.0	80.195(6)	0.76(1)	2.0291(1)	390
	15.7	80.122(7)	0.73(2)	2.0307(2)	1180
	14.7	80.101(8)	0.73(2)	2.0311(2)	1380
	13.7	80.107(8)	0.74(2)	2.0310(2)	1330
	11.7	80.149(8)	0.72(2)	2.0301(2)	890
	9.7	80.157(7)	0.78(2)	2.0299(2)	790
	7	15.7	80.177(6)	0.68(1)	2.0295(1)
14.7		80.183(8)	0.71(2)	2.0294(2)	540
13.7		80.185(6)	0.72(1)	2.0293(1)	490
11.7		80.190(8)	0.77(2)	2.0292(2)	440
9.7		80.192(10)	0.73(2)	2.0292(2)	440
7.0		80.211(9)	0.77(2)	2.0288(2)	250
5.0		80.211(12)	0.76(3)	2.0288(3)	250
2.0		80.223(8)	0.73(2)	2.0285(2)	100
1.0		80.217(7)	0.68(1)	2.0287(1)	200
11		15.7	80.234(7)	0.71(1)	2.0283(1)
	14.7	80.234(6)	0.68(1)	2.0283(1)	0
	13.7	80.229(10)	0.72(1)	2.0284(2)	50
	11.7	80.233(7)	0.74(2)	2.0283(2)	0
	9.7	80.252(11)	0.81(3)	2.0279(2)	-200
	7.0	80.211(15)	0.80(4)	2.0288(3)	250
	5.0	80.240(10)	0.74(2)	2.0282(2)	-50
	2.0	80.238(10)	0.72(2)	2.0282(2)	-50
	1.0	80.246(7)	0.67(1)	2.0280(1)	-150
	15	15.7	80.248(6)	0.69(1)	2.0280(1)
14.7		80.235(8)	0.72(2)	2.0283(2)	0
13.7		80.238(8)	0.73(2)	2.0282(2)	-50
11.7		80.254(8)	0.74(2)	2.0279(2)	-200
9.7		80.230(8)	0.76(2)	2.0284(2)	50
7.0		80.220(12)	0.79(3)	2.0286(3)	150
5.0		80.240(8)	0.74(2)	2.0282(2)	-50
2.0		80.244(8)	0.69(2)	2.0281(2)	-100
1.0		80.240(6)	0.67(1)	2.0282(1)	-50

19	15.7	80.250(8)	0.70(2)	2.0280(2)	-150
	14.7	80.251(6)	0.71(1)	2.0279(1)	-200
	13.7	80.248(6)	0.71(1)	2.0280(1)	-150
	11.7	80.255(8)	0.75(2)	2.0279(2)	-200
	9.7	80.260(8)	0.79(2)	2.0278(2)	-250
	7.0	80.245(11)	0.78(3)	2.0281(2)	-100
	5.0	80.244(8)	0.77(2)	2.0281(2)	-100
	2.0	80.233(7)	0.69(2)	2.0283(2)	0
	1.0	80.236(6)	0.67(1)	2.0283(1)	0
23	7.0	80.242(12)	0.76(3)	2.0281(3)	-100
	5.0	80.228(8)	0.74(2)	2.0284(2)	50
	2.0	80.243(8)	0.68(2)	2.0281(2)	-100
	1.0	80.239(7)	0.67(2)	2.0282(2)	-50
27	7.0	80.240(11)	0.75(3)	2.0282(2)	-50
	5.0	80.237(12)	0.76(3)	2.0282(3)	-50
	2.0	80.222(10)	0.72(2)	2.0286(2)	150
	1.0	80.243(6)	0.69(1)	2.0281(1)	-100
2	7.0	80.179(7)	0.77(2)	2.0295(2)	590
5	7.0	80.182(10)	0.74(2)	2.0294(2)	540
9	7.0	80.222(14)	0.74(4)	2.0286(3)	150
13	7.0	80.239(11)	0.78(3)	2.0282(2)	50

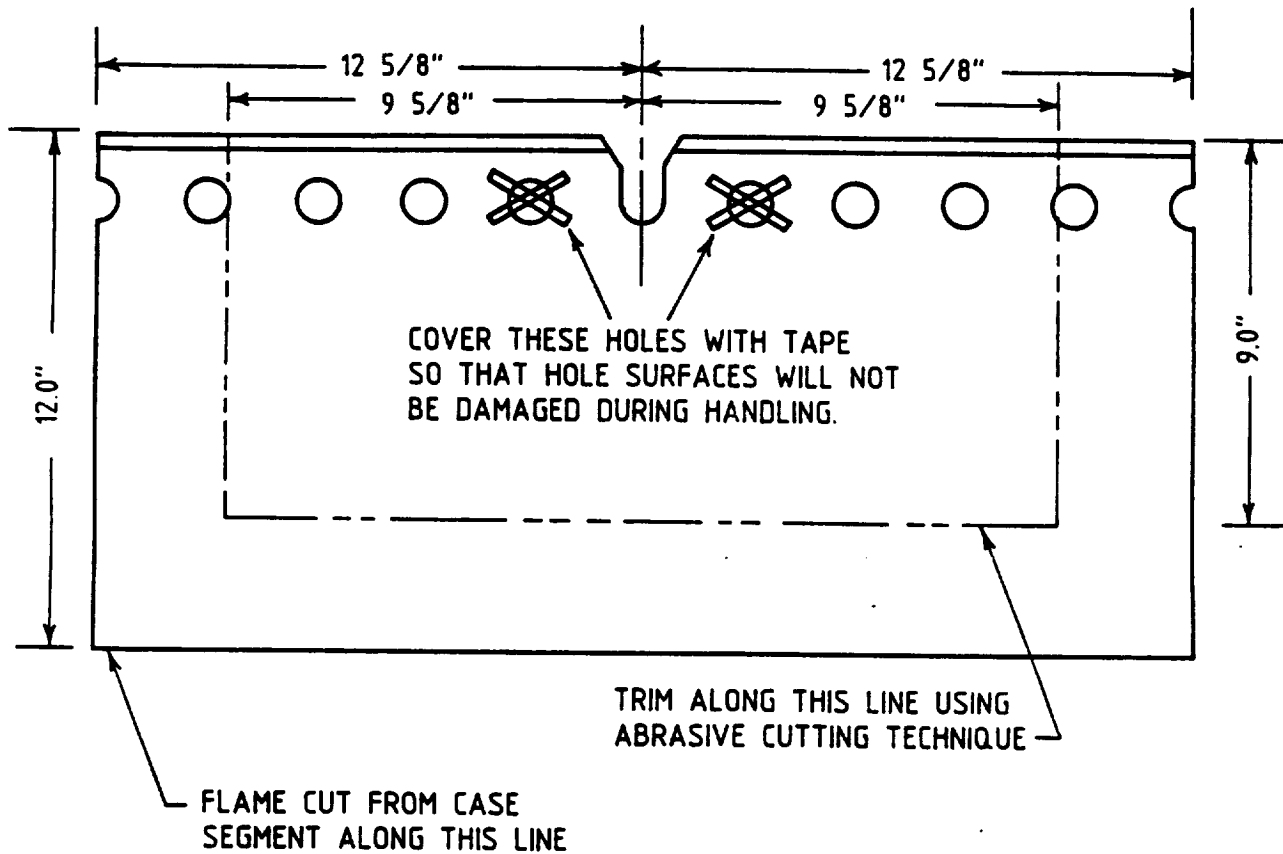
TABLE 5

HOOP STRAINS

Distance from pin hole mm	Distance from outside wall mm	$2\theta$ deg.	$\Delta(2\theta)$ deg.	$d_{110}$ Å	Strain ( $\times 10^6$ )
3	11.0	80.457(13)	0.81(4)	2.0236(3)	-2320
	10.0	80.434(16)	0.85(4)	2.0241(3)	-2070
	8.0	80.404(15)	0.90(4)	2.0248(3)	-1730
	7.0	80.418(15)	0.83(4)	2.0244(3)	-1920
	5.0	80.392(13)	0.90(4)	2.0250(3)	-1630
	2.0	80.379(14)	0.84(4)	2.0253(3)	-1480
	1.0	80.378(16)	0.81(4)	2.0253(3)	-1480
	7	11.0	80.263(13)	0.80(3)	2.0277(3)
10.0		80.267(11)	0.84(3)	2.0276(2)	-350
8.0		80.219(14)	0.81(3)	2.0286(3)	150
7.0		80.270(14)	0.75(4)	2.0275(3)	-390
5.0		80.223(10)	0.75(2)	2.0285(2)	100
2.0		80.215(13)	0.79(3)	2.0287(3)	200
1.0		80.249(12)	0.85(3)	2.0280(3)	-150
11		11.0	80.193(11)	0.76(3)	2.0292(2)
	10.0	80.192(12)	0.81(3)	2.0292(3)	440
	8.0	80.156(12)	0.74(3)	2.0299(3)	790
	7.0	80.174(14)	0.76(4)	2.0296(3)	640
	5.0	80.168(11)	0.79(3)	2.0297(2)	690
	2.0	80.204(15)	0.80(4)	2.0289(3)	300
	1.0	80.197(13)	0.77(3)	2.0291(3)	390
	15	11.0	80.184(13)	0.78(3)	2.0294(3)
10.0		80.212(12)	0.74(3)	2.0288(3)	250
8.0		80.205(13)	0.84(3)	2.0289(3)	300
7.0		80.199(16)	0.84(4)	2.0290(3)	350
5.0		80.222(17)	0.89(4)	2.0286(4)	150
2.0		80.237(9)	0.81(2)	2.0282(2)	-50
1.0		80.234(17)	0.80(4)	2.0283(4)	0
19		11.0	80.188(14)	0.78(3)	2.0293(3)
	10.0	80.201(13)	0.80(3)	2.0290(3)	350
	8.0	80.226(13)	0.76(3)	2.0285(3)	100
	7.0	80.208(14)	0.82(4)	2.0289(3)	300
	5.0	80.207(14)	0.82(3)	2.0289(3)	300
	2.0	80.212(13)	0.78(3)	2.0288(3)	250
	1.0	80.246(14)	0.81(4)	2.0281(3)	-100

23	7.6	80.200(11)	0.76(3)	2.0290(2)	350
	6.6	80.217(11)	0.80(3)	2.0287(2)	200
	5.6	80.224(9)	0.76(2)	2.0285(2)	100
	3.6	80.216(9)	0.77(2)	2.0287(2)	200
	2.6	80.223(11)	0.77(3)	2.0285(2)	100
27	9.4	80.203(11)	0.73(3)	2.0290(2)	350
	7.4	80.216(6)	0.72(1)	2.0287(1)	200
	5.4	80.222(7)	0.73(2)	2.0286(2)	150
	3.4	80.226(9)	0.73(2)	2.0285(2)	100
	1.4	80.239(6)	0.76(1)	2.0282(2)	-50

CUT THREE FROM TANG OF STIFFENER SEGMENT  
WHICH WAS IMMEDIATELY AFT OF ET ATTACH SEGMENT



TAG SPECIMENS

Fig. 1 - Cutting sketch for tang specimens taken from a segment of a solid fuel booster rocket.

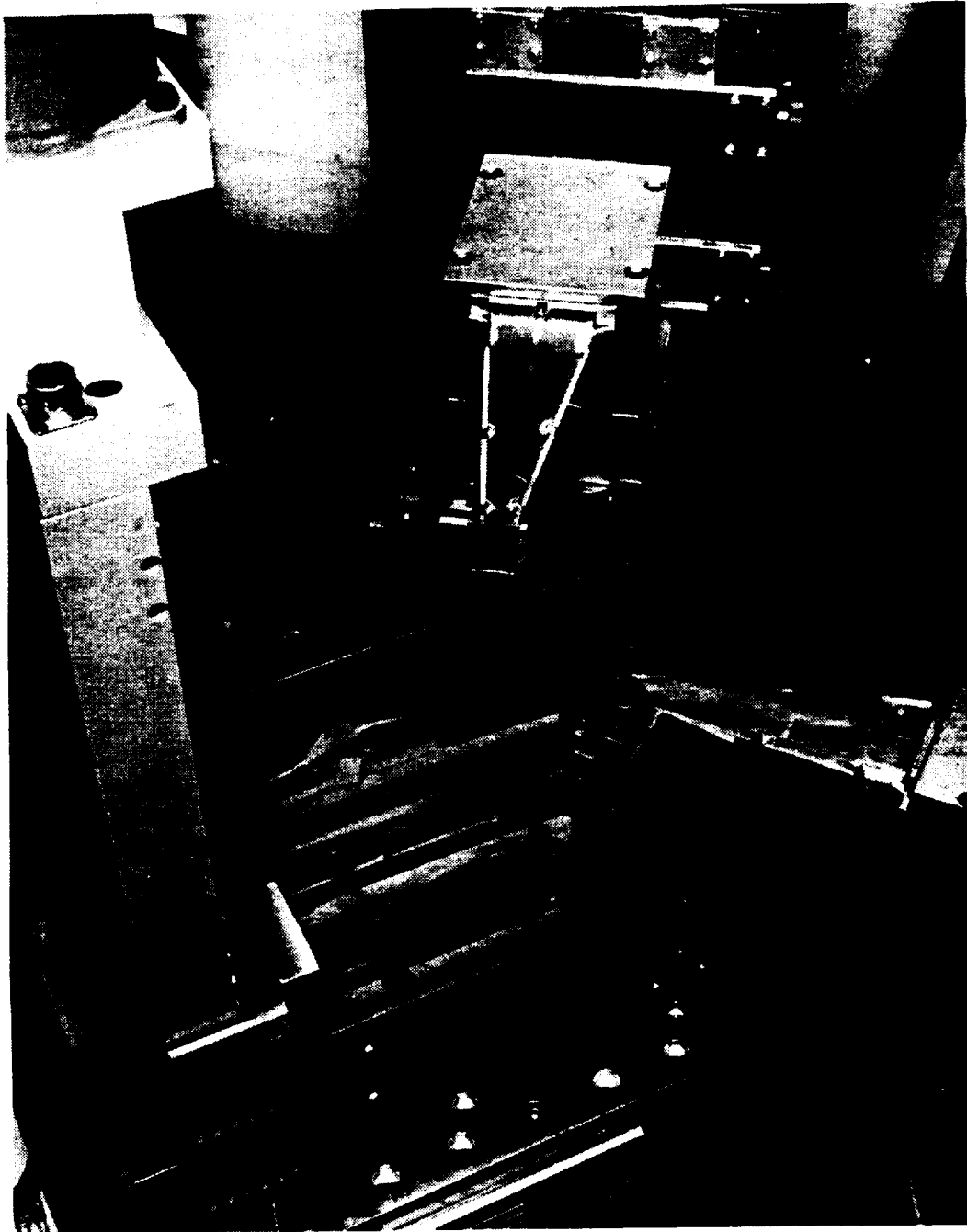


Fig. 2 - Photograph of the solid fuel booster rocket casing on the L3 spectrometer at the NRU reactor.

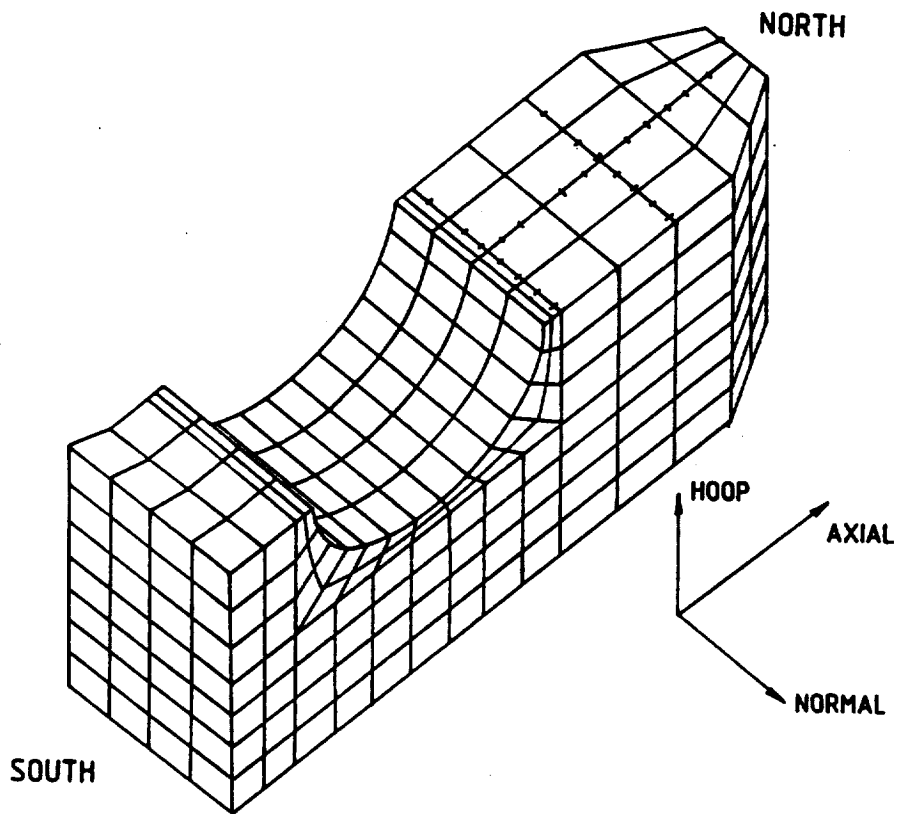


Fig. 3 - Schematic diagram of the tang end of a solid fuel booster rocket casing indicating axial, hoop and normal directions. The plane in which the measurements were taken is the top plane of the diagram defined by the axis of the bolt hole and a North-South axis indicated on the diagram.

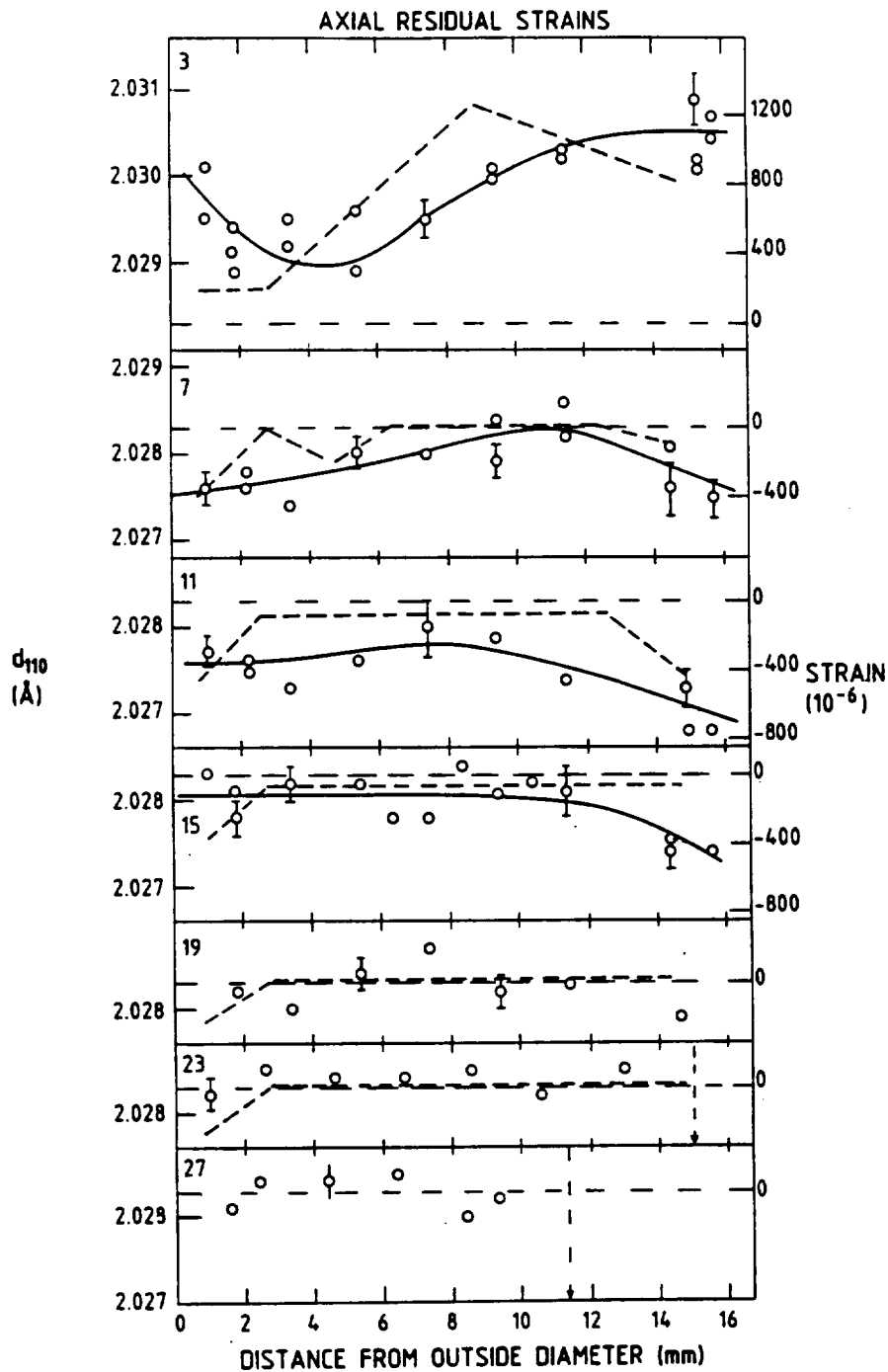


Fig. 4 - Variation of the axial strain through the wall of the casing from the outside wall for distances of 3, 7, 11, 15, 19, 23 and 27 mm from the outside diameter of the bolt hole. Short dashed lines indicate the results of finite element calculations.

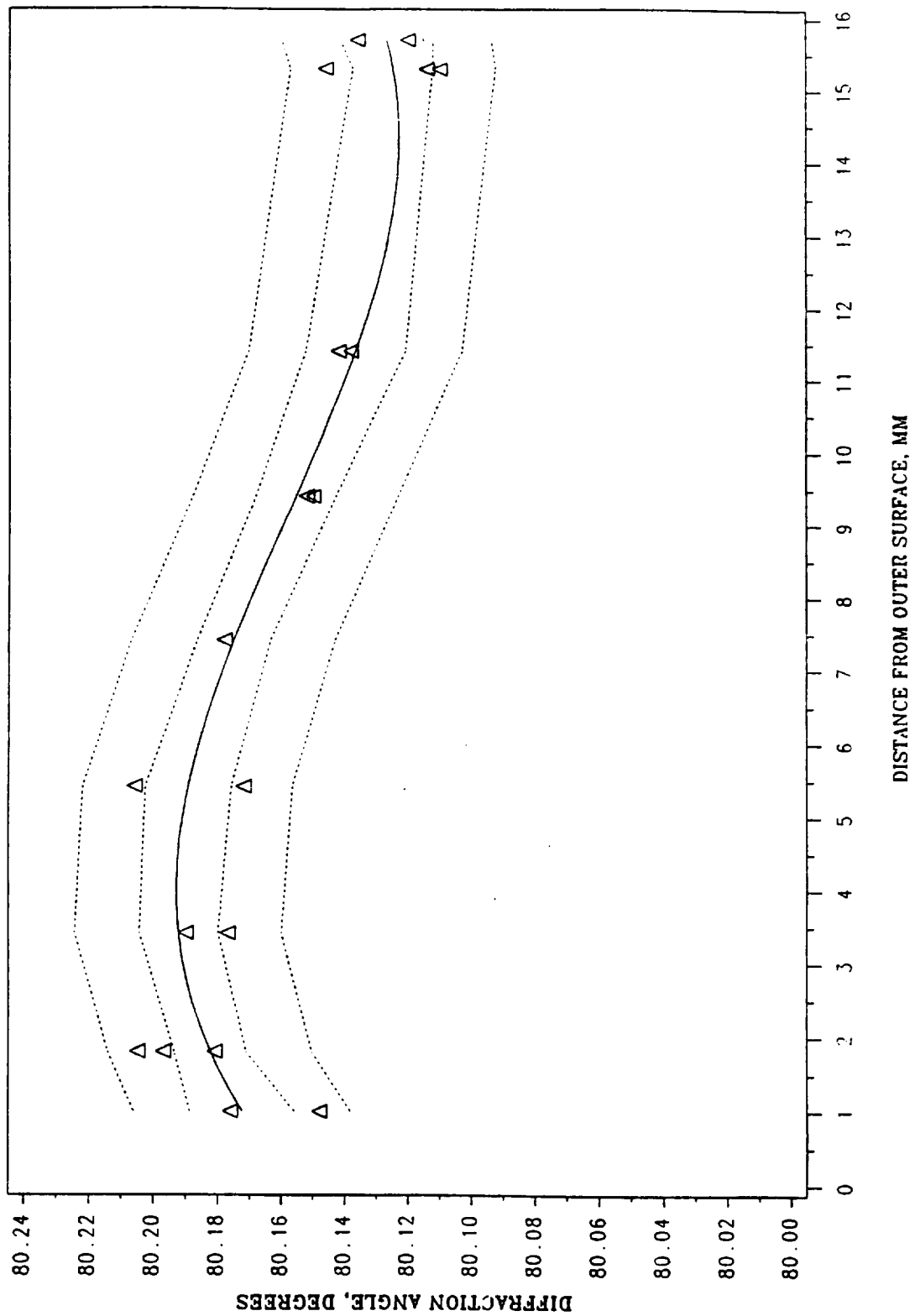


Fig. 5 - Third order polynomial fit to the twenty measurements of diffraction angle for the axial strain component measured at a distance of 3 mm from the edge of the pin hole. Error bands for  $\pm\sigma$  and  $\pm 2\sigma$  are shown by dotted curves.

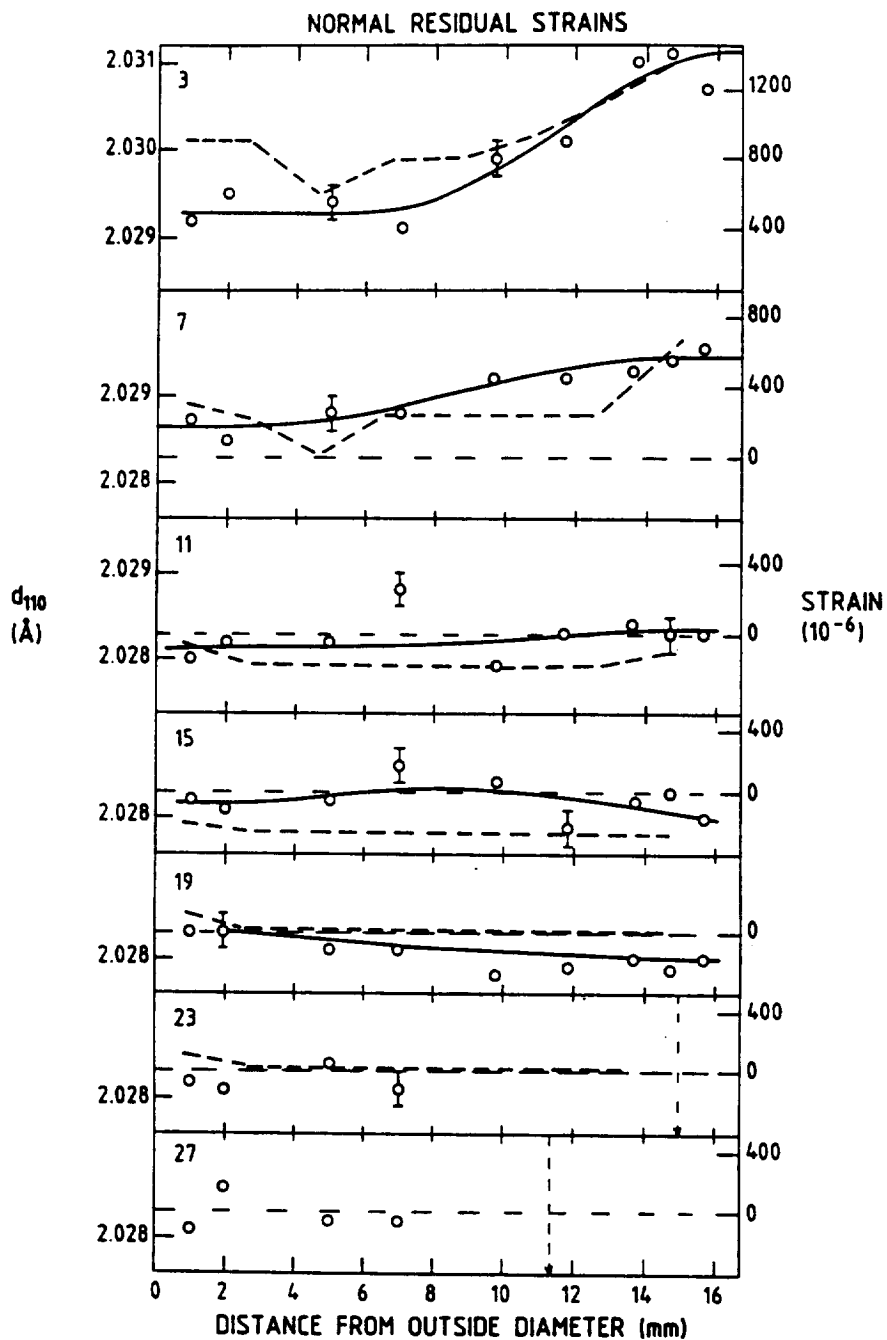


Fig. 6 - Variation of the normal strain through the wall of the casing for distances of 3, 7, 11, 15, 19, 23 and 27 mm from the outside diameter of the bolt hole. Short dashed lines indicate the results of finite element calculations.

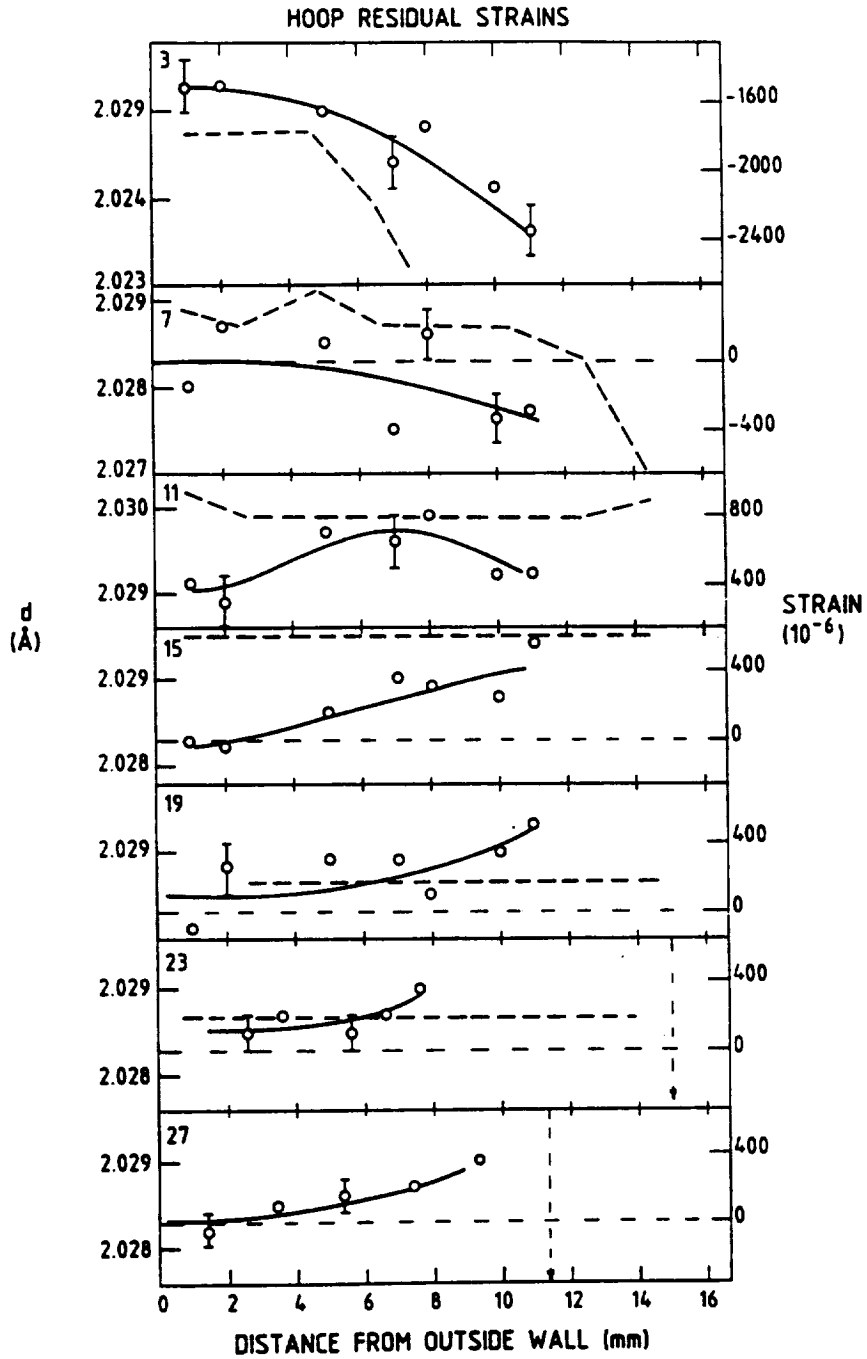


Fig. 7 - Variation of the hoop strain through the wall of the casing for distances of 3, 7, 11, 15, 19, 23 and 27 mm from the outside diameter of the bolt hole. Short dashed lines indicate the results of finite element calculations.

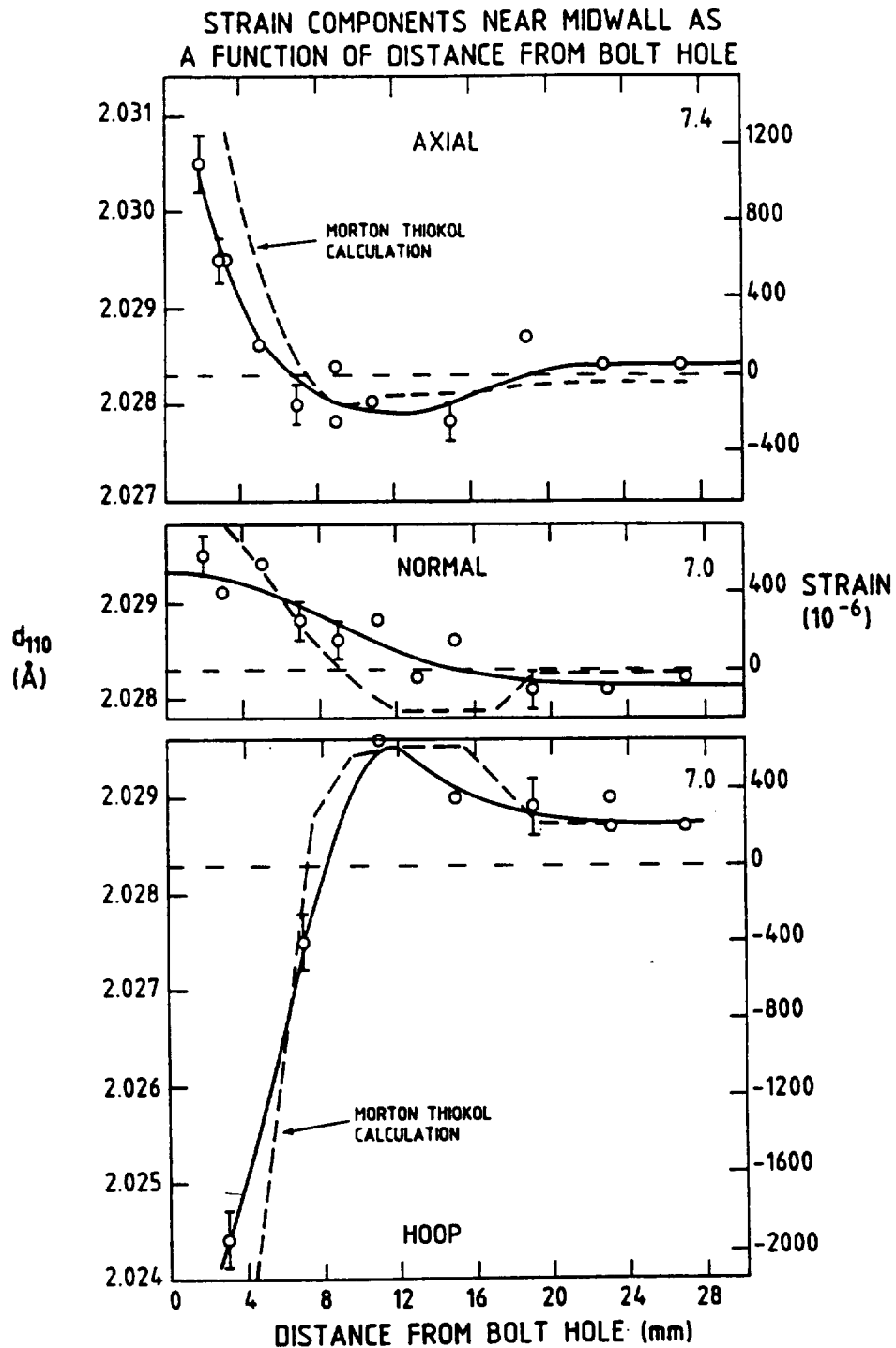


Fig. 8 - The axial, normal and hoop components of residual elastic strain as a function of distance from the outside diameter of the bolt hole at a position close to the mid-wall of the casing. Short dashed lines indicate the results of finite element calculations. The numbers 7.4, 7.0, 7.0 refer to the precise distance from the outside wall.

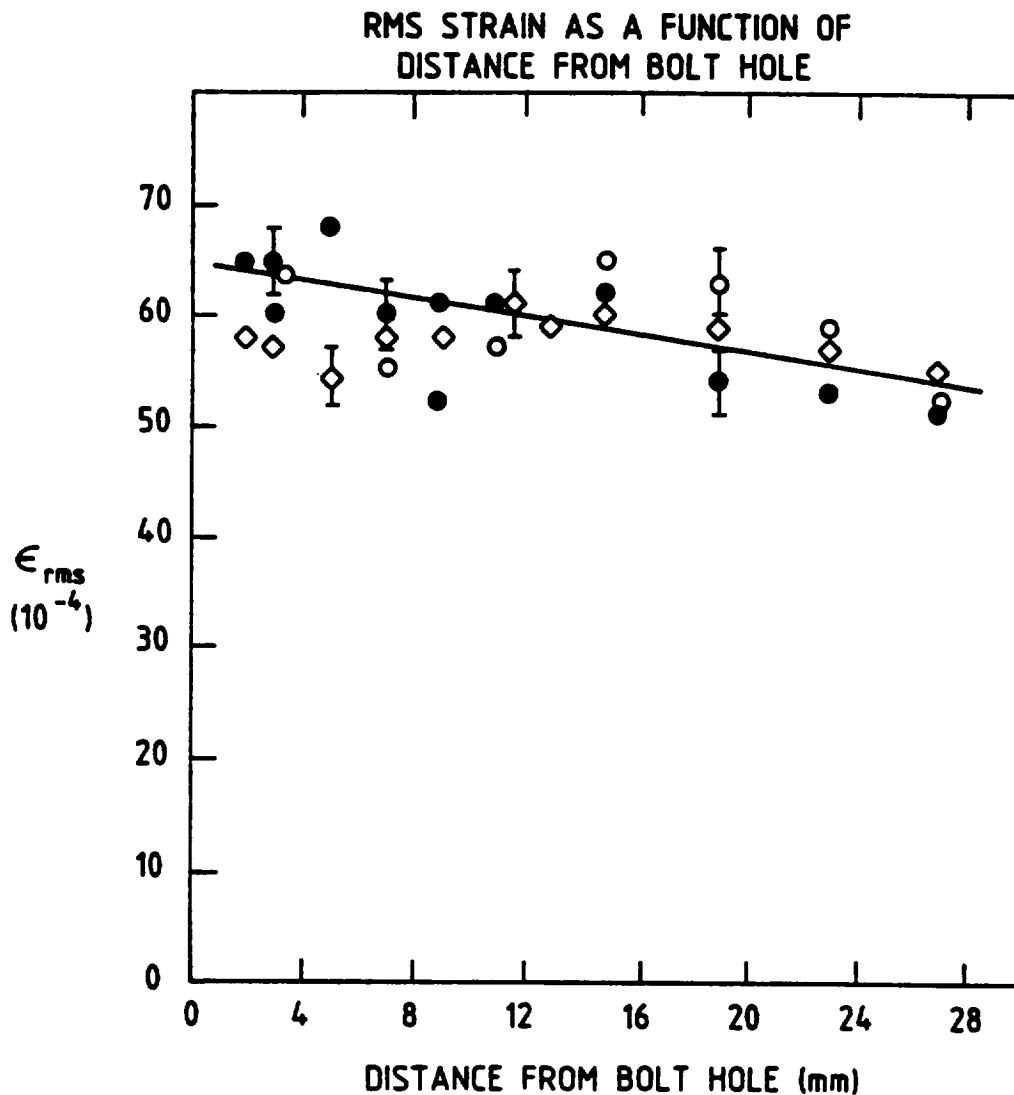


Fig. 9 - Root mean square strain derived from the intrinsic linewidth of the diffraction peaks as a function of distance from the bolt hole near the midwall. Solid circles, open circles, and diamonds correspond to axial, hoop and normal results respectively.